PŘÍRODOVĚDECKÁ FAKULTA UNIVERZITY
PALACKÉHO V OLOMOUCI

SPOLEČNÁ LABORATOŘ OPTIKY

Kvantové a klasické strojové učení pro kvantově informační protokoly

DIZERTAČNÍ PRÁCE

Jan Roik

školitel

doc. Mgr. Karel Lemr, Ph.D.

OLOMOUC   6. března, 2023

FACULTY OF SCIENCE, PALACKÝ UNIVERSITY OLOMOUC

JOINT LABORATORY OF OPTICS

Quantum and classical machine learning for quantum information protocols

Ph.D. THESIS

Jan Roik

supervisor

assoc. prof. Karel Lemr, Ph.D.

OLOMOUC   March 6, 2023

Bibliografická identifikace

Název práce	Kvantové a klasické strojové učení pro kvantově informační protokoly
Typ práce	Disertační
Autor	Jan Roik
Vedoucí práce	doc. Mgr. Karel Lemr, Ph.D.
Studijní obor	Nanotechnologie
Pracoviště	Společná laboratoř optiky
Jazyk	Angličtina
Klíčová slova	Kvantové provázání, klasifikace kvantového provázání, kvantifikace kvantového provázání, strojové učení, neuronové síte, kvantové sítě, proximální optimalizace politiky
Rok	2023
Počet stran	118
Dostupná na	http://portal.upol.cz

Bibliographic details

Title	Quantum and classical machine learning for quantum information protocols
Type	Ph.D. thesis
Author	Jan Roik
Supervisor	assoc. prof. Karel Lemr, Ph.D.
Study program	Nanotechnology
Department	Join Laboratory of Optics
Language	English
Key words	Quantum entanglement, quantum entanglement classification, quantum entanglement quantification, machine learning, neural networks, quantum networks, proximal policy optimization
Year	2023
Pages	118
Available at	http://portal.upol.cz

Declaration of originality

I hereby declare that this thesis is my own work and that, to the best of my knowledge and belief, it contains no material previously published or written by another person nor material which, to a substantial extent, has been accepted for the award of any other degree or diploma of the university or other institute of higher learning, except where due acknowledgment has been made in the text.

In Olomouc,..................................... ....

Submitted on ....

The author grants Palacký University in Olomouc permission to store and display this thesis and its electronic version in a university library and on the official website.

Acknowledgment

-The author

Contents

Chapter 1

Introduction

"The man who asks a question is a fool for a minute, the man who does not ask is a fool for life."

-Confucius

Since the dawn of time, humankind has manifested a deep desire to explore the world and unveil every mystery in the universe. These urges are deeply rooted in our nature and motivated by survival instincts [1]. Initially, we compensated for our lack of knowledge by inventing various stories about gods and monsters [2]. These were the initial attempts to understand the world around us. Similar endeavors have been typical for every civilization worldwide throughout history [3, 4]. As humankind evolved, we replaced these initial explanations (myths and legends) created by our imagination with a systematic study of the structure and behavior of the physical and natural world through observation and experiment[1]. Thus science was born. It is remarkable how fast our understanding of the universe has expanded since then. What started with the simple observation of the falling apple evolved into a search to understand the creation of the universe itself.

One of the most intriguing scientific discoveries was that nature is, in its essence, unpredictable. The "God", indeed, plays dice with us[2]. These findings introduced by the "Quantum" theory were shocking and brutal to accept [5, 6]. Since its introduction at the beginning of 20th century, it took nearly a century to collect enough evidence to convince the majority

---

[1]Definition of science from the Cambridge Advanced Learner's Dictionary & Thesaurus.
[2]The contradiction of Einstein's famous quote.

of the academic community that quantum theory is valid [7–9]. Despite several attempts so far, there has been no proper experiment to contradict its validity.

1.1 Quantum physics

The origin of quantum physics can be traced to the black-body radiation problem first described by Gustav Kirchhoff in 1859 [10]. In order to create a theoretical model matching observed patterns of black-body radiation, Max Planck had to consider that energy is radiated and absorbed in discrete energy packets, "quanta" [11]. However, for him, quantification was just a mathematical trick that did not reflect reality. It took another five years to confirm that quantization indeed describes reality when Albert Einstein also used it to explain the photoelectric effect[3] [12]. Quantum physics as we know it was established in 1925 when Werner Heisenberg composed matrix mechanics [13], and Erwin Schrödinger formulated wave mechanics [14].

Quantum physics is currently the most accurate way of describing the physical properties of nature on a fundamental level. Thus far, we formulated the quantum description of the weak [15], strong [16], and electromagnetic [17] interactions. That is why quantum theory has become essential for many scientific fields, such as quantum chemistry [18], quantum optics [19], quantum electronics [20], solid-state physics [21], materials science [22], computer science [23]. However, quantum physics is not just used for theoretical research. In fact, it is also essential for applied research [24], such as quantum communication [25], quantum cryptography [26], quantum biology (production of an "artificial leaf" for energy conversion by photosynthesis) [27], quantum computers [23], quantum sensor technology [28], quantum metrology [29], quantum electronics (including single electron transistors) [30] to mention a few.

1.2 Quantum information processing

Quantum information processing is a multidisciplinary field of research [31], including quantum information theory [32], quantum communications [25], quantum computation [33], and quantum algorithm design [34].

---

[3]The Nobel Prize in Physics 1921: Albert Einstein "For his services to Theoretical Physics, and especially for his discovery of the law of the photoelectric effect".

Quantum physics introduced new tools into data processing based on the properties of the quantum object, such as superposition and entanglement[4] [5]. These properties are the sole reason the new quantum protocols can solve classically unsolvable problems or make the standard protocols more efficient.

Where classical information theory works with bits representing the single quanta of information [35], quantum information theory, on the other hand, works with qubits represented by superposition [32], containing potentially unlimited amount of classical information. Qubits are typically encoded using discrete-level quantum mechanical systems. However, it was shown that even continuous variable could be a viable alternative [36, 37]. Historically the most prominent methods were encoding into the spatial or polarization modes of photons [38] and encoding into electrons that can be either in the ground or excited state [39]. Currently, the most promising methods are encoding either into the superconduction qubits [40] to construct large-scale quantum computers or into time bins [41] for quantum cryptography.

Working with qubits allows using the similar class of operations known from classical information theory, except for the restriction on perfect cloning of unknown qubit state. The list of permitted operations includes constructing quantum logic gates, executing quantum measurements, initializing to a known value, and propagating through quantum channels. Given operations are sufficient to design quantum circuits and even construct devices capable of executing them[5].

These so-called quantum computers showed the potential to solve complex tasks such as finding prime factors of an integer by running Shor's algorithm in polynomial time [43, 44]. Furthermore, many believe that quantum computers may offer a solution to non-deterministic polynomial-time hardness (NP-hard) problems, such as Tail Assignment Problem recently demonstrated on a smaller scale by Vikstål *et al.* [45]. In 2020 Zhong *et al.* published an article claiming they achieved true quantum supremacy on the gaussian boson sampling problem using only 76 qubits [46]. In November 2022, IBM published an article claiming the development of a 433-qubit quantum computer [47, 48].

---

[4]The Nobel Prize in Physics 2022: Alain Aspect, John F. Clauser and Anton Zeilinger "For experiments with entangled photons, establishing the violation of Bell inequalities and pioneering quantum information science".

[5]In 1998 Isaac Chuang, Neil Gershenfeld and Mark Kubinec created the first quantum computer [42].

This rapid evolution of quantum computing will offer a powerful tool to efficiently address problems such as quantum encryption [26], simulation of quantum systems [49], combinatorics problems [50], supply chain logistics [51], drug development [52], data analysis [53], machine learning [54], and much more [55].

Unfortunately, although quantum computing offers a solution to many fundamental problems, it also raises some concerns [56]. For example, it was shown that quantum computers can be very efficient at breaking prominent classical cryptography methods based on prime number factorization [57]. As a solution, a whole new field of cryptography was born [58]. This so-called "quantum" cryptography is based on the impossibility of perfectly cloning unknown quantum states [59]. The security of this encryption method is hence insured by the laws of nature and cannot be cracked under ideal conditions. The alternative method to quantum cryptography is co-called "post-quantum" cryptography, which focuses on developing a classical coding method unbreakable even by large-scale quantum computers [60].

The goal for the future is to create quantum communicational networks, aka quantum internet [61]. Such networks would provide a secure way to distribute quantum information among its users [62]. It would also help connect quantum processes to make even more complex calculations possible [63] or offer more accurate clock synchronization for the positioning systems [64]. Unfortunately, some open problems still need to be addressed before the experimental realization of a full-scale quantum internet [65–68].

1.3   Artificial intelligence

Artificial intelligence is one of the most exciting fields evolving in today's world. This general term refers to a computer system capable of accomplishing a task that requires human intelligence, such as using available information to make informed decisions, communicating with people using their natural language, identifying data patterns, acting on previous experiences, and adapting to new situations[6].

Artificial intelligence requires training to gain experience. We distinguish three base types of machine learning based on the degree of human involvement in the learning process. The first is supervised learn-

---

[6]Definition of artificial intelligence by: Oxford Languages and Google.

ing [69] which requires a labeled training data set to establish its policy. When trained properly, it should accurately predict future outcomes based on past processed data. The second method, unsupervised learning [70], can identify hidden patterns in unlabeled input data. As an output, it gives us more readable, organized data that may reveal patterns, similarities, or anomalies. Finally, the third method, reinforcement learning [71], is used in scenarios with clearly defined goals, actions, and reward structures. The agent receives a reward or punishment based on the action taken, and as a result, it should be able to find the optimal solution to a given task.

There is a large variety of approaches toward machine learning, each with its downsides and benefits. Therefore, the optimal machine learning method is chosen based on the type of artificial intelligence we want to create. We can highlight linear regression [72], clustering [73], and dimensionality reduction [74] as an example of the most prominent ones.

As mentioned above, one of the goals of artificial intelligence is to mimic human behavior. The field addressing this specific task is called deep learning [75]. This type of machine learning uses artificial neural networks to create a structure resembling the topology of the neurons inside a human brain [76]. The recent development of this branch of artificial intelligence introduced a technique known as generative machine learning [77]. Here two neural networks compete agent each other to achieve their goal. This advanced artificial intelligence can handle even complex tasks, such as creating art (see Fig. 1.1) or producing genuine photos of people that never existed.

Artificial intelligence has become an invaluable tool for many fields with immense application potential in the last decade. Thus far, machines have learned how to generate art [78], translate to hundreds of languages [79], drive cars [80], recommend content based on our preferences [81], and so much more. Artificial intelligence can best even the greatest players in the world in complex games such as chess [82], Go [82], or starcraft [83]. We even teach machines how to diagnose patients to increase the efficiency of health care [84, 85]. Despite all this recent progress, we are still far from general artificial intelligence, which some consider unachievable [86].

Figure 1.1: A *"Mystery pirate girl"* on the left and *"Popcorn octopus"* on the right were both created with the V4 version of Midjourney's algorithm. Author: D & L Ebers.

1.4 Outline

The presented thesis was written with the intention to summarize and consolidate the authors' published research focused on the potential of machine learning in quantum information processing. The research was carried out at the Joint Laboratory of Optics, Palacký university and Institute of Physics of Academy of Sciences of the Czech Republic[7]. This research facility offered decades of collective experiences in quantum information processing and machine learning [87–89]. The author also collaborated with theoreticians from the University of Adam Mickiewicz in Poznan[8].

Foundings presented in Chapters 3–5 are adopted from authors' journal publications containing the original results. Declarations of author's contribution are attached in the Appendix.

The rest of this chapter will briefly introduce the investigated problems and summarize the authors' other scientific projects. The first part of the second chapter introduces terminology connected to artificial intelligence, such as machine learning, neural networks, and reinforcement learning utilizing proximal policy optimization. The second part estab-

---

[7]17. listopadu 50A, 772 07 Olomouc, Czech Republic
[8]Uniwersytetu Poznańskiego 2, 61-614 Poznań, Poland

lishes terms connected to quantum information processing, such as entanglement classification, entanglement quantification, and entanglement witnesses.

Accuracy of entanglement detection via artificial neural networks and human-designed entanglement witnesses

Quantum entanglement is one of the most intriguing phenomena ever discovered by humankind. It has become a cornerstone for many applications, such as quantum cryptography [58], superdense coding [90], teleportation [91], and quantum computation [33]. Therefore it is essential to know how to distinguish entangled states. However, even nowadays, we still lack efficient and general methods to do so.

Currently, the most popular methods are full-state tomography and entanglement witnesses. Unfortunately, neither of them is optimal. Full-state tomography offers a complete quantum state description but is experimentally demanding and scales undesirably with the complexity of the investigating state. On the other hand, prominent entanglement witnesses such as collectibility [92], Clauser, Horne, Shimony, Holt (CHSH) nonlocality [93], fully entangled fraction [94], and entropy witnesses [95] do not guarantee correct classification of the investigated state. The idea of using a neural network to classify entangled states was initially demonstrated by Gao *et al.* in 2018 [96]. However, they considered only entangled linear witnesses, which allowed them to classify only a limited class of states.

Under those presumptions, we set our research goal to use the artificial neural network as the nonlinear entanglement witness, aiming to maximize the classification success rate for all general two-qubit stats while reducing required resources. The neural network performance was compared against the prominent analytical witnesses for random general 2-qubit quantum states.

Entanglement quantification from collective measurements processed by machine learning

Based on Author's publication: J. Roik, K. Bartkiewicz, A. Černoch, and K. Lemr, Physics Letters A, vol. 446, p. 128270, 2022 [A-2].

The promising performance of the artificial neural network to detect entangled states demonstrated in prior research [A-1] has motivated us to extend our effort to a more general task. This follow-up research aimed not only to classify general two-qubit states but quantify them, i.e., determine their degree of entanglement. Conventionally, one must perform full state tomography to reconstruct the investigated state's density matrix and subsequently calculate entanglement measures [97], which both scales unfavorably with the complexity of investigated state.

The research goal was to employ the artificial neural network to reduce the number of projections required for accurate entanglement quantification based on the results of collective measurement using a minimal set of tomographic projections [98]. We investigated correlations between the precision of the quantification as a function of the measurement configuration. The investigation was carried out on the general two-qubit states, and the negativity was used as an entanglement quantifier [99]. In the end, the performance of the artificial neural network was benchmarked against the capabilities of the polynomial regressions method.

Routing in quantum communications networks using reinforcement machine learning

Based on Author's publication: J. Roik, K. Bartkiewicz, A. Černoch, and K. Lemr, submitted (2023) [A-3].

With the recent evolution of quantum technologies, concepts such as the large-scale quantum networks "quantum internet" are steadily becoming a reality. Although we have already overcome many obstacles, few remain unaddressed [65]. One of the most crucial is identifying an effective protocol for route-finding in a teleportation-based quantum network [67]. The quantum nature of these networks introduces properties unique to the quantum world, such as non-additive noise (amplitude dumping [100], correlated phase noise [101]). Non-additive noise is the main reason we cannot simply use classical graph path and tree-finding algorithms because they cannot handle non-additivity, which often leads to suboptimal

solutions.

In order to maintain stable and safe communication, one needs to use as error free roads as possible (i.e., find the optimal solution). Therefore, we focused our research efforts on identifying the protocol capable of route-finding in a quantum network, emphasizing the maximization of the entangled fraction between the shared state.

In our research, we promote reinforcement learning represented by the proximal policy optimization (PPO) algorithm [102] as an efficient solution to the outlined problem. This algorithm was benchmarked against the Monte-Carlo search. We demonstrate the performance of both algorithms on various scenarios set in the quantum network. [9]

The author's other projects unrelated to this thesis included the development of the calibration method for commercially available colorimeters [A-4, A-5] and the experimental comparison of alternative approaches toward weak measurement [A-6]. Currently, the author supervises bachelor theses dealing with the capability of artificial intelligence to design quantum circuits. He is also a member of the group investigating synergic quantum generative machine learning [A-7]. The author was also the principal investigator of the DSGC grant (Doctoral Student Grant Competition) on the topic "Efficient preparation of non-classical discrete photon states for quantum information applications."

---

[9]Topology was inspired by one of the possible topologies of 6G networks [103].

Chapter 2

Methods and tools

This chapter will introduce the methods and tools used in upcoming chapters. Section 2.1 will briefly describe the artificial neural network (ANN). The goal is to shed some light on its training process and highlight which parameters are essential for the ANN's proper functionality. Section 2.2 will introduce proximal policy optimization (PPO), focusing on its working principles and establishing field-specific terminology, and Section 2.3 summarizes how to define tasks in a "gym" library. The second half of this chapter, Section 2.4, Section 2.5, and Section 2.6, will establish quantum states, entanglement witnesses, and quantum teleportation.

2.1   Artificial neural networks

Artificial neural networks are computer algorithms inspired by the brain structure of living organisms. Neurons fulfill the role of fundamental building blocks of every artificial neural network. By clustering neurons into layers, they determine the topology of the ANN [104]. In principle, two layers (input and output) are already sufficient for ANN to function. However, incorporating additional "hidden" layers into the ANN structure is common practice to enhance ANN performance [105]. Each neuron is represented by the activation number, $a \in \langle 0, 1 \rangle$. For better visualization of the ANN functionality, it is convenient to assign a grayscale value to a ranging from black for $a = 0$ to white for $a = 1$ (see Fig. 2.1).

ANN's initial layer contains n neurons, where n represents the corresponding input data size. Each segment of the input data provides an activation value $a_n^{(0)}$ for the neurons in the first layer. The activation numbers

of the neurons in the subsequent layers are given as a weighted sum

$$a_n^{(L)} = a_0^{(L-1)} w_{0,n} + a_1^{(L-1)} w_{1,n} + \ldots + a_m^{(L-1)} w_{m,n}, \tag{2.1}$$

$$a_n^{(L)} = \sum_m a_m^{(L-1)} w_{m,n}, \tag{2.2}$$

of all activation numbers $a_m^{(L-1)}$ from the previous layer multiplied by the weights $w_{m,n}$ which represent the strength of activation in the visualization of ANN they are represented as connection lines between neurons. The count of the neurons in the last layer sets the number of possible outcomes. Their corresponding activation values represent how confident the ANN is about a given output [106]. To introduce nonlinearity [107] and ensure that the activation values remain in the desired region, typically between 0 and 1, the activation function [108] σ, such as sigmoid [109], ReLU [110], Softmax [111], or Swish [112], is applied to the result of the weighted sum

$$a_n^{(L)} = \sigma \left(\sum_m a_m^{(L-1)} w_{m,n} \right). \tag{2.3}$$

One can also add bias $b_{m,n}$ to every node as an additional parameter

$$a_n^{(L)} = \sigma \left(\sum_m a_m^{(L-1)} w_{m,n} + b_n \right), \tag{2.4}$$

to influence the decision process of the ANN by setting how high the weighted sum needs to be before the neuron gets meaningfully activated. All adjustable parameters are incorporated into vector

$$\vec{W} = \left[w_{0,0}, \ldots, w_{m,n}, b_0, \ldots, b_n \right]. \tag{2.5}$$

Let us consider an illustrative case where we task a neural network to classify handwritten digits on the 10×10 pixel display. Given that each pixel contributes to the input data size, the ANN will have 100 neurons in the initial layer, each representing one pixel of the display grid. Activation values correspond to normalized grayscale intensity values displayed on the pixels (see Fig. 2.1). Under the presumption that given ANN can distinguish only digits $1-4$, the last layer in the network will contain four neurons. Additionally, one hidden layer with five neurons should be sufficient to solve outlined task efficiently, considering the complexity of the presented task. From the visual representation of the ANN (see Fig. 2.1), one can see that every distinctive input has activation values that form unique patterns in
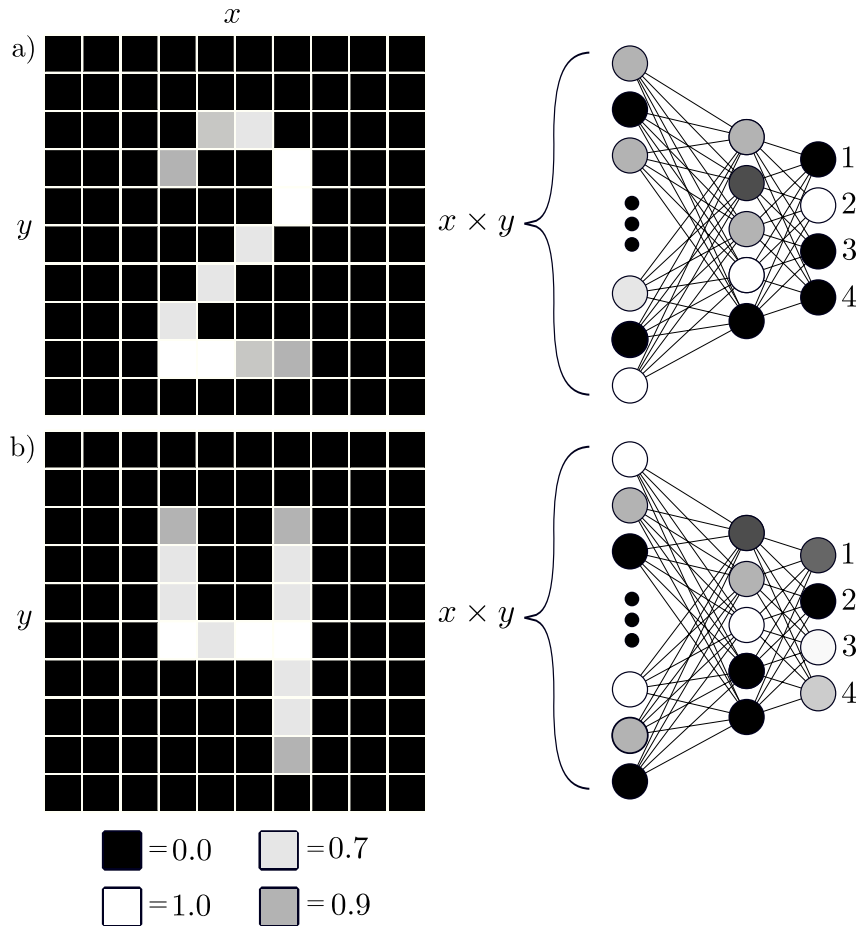
Figure 2.1: Visual representation of the artificial neural network task to classify handwritten digits on the pixel screen, where each pixel serves as an activation value in the initial layer of the ANN. a) The correct classification of the digit two. b) The incorrect classification of the digit four.

the ANN layers. During the training stage, the ANN tries to identify these patterns to make informed guesses of the input state [113].

With the topology established, the ANN is ready to learn. In the first step, we need to divide the data set into at least two mandatory groups training data set and testing data set. During the training, ANN will repeatedly process all elements of the training data set and continuously adjust all its weights and biases $\vec{W}$ to maximize the prediction success rate. Initially, all parameters of $\vec{W}$ are set randomly. The hope is that given a sufficient quantity of training data, ANN will adjust its $\vec{W}$ accordingly to be then able to classify input data correctly beyond the training data set. The actual "learning" of the ANN can be described as merely searching for the local and global minima of specific functions (cost function) [114]. This function takes ANN's $\vec{W}$ as an input and returns a single number as an output corresponding to learning efficiency during training. The cost function

$$C = \frac{\sum_{f=1}^{Q} C_f(\vec{W})}{Q},$$　　　　(2.6)

is the average cost of all training data, where $C_f(\vec{W})$ is the cost of the single training examples, and Q is the number of examples preceded before the policy update. $C_f(\vec{W})$ is obtained by comparing the activation numbers $a^{(T)}$ of the network's last layer with the activation numbers of the desired outcome $\vec{d}$ as

$$C_f(\vec{W}) = (a_1^{(T)} - d_1)^2 + (a_2^{(T)} - d_2)^2 + \ldots + (a_j^{(T)} - d_j)^2.$$　　　　(2.7)

Suppose the $C_f(\vec{W})$ is close to 0. That means ANN classified the current example correctly. On the other hand, if the $C_f(\vec{W})$ is large, the network guessed poorly.

However, a mere cost function is insufficient for the ANN to make appropriate changes to $\vec{W}$ to maximize the decision success rate. There is a need for a specific guide on how to adjust them. The solution is to make a gradient descent [114] of the cost function $-\vec{\nabla}C(\vec{W})$. Gradient descent provides the ANN method for adjusting $\vec{W}$ to follow the steepest descent of the $C(\vec{W})$. This method should ideally lead to reaching the local minima of the $C(\vec{W})$, but the result can vary according to the randomly chosen initial parameter of $\vec{W}$ (i.e., it is not guaranteed that obtained minimum is global). Each element of the gradient descent function gives us an idea of how crucial role the corresponding element of $\vec{W}$ plays in ANNs' decision making (i.e., how noticeable will be the impact of its change on the cost function).

Cost of the single training example

$$\sum_{j=1}^{m}(a_j^{(T)} - d_j)^2$$

1 $\left(\boxed{0.9} - \boxed{0.0}\right)^2 +$
2 $\left(\boxed{0.0} - \boxed{1.0}\right)^2 +$
3 $\left(\boxed{0.1} - \boxed{0.0}\right)^2 +$
4 $\left(\boxed{0.0} - \boxed{0.0}\right)^2 = C_f(\vec{W})$

Cost function

$$C = \frac{\sum_{i=1}^{Q} C_f(\vec{W})}{Q}$$

Gradient descent

$-\nabla C(\vec{W})$

$C(\vec{W})$

$\vec{W}$

Dividing into batches
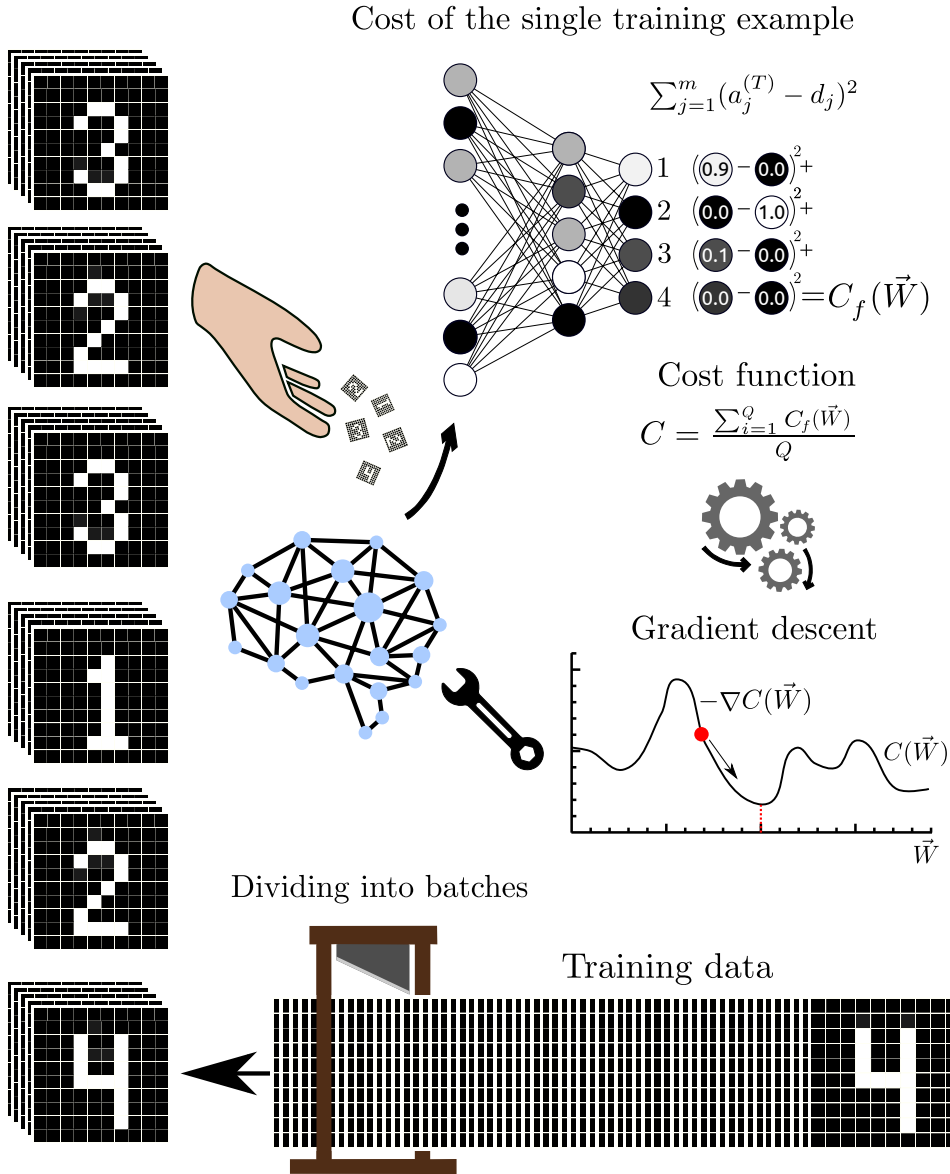
Training data

Figure 2.2: Illustration of the learning process of artificial neural network. Here one can see how the training data set is divided into batches of the size Q and fed to ANN. After processing each batch, the ANN waits are updated according to the gradient descent of the cost function. In the ideal case, the gradient descent should guide ANN from the current state (visualized by the red dot) to the global minima of the cost function.

Figure 2.3: Illustration of the stochastic gradient descent. The red line represents rapid descent in semi optimal gradient descent direction. The blue line represents well-calculated steps in the optimal downhill direction.
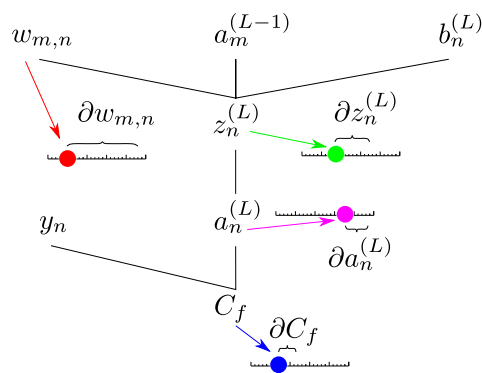
Figure 2.4: Depiction of the chain rule of the last two layers of the ANN. It illustrates how the change in the ∂C_f (blue dot) cause deviation of $\partial a_n^{(L)}$ (purple dot), $\partial z_n^{(L)}$ (green dot) and, finally, $\partial w_{m,n}$ (red dot).

As mentioned before, the ANN should, in principle, update $\vec{W}$ after processing all samples from the training data set (i.e., after every epoch). In reality, at the beginning of every epoch, the training data set is randomly shuffled and divided into smaller groups "batches", and the policy is updated after processing each batch to make the process feasible to calculate. It is more efficient to do fast and less considered steps downhill, "stochastic gradient descent" [115], than spend an extended time in one place and then make optimal step (see Fig. 2.3).

Backpropagation is the method describing how the parameters of the ANN are updated [116]. It gives information on the dependence of the cost function on infinitesimal changes in weights, activations, and biases

$$\frac{\partial C_f}{\partial w_{m,n}} = \frac{\partial z_n^{(L)}}{\partial w_{m,n}} \frac{\partial a_n^{(L)}}{\partial z_n^{(L)}} \frac{\partial C_f}{\partial a_n^{(L)}}, \tag{2.8}$$

$$\frac{\partial C_f}{\partial a_m^{(T-1)}} = \sum_{j=1}^{n} \frac{\partial z_n^{(L)}}{\partial a_m^{(L-1)}} \frac{\partial a_n^{(L)}}{\partial z_n^{(L)}} \frac{\partial C_f}{\partial a_n^{(L)}}, \tag{2.9}$$

$$\frac{\partial C_f}{\partial b_n^{(L)}} = \frac{\partial z_n^{(L)}}{\partial b_n^{(L)}} \frac{\partial a_n^{(L)}}{\partial z_n^{(L)}} \frac{\partial C_f}{\partial a_n^{(L)}}, \tag{2.10}$$

where $z_n^{(L)} = w_{m,n} a_m^{(L-1)} + b_n^{(L)}$. Following the chain rule depicted in Fig. 2.4, one can monitor the effect of the changes to parameters of the cost function throughout the network. Generalizing the chain rule allows us to backtrack the impact of the change from the last layer to the initial layer.

2.2   Proximal policy optimization

Before we dive into proximal policy optimization, let us briefly introduce reinforcement learning in general. We usually talk about reinforcement learning when the core of the machine learning algorithm is based on the interaction between the agent "player", and the environment "game" [71]. This interaction mediates the learning process. The environment is usually described as a collection of states. Given the initial state, the agent will take action, and the environment will respond by changing the state and rewarding the agent. The agent does not have direct information about the environment. His knowledge and experience are obtained through monitoring changes in reward based on the action taken. Reinforcement learning is, therefore, ideal for solving problems, which are often very complex with unknown optimal solutions [117].

Proximal policy optimization [102] is a type of deep reinforcement learning algorithm developed as a successor to Deep mind [118]. Unlike Deep mind, PPO uses online learning, which means that PPO does not use a replay buffer to store past experiences. Once the batch of experiences has been used to do gradient updates of the policy, these experiences are discarded. PPO also simplified the implementation of the trust region, which significantly improved the efficiency of the reinforcement learning method. The primary motivation behind the trust region is to limit rapid changes in the policy, thus allowing the agent to train more efficiently. Unlike the original trust region policy optimization TRPO [119], which introduces a rather complex clip function, PPO simplified the implementation of this function, making it much more practical.

Let us define the PPO policy as

$$L_t^{\text{PPO}}(\theta) = \hat{E}_t \left[L_t^{\text{CLIP}}(\theta) - c_1 L_v^{VF}(\theta) + c_2 S[\pi_\theta](s_t) \right], \qquad (2.11)$$

where L_t^{CLIP} represents the clipped version of the normal gradient objective, L_t^{VF} is squared-error loss responsible for updates of the baseline network, S stand for entropy bonus term, which ensures that the agent does enough exploration during training, and s_t represents the current state. Hyperparameters c_1 and c_2 set the contribution of L_t^{VF} and S to the final policy. The clipped version of the normal gradient objective

$$L_t^{\text{CLIP}}(\theta) = \hat{E}_t \left[\min \left(r_t(\theta) \hat{A}_t ; \text{clip}(r_t(\theta), 1 - \epsilon, 1 + \epsilon) \right) \hat{A}_t \right], \qquad (2.12)$$

represents the core of the whole algorithm. The expectation operator $\hat{E}_t$ is taken over the minimum of the two terms r_t and $\text{clip}(r_t, 1 - \epsilon, 1 + \epsilon)$ where ϵ ranges from $\{0, 1\}$. r_t defines the objective for normal policy gradients, which pushes policy toward actions that yield a higher positive advantage over the baseline. Estimation of the advantage function $\hat{A}_t$ can be positive or negative, which dictates the effect of the "min" operator [102]. The probability ratio r_t determines the relation between newly updated policy outputs and the previous old version of the network. If the $r_t > 1$, the action becomes more likely than it was in the old policy version. On the other hand, if $r_t < 1$, the action becomes less likely than it was before the last gradient step. Policy π_θ is represented by a neural network fed by observed states of the environment as input and gives suggestions of action as output. Estimation of the advantage function

$$\hat{A}_t = D_t - B_t, \qquad (2.13)$$

has two contributors, discounted sum

$$D_t = \sum_{k=0}^{\infty} \gamma^k r_{t+k},$$ (2.14)

and baseline estimation B_t. A discounted sum of rewards D_t is a weighted sum of all rewards r_{t+k} the agent receives during each time step k of the current episode. Parameter γ ranges from 0 to 1 and sets how much the agent values immediate reward r_t over future rewards. Baseline estimation B_t gives an estimate of the $\hat{A}_t$, trying to predict the final return of the episode from the current state. Since B_t is also implemented as a neural network, the result is a noisy value function estimation.

2.3 Gym library

Now, with the working principle of the PPO established, we only need to establish a method capable of defining the task in the way PPO can process. One of the most prominent API application programming interface for this task is the openAI "gym" library [120]. This library allows us to define tasks in the form of games. Before diving into detail, let us establish our illustrative game, "Find the cheese". In this game, the player "mouse" needs to find a safe path to cheese while avoiding threats such as cats, poisons, and traps (see Fig. 2.5). Let us follow the description of the gym environment with this illustrative game in mind.

There are three essential parts required for every gym environment. The first is the initialization process which defines the environment of the game. It also establishes the observation space used to evaluate a player's progress. In the case of our "Find the cheese," the initialization would define the layout of the labyrinth, including information about the location of all threats (poisons, cats, and traps), the initial position of the player (mouse), and the location of the final objective (cheese). In this case, the observation space could be the mouse's current position in the labyrinth and the steps taken during one game.

The second requirement is to define the reset function. Reset is utilized every time the player finishes the game. This function is straightforward to describe because it simply resets an environment and observation space to the default position.

The final mandatory part of the gym environment is defining the step. Each step describes the consequences of the player's actions in the game's
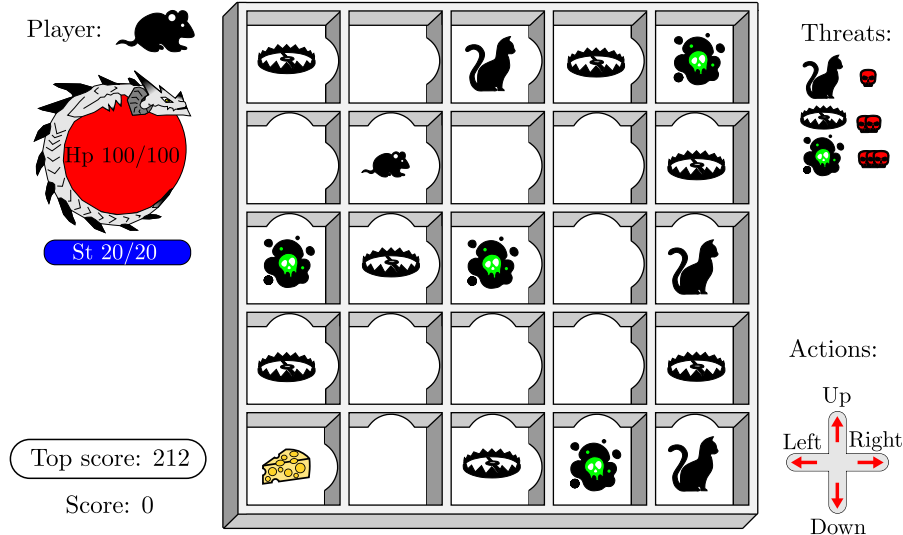
Figure 2.5: Graphical representation of the "Find the cheese" game. This illustrative case is a visualization of the game designed in the gym environment. Here a mouse has limited health points and stamina to reach the cheese using only four actions (up, down, right, left).

current state. The step also defines a reward structure, which provides feedback for the player during learning. There are two types of rewards, each with its unique role. First is the preliminary reward R_p, which is awarded after each step and serves as a direct evaluation of the taken action. The second is the final reward R given only after the end of the game. R describes the overall performance of the player during a game. In the case of "find the cheese", the step would describe the movement of the mouse throughout the labyrinth based on the action (go: left, right, up, and down) taken. The preliminary reward structure can award the mouse for choosing a direction leading to a safe room and punish it for choosing directions leading to danger.

We can establish the mouse's health points (100 Hp) and stamina (20 St) as parameters, which serve as additional conditions for ending the game. Each step will exhaust the mouse (-1 St), restricting the number of steps it can take to reach the cheese. Simultaneously every visited dangerous room will reduce mouse health points accordingly to room lethality by -30 Hp, -60 Hp, and -90 Hp for cat, trap, and poison, respectively. The game

now has three conditions to track. The mouse will get the final reward if any of them is fulfilled. The first condition is Hp < 0 mouse sadly died, so it gets $R = -100$. Second condition St = 0 mouse survived but remains hungry $R = 0$. The third and final condition is fulfilled if the mouse reaches the cheese. In that case, the mouse is alive and well-fed $R = 100$. Alternatively, we can also consider the remaining Hp and St of the mouse after reaching the cheese. In that case, $R = 100 + (Hp + St)$. With all the essential parts of the game defined, one can choose from a plethora of reinforcement learning algorithms, such as PPO, to play the game and find the optimal solution.

2.4   Quantum states 101

Quantum states are mathematical objects that describe a given particle's physical properties. Let us consider two (pure) quantum states $|\psi_1\rangle$ and $|\psi_2\rangle$ expressed in Dirac notation [121]. Assuming that some object can exist in either of these states, one can create a weighted linear combination of them and thus define a new valid (pure) quantum state

$$|\psi\rangle = \alpha|\psi_1\rangle + \beta|\psi_2\rangle. \tag{2.15}$$

Here α, β are complex probability amplitudes that must satisfy the normalization condition

$$|\alpha|^2 + |\beta|^2 = 1. \tag{2.16}$$

Such a linear combination of quantum states is referred to as superposition [122]. So far, have considered considered only pure quantum states. In reality, however, most states are probabilistic mixtures of multiple quantum states. One needs to establish a density matrix representation to describe these so-called mixed states. The density matrix $\hat{\rho}$ [123] defines a general quantum state as

$$\hat{\rho} = \sum_i p_i |\psi_i\rangle\langle\psi_i|, \tag{2.17}$$

where

$$\sum_i p_i = Tr\left(\hat{\rho}\right) = 1. \tag{2.18}$$

Here p_i corresponds to the contribution of the respective state $|\psi_i\rangle$ towards general state $\hat{\rho}$. Considering a case where only one $p_i > 0$, we obtain a description of the pure states.

Now let us consider an arbitrary pure quantum state

$$|\psi_{AB}\rangle = \sum_{ij} \gamma_{ij} |\psi_i\rangle_A \otimes |\psi_j\rangle_B, \tag{2.19}$$

where symbol $\otimes$ depicts a tensor product, $|\psi_i\rangle_A, |\psi_j\rangle_B$ represents pure quantum states, and γ_{ij} stands for collective complex probability amplitudes. State $|\psi_{AB}\rangle$ is separable if there exist complex probability amplitudes α_i and β_j so that $\gamma_{ij} = \alpha_i \beta_j$, yielding $|\psi\rangle_A = \sum_i \alpha_i |\psi_i\rangle_A$ and $|\psi\rangle_B = \sum_j \beta_j |\psi_j\rangle_B$. State $|\psi_{AB}\rangle$ is considered inseparable if $\gamma_{ij} \neq \alpha_i \beta_j$. In that case state $|\psi_{AB}\rangle$ is refereed to as entangled state [124].

2.5 Entanglement witnesses

We have already mentioned in the introduction that entanglement is one of the most intriguing properties of quantum states with immense application potential. However, to efficiently use this valuable resource [125], it is crucial to identify which states are entangled. Full state tomography and density matrix estimation represent the most robust solution to the outlined task [126]. Unfortunately, its complexity grows exponentially with the dimension of the investigated states [127,128]. Therefore, it rapidly becomes experimentally unfeasible. This observation motivated the search for a suitable replacement for full-state tomography by some alternative method, "entanglement witness," that would reduce the amount of information needed for reliable state classification. In principle, we can visualize the ideal entanglement witness as an oracle that would give us binary answers on whether the presented state is entangled. In reality, entanglement witnesses usually try to fulfill some conditions given by function or inequality to test the properties of the investigated state [97]. The most famous examples of entanglement witnesses is the Bell inequalities [6]. Bell inequalities

$$C_h(a,c) - C_h(b,a) - C_h(b,c) \leq 1, \tag{2.20}$$

were established in 1964 by John Stewart Bell. Here, C_h denotes correlations predicted by the local hidden variable theory, and a, b, and c represent three arbitrary measurement settings. Quantum physics predicted the violation of Bell inequality in case the investigated state is entangled. The Bell inequality was, unfortunately, problematic to prove experimentally. Therefore, Bell inequality was modified in 1969 by Clauser, Horne,

Shimony, and Holt to make experiments feasible. This so-called CHSH inequality [93]

$$S = \left| E(a, b) - E(a, b') + E(a', b) + E(a', b') \right| \leq 2, \tag{2.21}$$

became the first experimentally viable entanglement witness. Here a, a', b, and b' represent measurement settings, and E defines the measured expectation value for simultaneous measurements in the above-listed settings.

Another example of a well established entanglement witnesses is the so-called PPT criterion. This entanglement witness was derived in 1996 by the Asher Peres and Horodecki family [129, 130]. PPT criterion evaluates the smallest eigenvalue λ_i of the partially transposed density matrix $\hat{\rho}^{PT}$. If

$$\min(\lambda_i) < 0, \tag{2.22}$$

PPT ensures the state is entangled. However, in some cases, a state can still be entangled even if the smallest eigenvalue is positive (e.i. in terms of Eq. (2.22) PPT criterion serves as a mere sufficient condition of the entanglement). If we restrict the class of the investigated states to 2×2 and 2×3 dimensional systems, PPT acts as a necessary and sufficient condition of the entanglement (e.i. if the minimum eigenvalue is negative, the state is entangled, otherwise is separable).

In general, entanglement witnesses can be either linear or nonlinear. Linearity is achieved when the witness is expressed as a linear function of the density matrix, or the mathematical expression of the witness does not include any nonlinear terms of expectation values. Such a witnesses $\mathscr{F}$ can be expressed as

$$\mathscr{F} = \text{Tr}\left[\hat{\rho}\hat{W}\right], \tag{2.23}$$

where $\hat{\rho}$ is the density matrix, and $\hat{W}$ represents the witness operator. However, it is generally more efficient to use nonlinear entanglement witnesses because these witnesses can detect a larger group of entangled states due to their nonlinear contributions. The first approach toward deriving a nonlinear witness

$$\mathscr{F}(\hat{\rho}) = \text{Tr}\left[\hat{\rho}\hat{W}\right] + \chi(\hat{\rho}), \tag{2.24}$$

is based on adding nonlinear functions $\chi(\hat{\rho})$ of expectation values to existing linear witnesses. It was proven that every bipartite linear entanglement witness could be improved by such a nonlinear contribution [131]. Alternatively, the witness's nonlinearity can be achieved when the witness

$$\mathscr{F} = \mathscr{F}\left\{\text{Tr}\left[\hat{\rho}^{k_i}\hat{W}_i\right]\right\}, \tag{2.25}$$

is a nonlinear function of the density matrix where k_i is an integer. These witnesses rely on joint measurements on multiple copies of an investigated state, therefore "collective" entanglement witnesses [92, 132]. The collective witnesses will be further discussed in Chapter 3 and Chapter 4.

2.6   Quantum teleportation

Quantum teleportation is a protocol capable of transferring an unknown quantum state from sender to receiver without actually sending the physical object in which it is encoded through the quantum channel [133]. Imagine a scenario when Alice and Bob meet and decide to share the entangled state $|\Phi^+\rangle = \frac{1}{\sqrt{2}}(|0\rangle_A|0\rangle_B + |1\rangle_A|1\rangle_B)$ where $|0\rangle$ and $|1\rangle$ represent an orthogonal set of states refereed to as computational basis and subscripts A and B mark Alice's and Bob's particle respectively. After some time, Alice is contacted by Charlie, who shares with her an urgent quantum message $|\psi\rangle = \alpha|0\rangle_C + \beta|1\rangle_C$ for Bob, where subscript C is used to distinguish Charlie's message. Unfortunately, Alice no longer shares a quantum channel with Bob. Therefore, she cannot directly forward the message. Alice, however, still possesses particle A from the initial shared entangled state $|\Phi^+\rangle$. Alice can therefore perform a Bell measurement [134] between particle A and Charlie's message represented by C. This causes state $|\Psi^+\rangle$ to collapse and destroys message $|\psi\rangle$ shared with Alice (e.i. the message is not cloned). The result of Alice's measurement will be one of the following four Bell states.

$$|\Phi^\pm\rangle = \frac{1}{\sqrt{2}}(|00\rangle \pm |11\rangle), \tag{2.26}$$

$$|\Psi^\pm\rangle = \frac{1}{\sqrt{2}}(|01\rangle \pm |10\rangle). \tag{2.27}$$

After the measurement is done, Alice will contact Bob via the classical channel and inform him which Bell state she obtained. This information will hint Bob what correction he needs to make to his particle B ($|\Psi^+\rangle \rightarrow$ bit flip, $|\Phi^-\rangle \rightarrow$ phase flip, $|\Psi^-\rangle \rightarrow$ phase and bit flips and $|\Phi^+\rangle \rightarrow$ no correction). If Bob performs the proper corrections, his particle B will transform into Charles's message $|\psi\rangle$ (see Fig. 2.6).

If we return to the previously discussed scenario, imagine that Charlie wants to establish a shared entangled state with Bob but does not have a direct quantum connection with him. However, this time, he possesses a shared entangled pair with Alice. We also assume that Alice and Bob, once
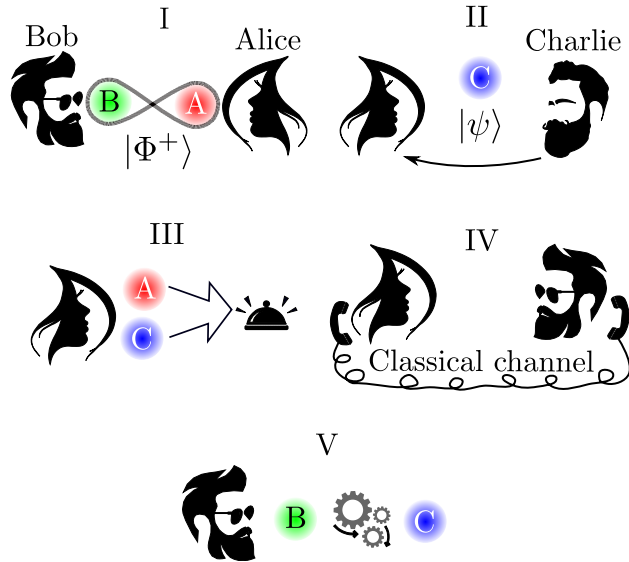
Figure 2.6: Scheme of quantum teleportation. I) Alice and Bob share an entangled pair. II) Charlie sends a quantum message to Alice. III) Alice performs Bell measurement. IV) Alice shares the classical result of the measurement with Bob. V) Bob applies correction to his particle B, transforming it into Charlie's message.

again, share an entangled state. Alice can again perform Bell measurement on her two particles, one belonging to the pair shared with Bob and the second to the pair shared with Charlie. Then Alice will finish this protocol by contacting Bob via a classical channel and telling him the result of the Bell measurement. Similarly, as described above, Bob will apply correction to his particle. Charlie and Bob will end up sharing an entangled state. We refer to this type of quantum teleportation as entanglement swapping [135].

Chapter 3

Accuracy of entanglement detection via artificial neural networks and human-designed entanglement witnesses

3.1   Introduction

Quantum entanglement is an intriguing phenomenon described almost a century ago by Schrödinger, Einstein, Podolsky, and Rosen [5, 136]. Since then many theoretical and practical papers alike, as well as vivid discussions, were dedicated to this topic [137–139]. The ability to effectively detect entangled state became essential mainly because of their application potential in quantum computing [140], quantum cryptography [58], and quantum teleportation experiments [141]. The most robust way of detecting it is via a full state tomography and density matrix estimation [126]. This method allows us to obtain all information about the state and thus correctly detect entanglement. Unfortunately this method is experimentally demanding because the number of required projections grows exponentially with the dimension of Hilbert space. There is also a variety of other methods that do not rely on full-state tomography [93, 132, 142–

160]. These methods include a wide range of linear entanglement witnesses [142–147] of the CHSH- Clauser Horne Shimony Holt type [93]. While for pure states, these methods give similar results, their outcomes might vary significantly when mixed states are considered. While requiring only a relatively few measurement configurations, these witnesses can not reliably function without some a prior information about the detected state. To circumvent this limitation, while not resorting to state tomography, non-linear entanglement witnesses have been proposed.

In 2011, Rudnicki *et al.* introduced a nonlinear entanglement witness called *Collectibility* [132, 155]. For a visual demonstration of this concept [see Fig. 3.1 a)]. For 2-qubit states, this witness requires two simultaneously prepared copies of the investigated state. Then a Bell state projection is imposed on a pair of corresponding qubits from each copy and the remaining qubits are subjected to local measurements. For a general 2-qubit state, this requires a combination of 5 local projections and, thus, fewer measurement configuration than full quantum state tomography which includes at least 24 projections. One can further decrease the time needed for a QST if measurements can be performed in parallel on multiple copies of the investigated state. When dealing with unknown quantum states, collectibility can detect a much broader range of states compared to linear witnesses. Namely, it detects all pure entangled states. Unfortunately, it detects entanglement of only a fraction of mixed states. This shortcoming is characterized by a rather big Type-II error (false negative), as we show later. On the other hand, all states which are classified as entangled by this method are classified correctly (Type-I error is null, there are no false-positive classifications). We demonstrate that significant improvement can be reached when collective entanglement witnesses are devised using an artificial neural network. As demonstrated by Gao *et al.* [96] and other groups [161, 162], neural networks can be used to identify quantum states. However, only linear entanglement witnesses were considered which significantly limited the class of detected entangled states. Note that neural network-based linear witnesses share the same shortcomings with their analytical counterparts, which is the need for a prior information about the investigated state.

We train a neural network to classify quantum states by providing it with results of collective measurements and demonstrate its significantly better performance over collectibility and other similar non-linear witnesses for a general 2-qubit state as well as for real experimental data for a fixed number of measurement configurations. Moreover, we show the
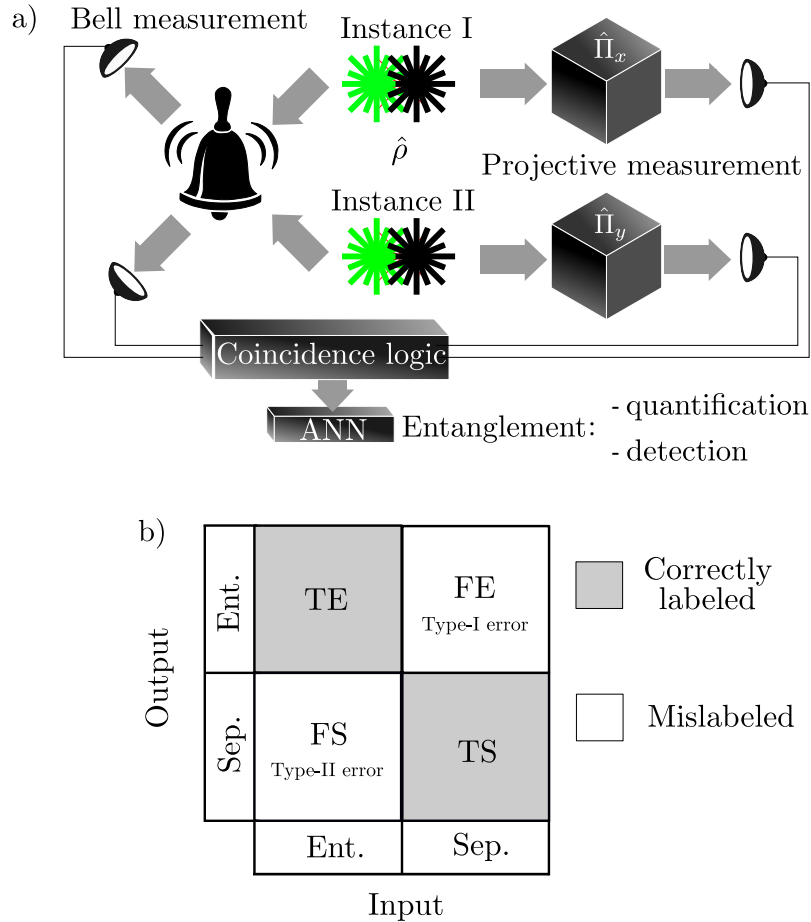
Figure 3.1: a) Scheme of a collective measurement: two instances of the investigated states $\hat{\rho}$ are subject to simultaneous measurement. While one qubit of each instance undergoes local projections, the other two qubits are nonlocally projected onto a Bell state. These coincidence detections can be fed to an artificial neural network that can serve as an entanglement witness or even entanglement quantifier (measure) for investigated state $\hat{\rho}$. b) Schematic depiction of the confusion matrix used for performance evaluation of the ANN. TE - truly entangled, FE - falsely entangled, TS - truly separable, FS - falsely separable, Sep. - separable, Ent. - entangled.

increasing capability of the neural network when provided with a larger amount of measurement configuration outcomes by comparing it against three other analytical methods that require 12 projections, namely FEF – fully entangled fraction [94, 163, 164], CHSH [93], and entropic witness [95, 165]. These projections are listed in Appendix A.1 Tab. A.2. We use confusion matrix as a method of performance evaluation for the ANN and previously known non -linear witnesses [see Fig. 3.1 b)]. Diagonal elements show the number of correctly labeled input states TE - truly entangled and TS - truly separable furthermore off-diagonal elements provide information about falsely labeled input states FE - falsely entangled and FS - falsely separable.

3.2   Collective measurements

Although our idea can be generalized, we focus our investigation on the entanglement of two-qubit states $\hat{\rho}$. In order to perform collective measurements on these states, one needs to start with the preparation of two instances of $\hat{\rho}$ resulting in an overall density matrix of the entire system $\hat{\rho}_4 = \hat{\rho} \otimes \text{SWAP}\, \hat{\rho}\, \text{SWAP}^\dagger$; where the SWAP operator interchanges the order of subsystems (see [Eq. A.4] in Appendix A.1). One qubit from each instance is projected locally, while the remaining qubits undertake a nonlocal Bell-state projection. For the visualization of this procedure, see Fig. 3.1 a). For a given pair of local projections, the result of collective measurement is the probability of a successful singlet Bell-state projection imposed on the nonlocally projected qubits

$$P_{xy} = \frac{\text{Tr}[(\hat{\rho}_4)(\hat{\Pi}_x \otimes \hat{\Pi}_{\text{Bell}} \otimes \hat{\Pi}_y)]}{\text{Tr}[(\hat{\rho}_4)(\hat{\Pi}_x \otimes \hat{\mathbb{1}}^{(4)} \otimes \hat{\Pi}_y)]}. \tag{3.1}$$

In this equation $\hat{\Pi}_x$ and $\hat{\Pi}_y$ are local projections onto single-qubit states $|x\rangle$ and $|y\rangle$, $\hat{\Pi}_{\text{Bell}}$ denotes projection onto the singlet Bell state and $\hat{\mathbb{1}}^{(4)}$ represents four-dimensional identity matrix [155]. One collective measurement configuration corresponds to the choice of one $\hat{\Pi}_x$ and one $\hat{\Pi}_y$. Obtained set of B probabilities[1] $P_{xy}^{(i)}$; $i = 1, ..., B$ is subsequently fed to a neural network for training together with labels obtained by the PPT- Peres-Horodecki criterion [129, 130].

[1]In the original paper referred to as N here relabeled to avoid confusion with Negativity.

3.3 Artificial neural network

TensorFlow 2.0 [166] was used to program a neural network capable of classifying quantum states. We experimented with the complexity of the network and our final layout of the network with 5 hidden layers containing $36, 180, 75, 180,$ and 75 nodes respectively seems to be the optimal choice to find a balance between obtained precision and computation time. The proposed network is capable of assigning any quantum state with a value $w \in [0; 1]$ which can be interpreted as a confidence factor from 0 (certainly entangled) to 1 (certainly separable). We defined decision threshold ϵ to convert the w values to a binary label: $w < \epsilon \Rightarrow$ entangled, $w \geq \epsilon \Rightarrow$ separable. By changing ϵ value we make the network biased towards the desired decision which allowed us to tune the trade-off between Type-I and Type-II errors. The network was trained on 4×10^6 samples and tested on the other 4×10^5 samples with distribution containing 67.74% entangled states and 32.26% separable states. For more details about the purity distribution of the samples see Fig. A.1 in Appendix A.1. The main goal was to test the network against collectibility, therefore, we start to train it using the same $B = 5$ projection settings (see Appendix A.2 for a brief overview on collectibility). In the next step, we also tested capability of the network for $B = 3, 6, 12, 15$ projection settings (see Appendix A.3 for more details).

3.4 Results

In the first step, we decided to test the neural network with decision threshold $\epsilon = 0.5$ for a several amounts of projection settings $B = 3, 5, 6, 12, 15$. As it turns out the neural network was capable of labeling entangled and separable states even using 3 projection settings with an overall success rate of around 83.33%. For an increasing number of projection settings success rate increased even further and reached 96.55% for 15 projections settings. We plot the probability of incorrect decision as a function of the smallest eigenvalue of the partially transposed density matrix $\hat{\rho}$ (see Fig. 3.2).

As expected, the neural network struggles with the states close to the PPT decision boundary (minimal eigenvalue close to zero). Unfortunately, the neural network is, to some extend, prone to Type-I errors (separable state classified as entangled). As it turns out the network is more likely to make a mistake when classifying separable states than entangled states. Our solution is to change the decision threshold ϵ to decrease the Type-I error. This means that we demand more certainty from the network when
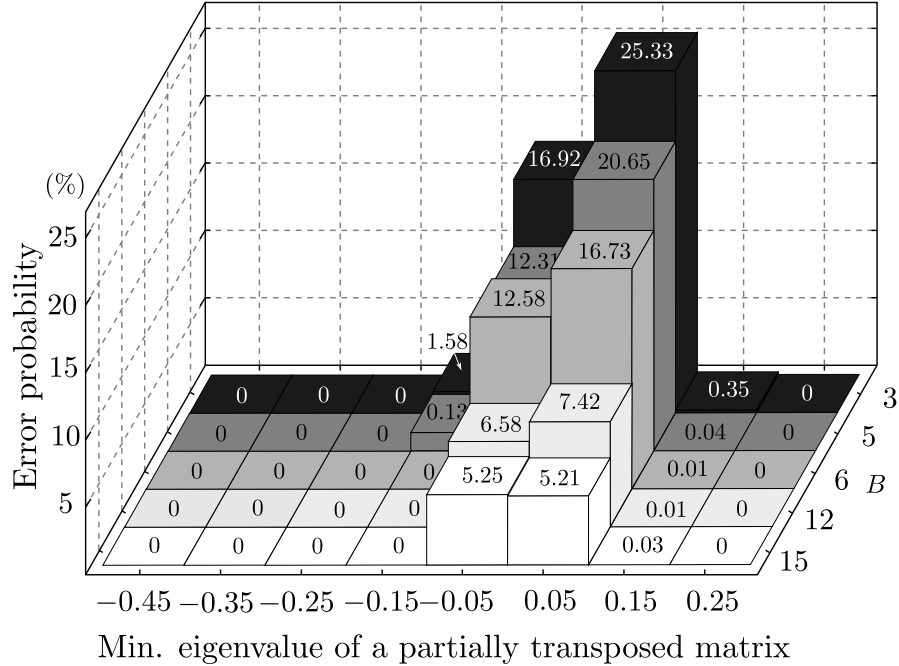
Figure 3.2: The result obtained by the neural network with decision threshold $\epsilon = 0.5$ for $B = 3, 5, 6, 12, 15$ and distribution containing 67.74% entangled states and 32.26% separable states. In this graph probability of false prediction is plotted against the minimal eigenvalue of a partially transposed matrix.

classifying the entangled state. By optimizing thresholds we manage to find the value which satisfies a condition of Type-I error < 1% which we find acceptable. It is possible to arbitrarily decrease the Type-I error by sacrificing the detection capability characterized by Type-II error. For more detailed dependence of Type-I and Type-II error on threshold for $B = 3, 5, 6$, $12, 15$ see Fig. 3.3, Tab. A.1, and Fig. A.3. In the next step we compared the network performance against collectibility. The neural network fed by outcomes of the same 5 projection settings also required by the collectibility was able to correctly classify 78.14% of all states while committing Type-I error of 0.96% ($\epsilon = 0.9$). This performance vastly surpassed the capability of the Collectibility which identifies only 36.59% of the states correctly (see Tab. 3.1). To further highlight the potential of ANN we compared its performance with analytical methods (FEF, CHSH, and EW) (see Tab. 3.1). The

ANN					
B	3	5	6	12	15
Type-I error (%)	0.93	0.96	1.18	0.24	0.22
Type-II error (%)	33.47	20.91	15.88	7.74	5.24
Success rate (%)	65.50	78.14	82.94	92.01	94.54

	Collectibility	FEF	EW	CHSH
B	5	12	12	12
Type-I error (%)	0	0	0	0
Type-II error (%)	63.41	14.00	42.00	54.00
Success rate (%)	36.59	86.00	58.00	46.00

Table 3.1: Comparison of the results obtained by ANN for $B = 3, 5, 6, 12, 15$ with prominent analytical methods (collectibility, FEF - fully entangled fraction, EW - entropic witness, CHSH nonlocality). Both Type-I and Type-II errors are taken for decision threshold $\epsilon = 0.9$ to ensure Type-I error < 1%.

success rate of the ANN surpass capabilities of FEF by 6.01%, EW by 34.01%, and CHSH by 46.01% while committing Type-I error 0.24%. This means that if we can accept some Type-I error, it is possible to achieve a major improvement in entangled states detection using the neural network. Note that the purpose of this research was not to use ANN simply to fit existing entanglement witnesses, but rather to devise completely new ones that we later compare with these already known analytical formulas.

We have investigated the possibility to derive approximate analytical formulas from the parameters of trained ANNs. This is a rather complex task and we were only able to find a reasonable formula for $B = 3, 5$ measurement configurations. Using logistic regression, a witness in the form of

$$W_B = \left[1 + e^{-z_B}\right]^{-1}, \tag{3.2}$$

where $z_B = \vec{w}_B \cdot \vec{p}_B$ and $\vec{p} = (1, P_{HH}, P_{VV}, P_{HV}, P_{DD}, P_{AA})$ for $\vec{w}_3 = $ (-2.3348, 19.3139, 21.5486, -11.4228, 0, 0) and $\vec{w}_5 = $ (0.0009, 7.7967, 9.6227, -25.8294, 21.9635, 22.0167) can be obtained. The states for which $W_B < 0.05$ are classified as entangled (separable otherwise). This decision boundary implies Type-I error of circa 0.9% and Type-II errors of 57.5% and 44.8% corresponding to $B = 3, 5$ respectively. Type-I errors can be made arbitrary small by lowering the threshold value of W_B for classifying a given state as entangled.
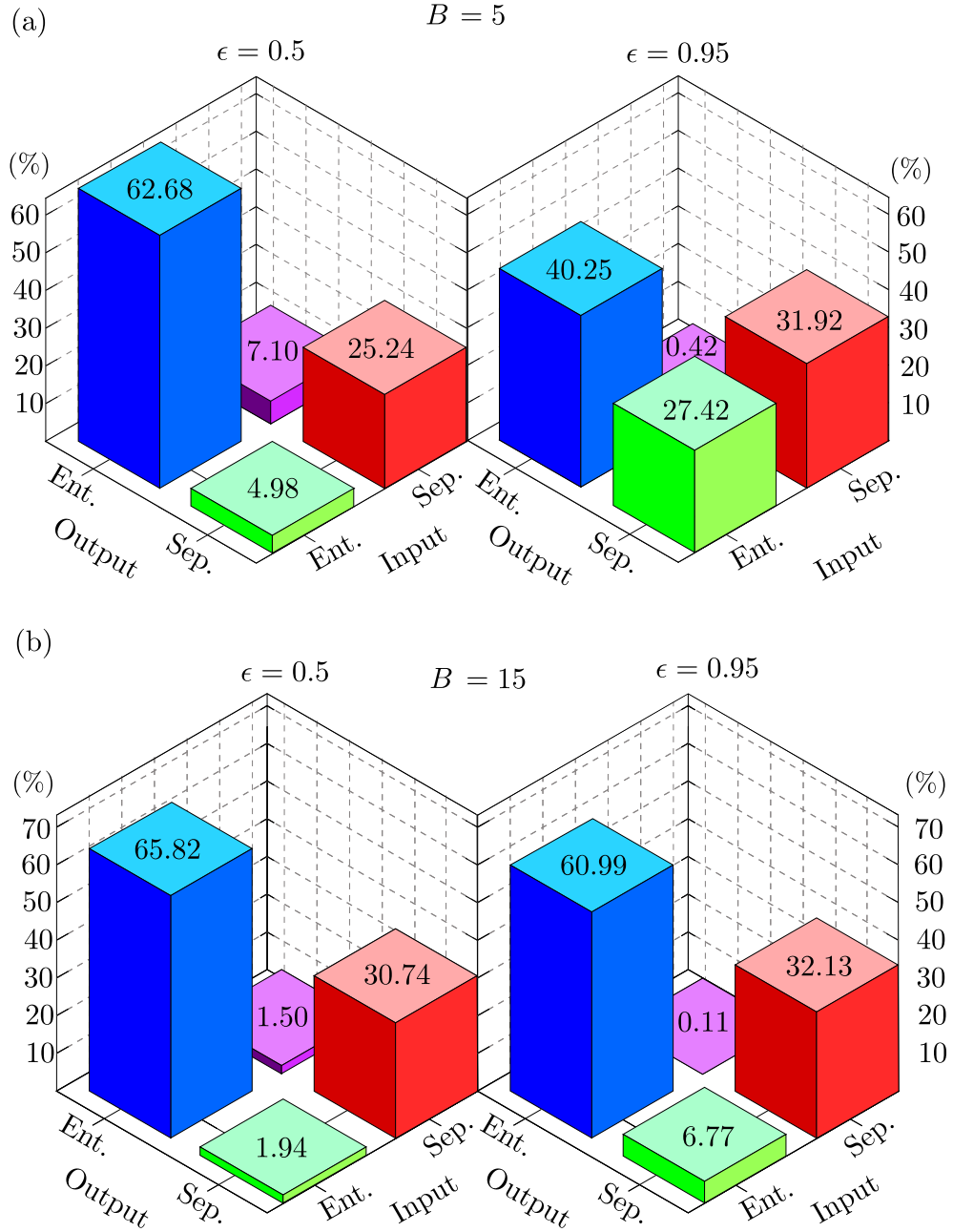
Figure 3.3: Performance dependence of the ANN on decision threshold $\epsilon = 0.5, 0.95$ with distribution containing 67.74% entangled states and 32.26% separable states depicted as confusion matrices for: a) $B = 5$; b) $B = 15$.

3.5 Experimental implementation
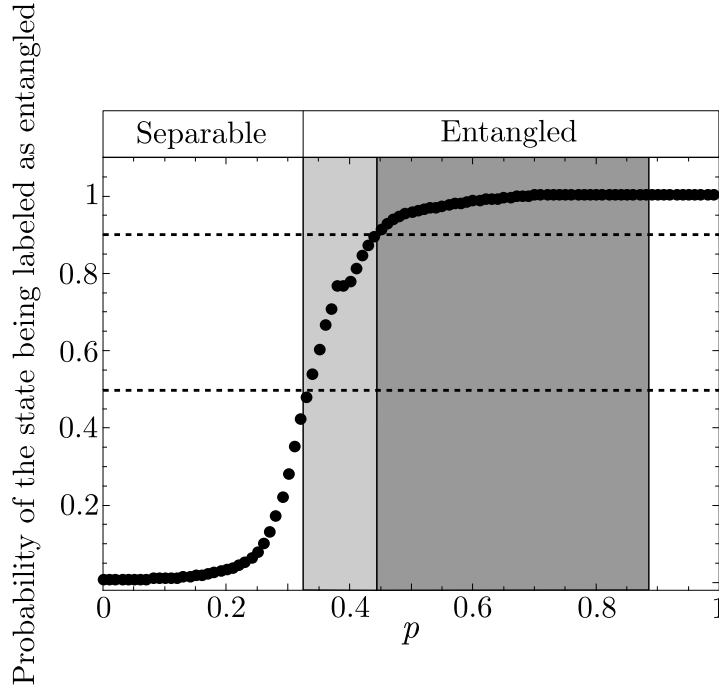
Figure 3.4: Results obtained by neural network and collectibility respectively from a real experimental data set $B = 5$. Black full dots show the probability of a Werner state being labeled as entangled by the ANN. The light-gray area covers the values of p which neither the neural network nor collectibility can classify correctly. The dark-gray area represents the range of p values for which the ANN classifies the Werner states correctly and collectibility fails. The dashed lines represent the decision thresholds $\epsilon = 0.9$ and 0.5 respectively.

To verify the network capability we decided to further test it on a set of real experimental data. For this purpose, we used the data set from the first-ever Collectibility measurement from 2016 [167]. In that particular experiment, a class of Werner states of the form of $\hat{\rho}_w = p|\psi^-\rangle\langle\psi^-| + (1 - p)\hat{\mathbb{1}}/4$, was investigated. $|\psi^-\rangle$ represents singlet Bell state, and $\hat{\mathbb{1}}/4$ stands for the maximally mixed state. We set the detection threshold to $\epsilon = 0.9$ like in the previous comparisons of the neural network with collectibility, to

be consistent and make test conditions as fair as possible. Results show that collectibility can classify states with $p > 0.89$ as entangled witch corresponds with its theoretical prediction. The neural network, on the other hand, detects entangled states when $p > 0.44$ (see Fig. 3.4). Note that it is known that Werner states are entangled for $p > \frac{1}{3}$.

3.6   Conclusions

We trained a neural network to classify general qubit states based on nonlinear collective witnesses. Our main goal was to compare the capability of this network against a prominent analytical representation of nonlinear witnesses: the collectibility. The network can classify the general twoqubit states significantly more efficiently than collectibility with Type-I error $< 1\%$. The ANN also surpasses FEF, CHSH, and entropic witness when taught on 12 projections (the same amount needed by the mentioned analytical witnesses). Increasing the number of projection settings improves the ANN's decision even more. We further support this claim by using the network on a real experimental data set. The network confirmed its potential by correctly labeling a broad range of states where collectibility fails. Moreover, it achieved a Type-I error = 0 on Werner states. Our research promotes the idea of using artificial intelligence towards a better understanding of the intriguing physical phenomena such as the entanglement. We have demonstrated that the neural network can quickly train to become a valid efficient collective entanglement witness. We have directly compared its performance with analytical formulas. Using nonlinear measurements (on two copies of the state), our network operates completely free of any a priory information that can bias comparison of its performance with analytical counterparts. Moreover, we have shown that the training performed on numerically generated states works very well on real experimental data corresponding to states completely unknown to the ANN.

Because of technical limitations on the possible complexity of our ANN and on the number of samples processed in ANN training, reaching the limit of zero Type-I error was not possible. However, we were able to tune this error to a fraction of a percent by choosing a proper value of ϵ. By extrapolating our results for the whole available range of ϵ, we conclude that the limit of vanishing Type-I error is reached by the ANN for $\epsilon = 0.9822$ and $\epsilon = 0.9994$ for 5 and 12 measurements, respectively. The Type-II errors for these values of ϵ are 31.26% (5 measurements, about 32% better then col-

lectibility) and 11.40% (12 measurements, 2.6% better than FEF). Thus, we have demonstrated that the best known analytical methods for certifying entanglement with a few measurements can be further improved. Notably, the 2.6% smaller Type-I error of ANN with respect to FEF, means that ANN fails relatively on about 20% less states than FEF using the same input. This demonstrates that there is still a place for improvement in the theory of experimentally-friendly entanglement detection. The extrapolation of functional the dependence of Type-I and II errors on ϵ was performed by fitting a quadratic and an exponential curve, respectively. We believe that the high quality of both fits and the proximity of the lowest Type-I error data point to 0 justify our conclusions. We hope that our results will stimulate further research in experimentally-friendly methods of classifying quantum states.

Further to that, the theoretical assumption of zero Type-I error of analytical witnesses does not hold operationally because of unavoidable experimental imperfections and finite precision of all measurements. As a result, separable states close to the decision boundary may be misclassified even using theoretically infallible witnesses. In this study, we have allowed the ANN a Type-I error of about 1% which we believe is still an admissible error that can be tolerated in practical implementations burdened by the above-mentioned experimental imperfections. Note that in case of 12 measurement configurations, the ANN misclassifies only 1 in about 400 separable states while simultaneously missclassifying about two times less entangled states then its best performing analytical counterpart, the FEF.

Chapter 4

Entanglement quantification from collective measurements processed by machine learning

Text adopted from *Jan Roik, Karol Bartkiewicz, Antonín Černoch, and Karel Lemr, Physics Letters A, vol. 446, p. 128270, 2022* [A-2].

4.1   Introduction

Quantum entanglement shows immense potential as a resource in various research fields, such as quantum computing [140, 168, 169], quantum cryptography [58] and quantum teleportation experiments [141]. Even though entanglement has been studied for about a century now [5, 136], finding a method for its experimentally feasible quantification for general quantum states is still an open and complex problem [170–173].

The most robust procedure so far seems to be the full quantum state tomography [98, 174], subsequent reconstruction of the density matrix [175], and calculation of entanglement measures. These measures include negativity [99], concurrence, [163, 176] or relative entropy of entanglement [95, 177]. For a review, see Ref. [97]. The problem of full state tomography lies in the unfavorable scaling of the number of measurement configurations as a function of the Hilbert space dimension. Even for a two-qubit system, one needs to apply at least 15 measurement settings while also inevitably obtaining some information on the investigated system that is irrelevant to entanglement quantification. In order to lower the number

of measurement configurations, entanglement witnesses have been proposed [93,132,142–160]. However, these instruments are designed to merely detect entanglement and can be used as measures only in limited cases such as quasi-pure states. The concept of nonlinear entanglement witnesses has been introduced [131] as a countermeasure to alleviate the problem of state dependency of entanglement detection. A noteworthy class of nonlinear witnesses is the class of so-called collective witnesses based on simultaneous measurement on multiple instances of the investigated state [132, 155]. Entanglement measures can be estimated from collective measures as well. Analysis reveals that 4 copies of a two-qubit system need to be investigated simultaneously which can prove experimentally too demanding [178]. We limit ourselves to having simultaneously only two copies of the investigated state to overcome this challenge. In this configuration, the relation between the outcomes of a collective measurement and an entanglement measure, say the negativity, is far from trivial.

Machine learning has penetrated many areas of science, helping with finding complex models based on large data sets [179]. Artificial neural networks (ANNs) are particularly well suited for recovering of nonlinear dependencies as they are effective universal function approximators [180]. Not surprisingly thus, ANNs and artificial intelligence, in general, has been used to investigate properties of quantum states, such as entanglement detection [96, 161, 162], quantification of various properties of quantum states [181–185], or compressed sensing [186, 187]. In this chapter, we use the predictive power of ANNs to estimate quantum state negativity based on the outcomes of collective measurement.

4.2 Collective measurements and data generation

We focus our investigation on quantifying the entanglement of two-qubit states $\hat{\rho}$. The generation of the investigated states and collective measurements were handled similarly, as described in the previous chapter. This investigation aims at efficient entanglement quantification in two-qubit states using as few projections as possible. To achieve this goal, we take inspiration from the concept introduced by Řeháček *et al.* called minimal qubit tomography [98]. The authors established that the minimal set of tomographic projections per one qubit consists of four projections corresponding to states forming a tetrahedral inscribed into a Bloch sphere (see
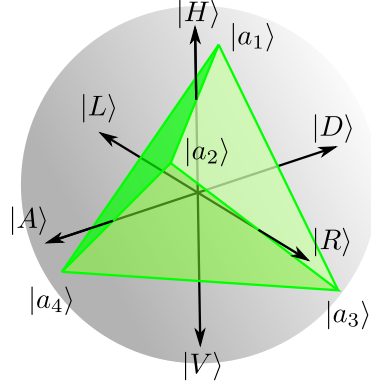
Figure 4.1:   Minimal set of tomographic projections visualized on the Poincaré sphere by $|a_j\rangle$ vertices, where $|a_1\rangle = \frac{1}{\sqrt{3}}(1,1,1)$, $|a_2\rangle = \frac{1}{\sqrt{3}}(1,-1,-1)$, $|a_3\rangle = \frac{1}{\sqrt{3}}(-1,1,-1)$, $|a_4\rangle = \frac{1}{\sqrt{3}}(-1,-1,1)$. Black arrows represent $|H\rangle$- horizontal, $|V\rangle$- vertical, $|D\rangle$- diagonal, $|A\rangle$- antidiagonal, $|R\rangle$- circular right-hand, $|L\rangle$- circular left-hand basis states.

Fig. 4.1). One possible set of these projections

$$
\begin{aligned}
\hat{\Pi}_1 &= \frac{1}{4}\left(\sigma_0 + \frac{1}{\sqrt{3}}\left(\sigma_x + \sigma_y + \sigma_z\right)\right), \\
\hat{\Pi}_2 &= \frac{1}{4}\left(\sigma_0 + \frac{1}{\sqrt{3}}\left(\sigma_x - \sigma_y - \sigma_z\right)\right), \\
\hat{\Pi}_3 &= \frac{1}{4}\left(\sigma_0 + \frac{1}{\sqrt{3}}\left(-\sigma_x + \sigma_y - \sigma_z\right)\right), \\
\hat{\Pi}_4 &= \frac{1}{4}\left(\sigma_0 + \frac{1}{\sqrt{3}}\left(-\sigma_x - \sigma_y + \sigma_z\right)\right),
\end{aligned}
\tag{4.1}
$$

is conveniently expressed in terms of Pauli matrices $\sigma_{0,x,y,z}$ [188].

Full two-qubit state tomography still requires at least 15 measurements for this optimal basis, assuming one knows constant state generation rate. A density matrix $\hat{\rho}$ can be estimated from the tomography, and the entanglement quantifier *negativity* is calculated as

$$
N_A = 2|\min(\lambda_i)|,
\tag{4.2}
$$

where $\min(\lambda_i)$ is the smallest eigenvalues of partially transposed density matrix $\hat{\rho}^{PT}$ [99].

For the collective measurement approach to be beneficial, it needs to require at most 7 measurement configurations which is less than one-half of the projections needed for a full state tomography (if we are using two instances simultaneously). Because of the symmetry of $\hat{\rho}_4$, the collective measurement is independent of the swap of local projections, i.e. $P_{xy} = P_{yx}$. Using this fact and considering the minimal basis set $\hat{\Pi}_{1,...,4}$, the maximal independent number of collective measurement configurations is $B = 10$ (see Tab. 4.1). To estimate negativity from a number of configurations $B < 10$, only a subset of the probabilities P_{xy} is selected as indicated in Tab. 4.1. Finding an approximated analytical formulae for quantum states negativity based on a specific number of collective measurement configurations B is a tedious and considerably difficult task. To solve this problem, we turn to the predictive power of artificial neural networks. To this end, uniformly random two-qubit states $\hat{\rho}$ are generated (for generation procedure, see Appendix A.1), and the respective probabilities P_{xy} (3.1), as well the analytical value of negativity N_A (4.2), are calculated using the method described above.

4.3   Artificial neural networks

We have programmed the artificial neural networks capable of quantifying the degree of entanglement in terms of negativity for general two-qubit states utilizing the technique of supervised learning. The input dataset is a collection of feature vectors of length B filled with a subset of collective measurement outcomes P_{xy} according to Tab. 4.1. Each vector thus represents B collective measurements carried out on two simultaneous copies of one randomly generated two-qubit quantum state. The output layer (dataset) consists simply of the single value of negativity corresponding to each input vector. The analytical value of negativity N_A is calculated for all randomly generated quantum states from their density matrices (4.2).

The ANN was trained on $4 \cdot 10^6$ feature vectors. A validation dataset of $1 \cdot 10^6$ independent feature vectors was used to implement regularization, and the training was interrupted whenever a stop condition was reached (mean square error on the validation set gets below $1 \cdot 10^{-4}$ and for 10 consecutive epochs does not decrease further). In addition to that, a third independent test set of $1 \cdot 10^6$ feature vectors was used to obtain an unbiased evaluation of the final model. Our ANN struck a balance between complexity and efficiency, allowing us to obtain the best results using two hidden layers with 200 and 150 nodes, respectively as depicted in Fig. 4.2. De-

creasing the size of the layers by a factor of two already starts affecting the model precision, and increasing it by a factor of two does not bring any benefits. Additional layers provide no improvement. The Rectified Linear Unit (ReLU) activation function

$$\text{ReLU}(x) = x^+ = \max(0, x), \tag{4.3}$$

where x is the input to a neuron, is used between all layers with the exception of the last hidden and the output layer. The output negativity (layer) is calculated using the SoftPlus activation function, a smooth approximation of the ReLU function,

$$\text{SoftPlus}(x) = \ln(1 + e^x). \tag{4.4}$$

Using SoftPlus between the last hidden and output layers outperforms ReLU at this position. We used adaptive moment estimation as an optimizer [189] and mean squared error (MSE) as a loss function

$$\text{MSE} = \frac{1}{n} \sum_{i=1}^{n} (N_A - N_p)^2, \tag{4.5}$$

where n represents the number of all training states, N_A corresponds to analytical values of negativity obtained from the density matrix, and N_p stands for the predicted value of negativity. Experimenting with dropouts did not enhance the learning process.

In summary, the ANNs are used as universal function approximators [180]. Their outputs can be expressed for a three-layer network as

$$f(x, W^{(1)}, W^{(2)}, W^{(3)}) = \phi_3(W^{(3)}\phi_2(W^{(2)}\phi_1(W^{(1)}(x)))), \tag{4.6}$$

where for $n = 1, 2, 3$ ϕ_n are element-wise nonlinear activation functions acting on the result of matrix multiplication of weight matrices $W^{(n)}$ (the ANN parameters). The activation functions, the number of layers, and the weight matrix dimensions are presented in Fig. 4.2. For a single input sample, x is a vector of B values representing the measurement outcomes given by Eq. (3.1).

We tested the capability of the ANN for various numbers of projections configurations B from 5 to 10, i.e., various lengths of feature vector B. For details on exact measurement configurations used in the case of given feature dimensions B, see Tab 4.1.

As mentioned above, the maximal independent number of collective measurement configurations is $B = 10$. Therefore, we chose this case as our
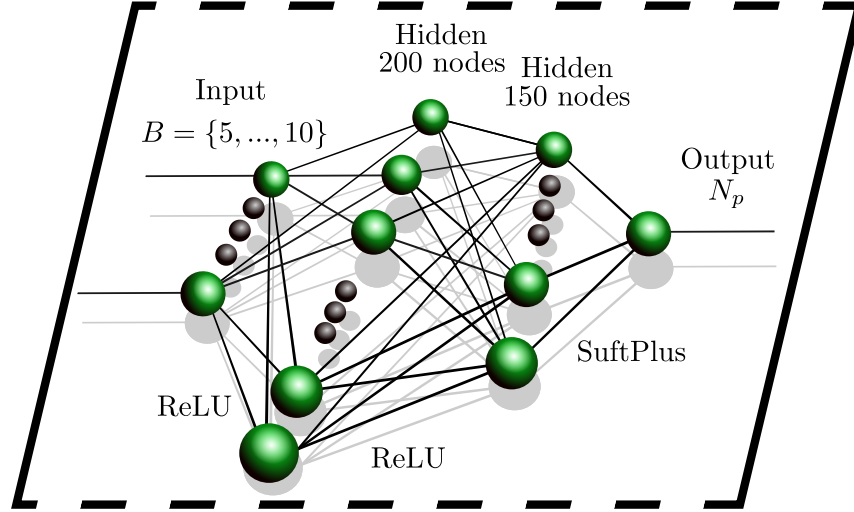
Figure 4.2: Topology of the final ANN model used for negativity N_P prediction from a vector of collective measurements of length B. Two hidden layers are used, containing 200 and 150 nodes, respectively. ReLU and Soft-Max are activation functions.

B	Specific projections
5	$\hat{\Pi}_1 \otimes \hat{\Pi}_1, \hat{\Pi}_2 \otimes \hat{\Pi}_2, \hat{\Pi}_3 \otimes \hat{\Pi}_3, \hat{\Pi}_4 \otimes \hat{\Pi}_4, \hat{\Pi}_1 \otimes \hat{\Pi}_3$
6	$B = 5, \wedge \hat{\Pi}_2 \otimes \hat{\Pi}_4$
7	$B = 6, \wedge \hat{\Pi}_1 \otimes \hat{\Pi}_4$
8	$B = 7, \wedge \hat{\Pi}_1 \otimes \hat{\Pi}_2$
9	$B = 8, \wedge \hat{\Pi}_2 \otimes \hat{\Pi}_3$
10	$B = 9, \wedge \hat{\Pi}_3 \otimes \hat{\Pi}_4$

Table 4.1: List of specific projection settings P_{xy} for a given number of measurements B. Note that B is consecutively the length of input feature vectors in the ANNs.

starting and reference point. From there, we gradually reduced the number of provided projections down to $B = 5$. The most impactful results are obtained for $B = 7$ because, at that point, the number of projections drops below one-half of the projections needed for a full state tomography making this setting our primary success indicator. We used the coefficient of determination R^2

$$R^2 = 1 - \frac{SS_{res}}{SS_{tot}},$$ (4.7)

and standard deviation

$$\tau = \frac{1}{\sqrt{n}}\sqrt{\sum_{i=1}^{n}((N_A - N_p) - \mu)^2},$$ (4.8)

to quantify the capabilities of the ANNs. Where the total sum of squares SS_{tot} and residual sum of squares SS_{res} are defined as

$$SS_{tot} = \sum_{i}(N_A - \bar{N})^2,$$
$$SS_{res} = \sum_{i}(N_A - N_p)^2,$$ (4.9)
$$\bar{N} = \frac{1}{n}\sum_{i=1}^{n}N_A,$$

$\bar{N}$ represents the mean value of analytically calculated negativity, and the mean average is obtained as

$$\mu = \frac{1}{n}\sum_{i=1}^{n}(N_A - N_p).$$ (4.10)

4.4   Results.

First, we provided the ANN with all available information about the investigated state (i.e., $B = 10$ projections) to set the benchmark. In this specific case, the ANN was able to reach $R^2 = 0.996$ and $\tau = 0.01$ (see Fig. 4.3). For $B = 10$, network model gives our best approximation of the negativity function $N(\hat{\rho})$ using only two copies of the investigated state and collective measurements. In the next step, we reduced the number of projections to $B = 9$. As expected, the performance of the network decreased to $R^2 = 0.993$ and $\tau = 0.02$. Further decrease in the number of projections to $B = 8$ did not reveal anything noteworthy but merely confirmed the trend

Figure 4.3: Comparison between analytically calculated negativity N_A and negativity predicted N_p by (a) artificial neural network and (b) quadratic regression for $B = 10$ and 7 configurations, respectively. In addition, the graphs include insets depicting histograms of the difference between N_A and N_p. Every tiny black dot corresponds to one of $1 \cdot 10^6$ tested random states. The coefficient of determination R^2 and standard deviation τ are also included in the legend. In an ideal case, all dots should lie on a diagonal line $N_A = N_p$. Green stripes depict standard deviation $\pm \tau$ from such an ideal case.
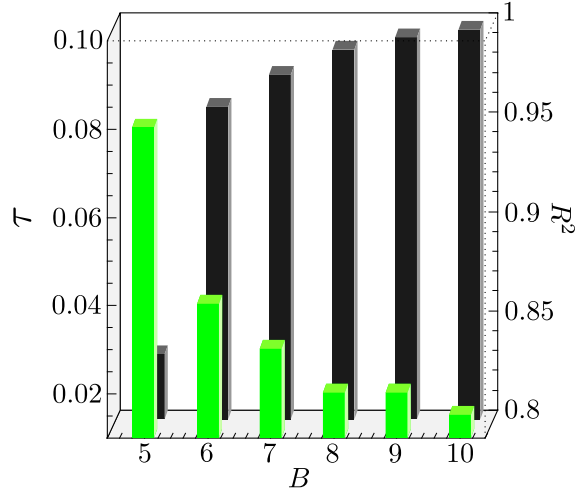
Figure 4.4: The coefficient of determination R^2 (represented by black back columns) and standard deviation τ (represented by green front columns) are plotted for all measurement configurations B to visualize trends in the results.

established above. The performance of the ANN taught on $B = 7$ projections represents the most notable result $R^2 = 0.976$ and $\tau = 0.03$ (see Fig. 4.3 for $B = 7, 10$ and Fig. 4.5 for other values of B) because, at this point, we reduced the number of projections under the full tomography requirements. Obtained results are similar to the limits of the analytical calculations performed on the estimated density matrix from actual experimental tomography data. Those calculations cannot be completely accurate due to unavoidable measurement uncertainties, which usually contribute to final analytical errors by a similar margin, i.e., $\tau = 0.03$ [190]. When the number of projections dropped to $B = 6$ we noticed some decline in the prediction capabilities ($R^2 = 0.961$ and $\tau = 0.04$). Even for $B = 6$ measurement configurations, the observed prediction error is still quite comparable to experimental full state tomography. We tried to limit the number of projections as much as possible, but we drew the line at $B = 5$. In this case, the ANN performance pecked at $R^2 = 0.841$ and $\tau = 0.08$. At this point, the prediction error is already significant, and therefore we did not proceed with further decreasing of B. For an overview of the results, see Fig. 4.4.

In Fig. 4.3, we have also compared the ANN models to quadratic regression models for $B = 7, 10$. The ANNs use significantly more model pa-
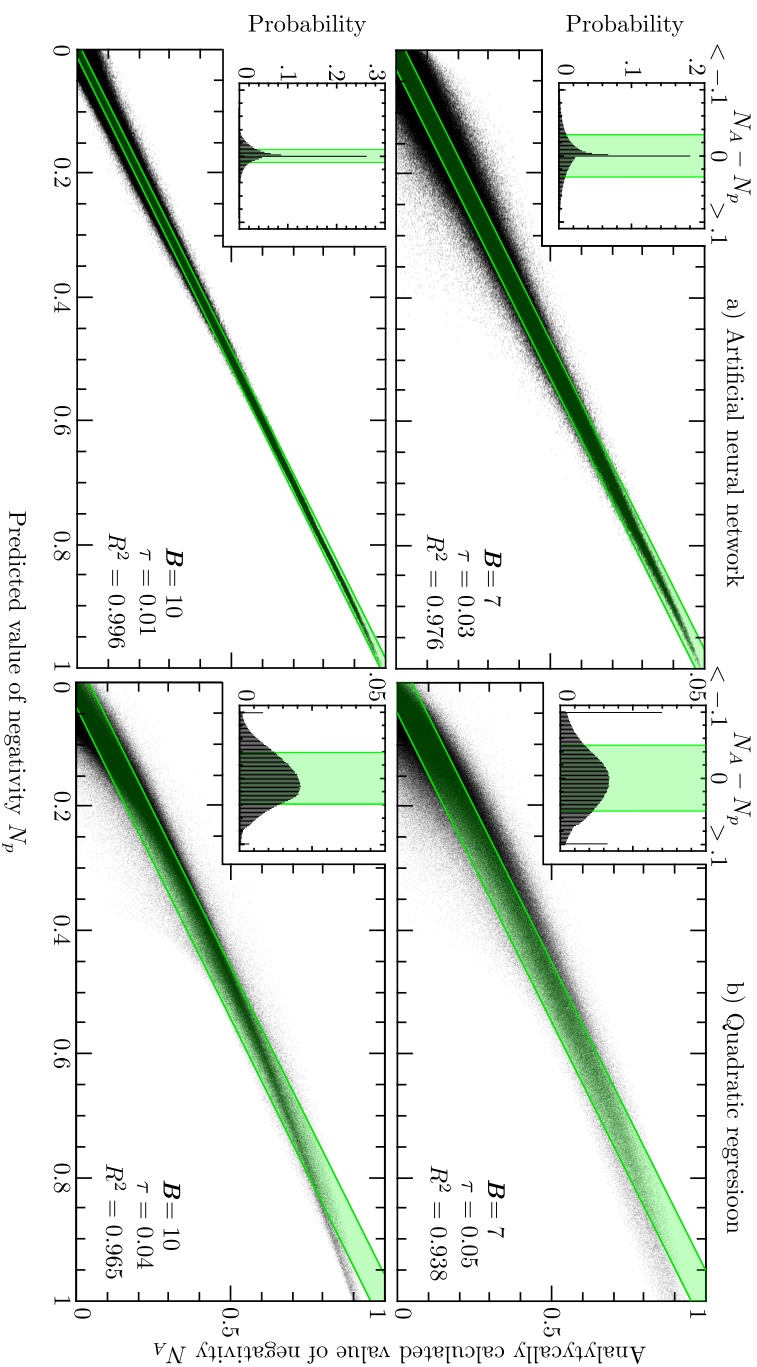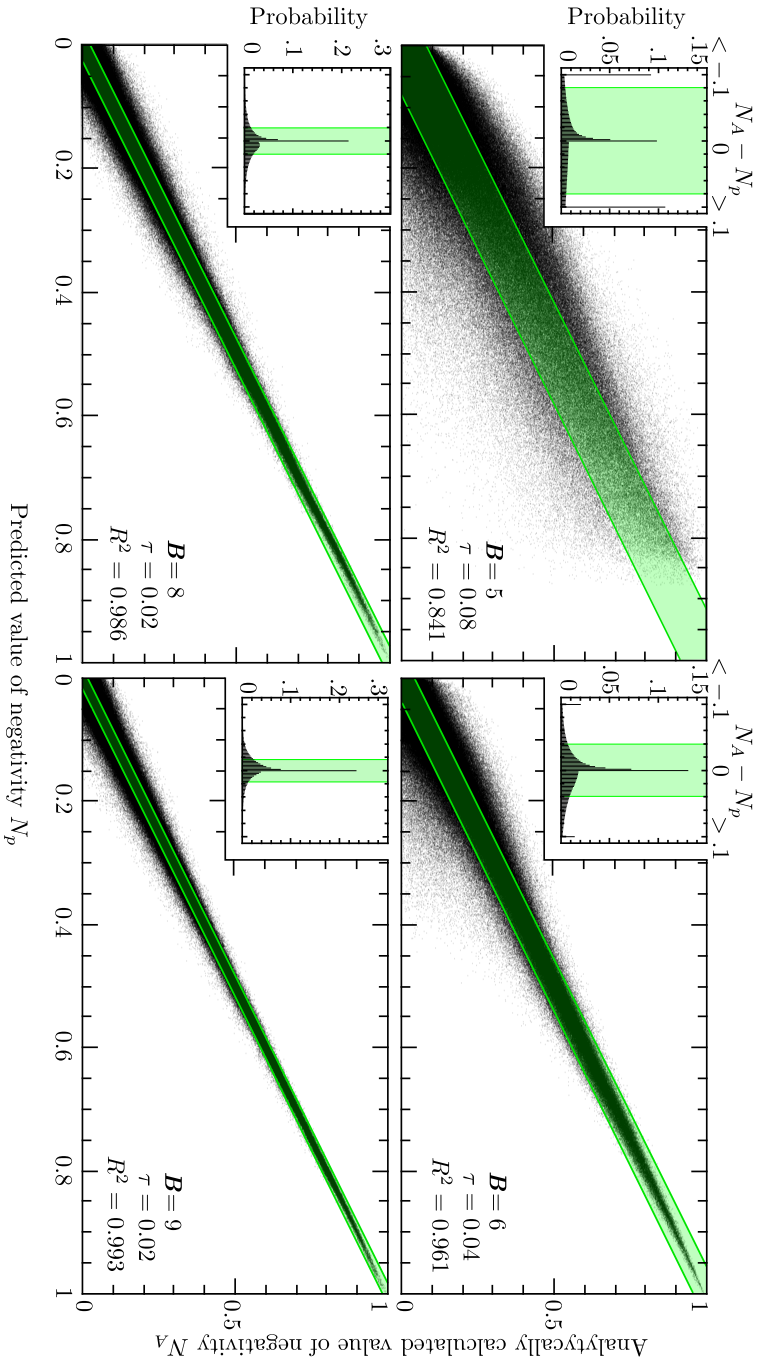
Figure 4.5: Comparison between analytically calculated negativity N_A and negativity predicted N_p by artificial neural network for $B = 5, 6, 8$ and 9 configurations respectively. In addition, the graphs include insets depicting histograms of the difference between N_A and N_p. Every tiny black dot corresponds to one of $1 \cdot 10^6$ tested random states. The coefficient of determination R^2 and standard deviation τ are also included in the legend. In an ideal case, all dots should lie on a diagonal line $N_A = N_p$. Green stripes depict standard deviation $\pm \tau$ from such an ideal case.

rameters than our regression models, but they perform much better. The coefficient of determination for the ANN models is typically larger by 0.03 if compared with the quadratic models. The typical root mean square difference between the predicted values N_p of the ANNs and quadratic regression models is circa 0.17, and it does not depend strongly on the number of measurement configurations B. However, there is an actual benefit of using the quadratic regression models because by doing so, we are able to directly obtain reasonably compact approximate analytical formulae for negativity as functions of assorted collective measurements. Note that regression models up to the fifth order were also tested and did not outperform the ANNs. More details on these models as well as their performance compared to the ANNs is presented in Appendix A.4.

4.5   Conclusions

The above-presented results demonstrate a significant potential of ANNs together with collective measurements for entanglement quantification. Even for $B = 6$ and 7 measurement configurations, the collective measurement performs similarly to experimental full quantum state tomography committing the predictive error of about 3% (in terms of standard deviation). Considering that the particular geometry of collective measurement also overlaps with the entanglement swapping setup [191], implementing entanglement quantification using this configuration can prove interesting for future quantum communication networks [192]. The method presented in this chapter can be used for effective entanglement quantification in entanglement swapping-based communication networks. Moreover, our previous research on the binary classification of entangled/ separable states indicates that the ANN trained on numerically generated quantum states also performs especially well on noisy experimental data [A-1] (at least on limited classes of quantum states). While nonlinear models are expected to function poorly on noisy data, they could perform reasonably well on data burdened with typical experimental error [178]. Although this work investigates the quantification of entanglement that is more demanding than comparison to simpler binary classification, we feel encouraged to conclude that the trained ANNs may also perform adequately on experimental data. However, the development of corresponding experimental setup implementing the set of projectors (4.1) and gathering a sufficient amount of real quantum state data goes well beyond the scope of this investigation. The ANNs were implemented using the TensorFlow

2.0 [166] and Keras [193] libraries.

Chapter 5

Routing in quantum communications networks using reinforcement machine learning

Text adopted from *Jan Roik, Karol Bartkiewicz, Antonín Černoch, and Karel Lemr, submitted (2023)* [A-3].

5.1   Introduction

Efficient communication has played a crucial role in the evolution of all civilizations since antiquity [194, 195]. As the evolution continued, our society began to globalize, and so have our communications needs, ultimately leading to the introduction of the Internet [196]. Nowadays, even these classical communications networks seem outdated, facing the development in the field of quantum communications [25]. The first proposed quantum communications protocols were designed for a one-to-one quantum key distribution (QKD) [197–199]. Subsequent strategies to encompass more parties have been proposed [199, 200]. One promising approach is the so-called teleportation-based quantum networks facilitated by standard or controlled teleportation [133, 201]. The idea is to concatenate many teleportation-based cells into a large global network, i.e., the quantum Internet [61]. Many studies have discussed this concept's po-
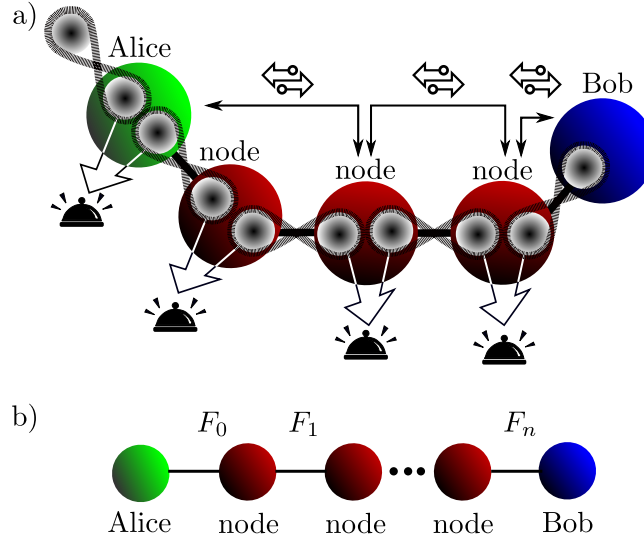
Figure 5.1: Schemes represent entanglement swapping from the initial to the final point in the quantum communications network. a) Each node possesses pair of particles belonging to two different entanglement states symbolized by the two black balls inside the nodes, black line between nodes depicts a quantum channel, green node symbolizes the initial point "Alice", red balls depict intermediate nodes used for entanglement swapping, and blue ball represents the final point "Bob". Bell icon mark where Bell measurement takes place and swap icon highlight where entanglement swapping is carried out. b) Characterization of the road between the initial and final point where $F_0, \ldots, F_n$ are singlet fractions shared by two neighboring nodes.

tential [66, 202, 203], the network's possible topologies [204], platforms to realize it on [205], and fundamental problems to overcome [65].

Quantum networks, however, aim beyond mere QKD, which we must consider when designing quantum networks. The major problem that needs to be addressed is finding an efficient method for optimal dynamic routing in these large-scale quantum networks. It seems that teleportation (entanglement swapping) is, for now, the best method for establishing connections between distant parties in quantum networks [206]. Also, note that entanglement swapping is the core ingredient for quantum repeaters [207] and relays [208], allowing combating unfavorable scaling of losses.

The unique features of quantum information prevent reliably employing classical tools such as shortest path and tree search algorithms [209]. This investigation provides solutions to the routing problem in teleportation-based networks using reinforcement machine learning. The connection between two distant parties (Alice and Bob) in these networks is established by repeated use of entanglement swapping by several intermediate nodes resulting in an entangled state $\hat{\phi}$ shared by the abovementioned parties, Alice and Bob (see Fig. 5.1) [191]. Once they share an entangled state, Alice and Bob are free to use it for secret key sharing [58], quantum state teleportation [91] or dense coding [210]. There are many possibilities to quantify the quality of the repeated entanglement swapping and the quality of the shared entangled state between Alice and Bob [97, 138]. We chose the singlet fraction F as the figure of merit because for bipartite entangled states, F can be directly used to evaluate the usefulness of $\hat{\phi}$ for quantum teleportation [211]. Singlet fraction

$$F(\hat{\phi}) = \max_{|\psi\rangle}\langle\psi|\hat{\phi}|\psi\rangle, \tag{5.1}$$

is defined as the maximal overlap of the investigated state $\hat{\phi}$ with any maximally entangled state $|\psi\rangle$. Maximal achievable teleportation fidelity f of a qubit state is then calculated as

$$f = \frac{2F+1}{3}. \tag{5.2}$$

One can naively think that the singlet fraction of the final state shared by Alice to Bob F_{AB} is obtained as a product of singlet fractions of the entangled states introduced in the repeated n entanglement swappings (see Fig. 5.1)

$$F_{AB} = \prod_{i=0}^{n} F_i, \tag{5.3}$$

alternatively, one can establish an effective *distance d* between Alice and Bob using a logarithm of the singlet fraction

$$d = -\log F_{AB} = -\sum_i \log F_i. \tag{5.4}$$

However, this is not generally true. For example, in cases of amplitude damping [100] or correlated phase noise [101], errors can cancel each other out. If Eq. (3) and Eg. (4) were to hold, one should be able to assign a single quantifier to each quantum channel between nodes and use any graph

path or tree-finding algorithm such as the Dijkstra algorithm and find the route minimizing the distance d [212]. As we show later in this chapter, this yields suboptimal solutions. Note that even prominent dynamic algorithms such as Bellman-Ford [213] and A* [214] cannot handle these types of errors.

One possible solution capable of handling quantum effects is a brute force in the form of the Monte Carlo algorithm. The only downside is Monte Carlo's exponential scaling with the number of nodes. Such a scaling becomes a game stopper, especially in the case of an evolving network where it needs to be repeatedly executed. Hence, a smarter strategy needs to be adopted. In this chapter, we propose using the proximal policy optimization (PPO), an artificial intelligence-based algorithm developed to solve complex evolving problems [102]. This algorithm is commonly used in the gaming industry, where we found inspiration for how to approach the routing problem. We designed our network as a map in a game for the agent to play, intending to find the optimal path through the quantum network. We compare the performance of the PPO against the Monte Carlo and the Dijkstra algorithm demonstrating PPO's virtues.

5.2   Quantum network topology

We found the inspiration for our network topology in the low-density parity-check code structure, one of the possible topologies considered for designing the 6G networks. For the details on the topology, see Fig. 5.2 [103]. This network simulates a real-world scenario where several local users form groups connected among themselves by central nodes. We chose this particular topology mainly due to its robustness against local connection problems, contributing to steady performance. In case of random malfunction in any specific node, this topology offers several possible reroutes to ensure stability. Each connection in the network structure represents a quantum channel using which two neighboring nodes share an entangled two qubit state. For simplicity, we limit the network topology to a maximum of 4 connections per node. Moreover, each node can perform entanglement swapping, i.e., Bell measurement. All shared entangled states are fully characterized by their density matrices. This representation allows us to fully describe how noisy or damaged each connection is. We can easily simulate different sources of disturbance, such as white noise in the channel or amplitude damping. These essential characteristics enable us to simulate various scenarios in the communications network that we later
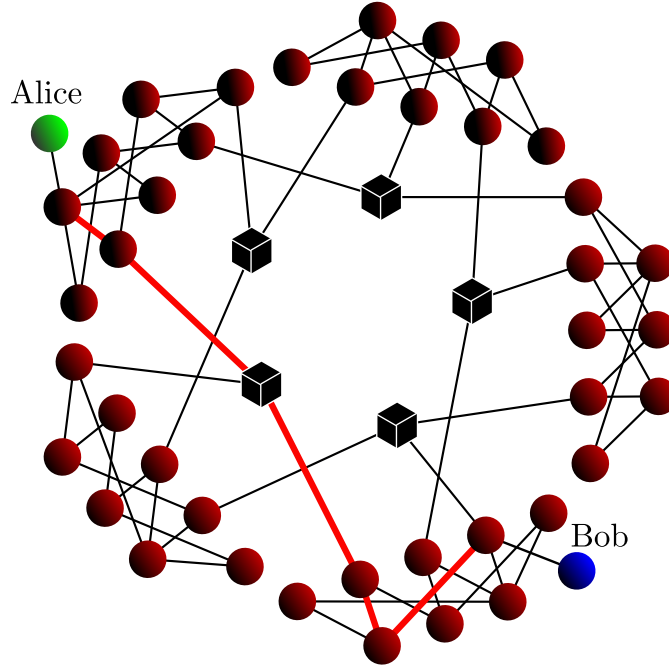
Figure 5.2: This figure shows a visualization of the quantum communications network. The entangled photon pair marked "Alice" represents the initial position for our agents, and blue circle named "Bob" marks the ending point of the route. Full black lines set possible routes for entanglement swapping, red thick lines highlight the optimal solution under ideal conditions, and black cubes represent primary connection nodes between local clusters.

present in the Results section.

The ultimate goal is to distribute entangled state between Alice and Bob. As mentioned in the previous section, the quality of this state is given in terms of singlet fraction F_{AB}, which we maximize. We cast this task as a "game" for the tested algorithms to play. The final reward is received in proportion to F_{AB}. Every connection can be used in each game only once because the used entangled pair is consumed in entanglement swapping. We choose the initial and final users' positions so that the agent can successfully connect them in a given number of actions. We made the routing in the network realistic by ensuring that even the unperturbed connections have a singlet fraction of the distributed state $F = 0.99$ by adding a

corresponding amount of white noise, forcing the PPO algorithm towards the shortest path solutions. To represent white noise, we model the shared entangled states in the form of Werner states

$$\hat{\rho}_w = p|\psi^-\rangle\langle\psi^-| + (1-p)\hat{1}/4. \tag{5.5}$$

$|\psi^-\rangle = (|01\rangle - |10\rangle)/\sqrt{2}$ represents singlet Bell state, $\hat{1}/4$ stands for the maximally mixed state, and p is the mixing parameter. Amplitude damping, on the other hand, is represented by generalizing the Bell states $|\psi^-\rangle$ to

$$|\psi_g^-(\theta)\rangle = \cos(\theta)|01\rangle - \sin(\theta)|10\rangle, \tag{5.6}$$

where $\theta \in [0; \frac{\pi}{2}]$ is the damping parameter. Lastly, an arbitrary phase shift can be described as

$$|\psi_s^-(\phi)\rangle = (|01\rangle - e^{i\phi}|10\rangle)/\sqrt{2}, \tag{5.7}$$

where $\phi \in [0; \pi]$ is the phase shift parameter and if uncompensated and random, renders the state shared between Alice and Bob effectively mixed.

5.3 Routing algorithms

We tested different algorithms capable to solve routing in quantum networks and compared their performance. Namely, we tested the PPO, Dijkstra algorithm, and Monte Carlo method on the quantum communications network. PPO is a policy gradient method for reinforcement learning which uses multiple epochs of stochastic gradient ascent to perform each policy update. It is well known for the simplicity of implementation to various problems and overall performance compared to similar family algorithms. We use stable baseline 3 framework [215] and its implementation of the PPO in our work.

The PPO agents starts at Alice's node. It can choose from at most four actions corresponding to the maximum number of connections any node can have. If the agent chooses an invalid action (i.e., a non-existing connection), the game ends with a negative reward. If a valid link is selected, the agent moves to the node connected by the chosen connection (action). At this point, entanglement swapping is implemented, leading to a shared entangled state between Alice and the connected node. Selecting action and implementing entanglement swapping constitutes one action. A maximum of 15 actions limits the agent; if depleted, the game ends. The preliminary reward is calculated at the end of each action using the formula

$$R_p = F_{A_i} - F_{A_{i-1}}. \tag{5.8}$$

where F_{A_i} stands for the singlet fraction of the newly established entangled state while $F_{A_{i-1}}$ is the singlet fraction resulting from entanglement swapping in the preceding action ($F_{A_0} = 1$ in case of the first action). We tuned the n-steps hyperparameter of the PPO according to the complexity of the designed quantum network topology. Note that the n-steps hyperparameter determines the number of actions the agent takes before updating the parameters of its policy. We kept all other hyperparameters in default values because we did not notice significant changes when tuning them. It is the reward function structure that has the most noticeable influence on the agent's performance. We save the PPO's policy after every 100–5000 games based on the scenarios' complexity. If the agent reaches the final destination (Bob), it receives a final reward

$$R = 100 F_{AB}. \tag{5.9}$$

In case of the Monte Carlo algorithm, we applied the same game rules as for the PPO. So, we can obtain a straightforward comparison. The only difference is that Monte Carlo chooses its actions randomly in each game with no intelligent policy.

Dijkstra's algorithm, on the other hand, needs more information and the data structure of the task. Unlike the previous agents, it needs to know the exact topology of the communications network ahead as well as information about each connection. Therefore, the Dijkstra algorithm does not operate under the same conditions as the previously mentioned agents. At the expense of requiring all the information, it is very efficient at finding distance d from Alice to Bob. A brief description on the working principle of the PPO and Djikstra algorithms is presented in the Appendix A.5.

5.4   Results

Firstly, we investigate routing in a quantum network burdened solely by white noise. This scenario is close to the classical network because white noise is additive and can not be compensated. In a quantum network, however, other types of errors can occur. As examples of such errors, we consider amplitude damping and correlated phase noise which we investigate in the second and third subsections. Finally, a dynamically evolving network noise is considered in the last subsection.

Intermediary nodes (count)	6	8	10	12	14	16
			Number of iterations			
PPO	780	1280	6880	7680	11840	41K
Monte Carlo	644	4310	95K	250K	4M	200M
Dijkstra				1012		

Table 5.1: Results of the three agents applied to the networks of different complexity. This complexity is parametrized by the minimal number of intermediary nodes (first row of the table) that need to be visited in order to find a valid routing solution. The number of iterations is the average number of iterations required to find a solution for a particular topology. Here $M = 10^6$ and $K = 10^3$.

5.4.1 Network affected by white noise

We start with a completely operational network (see the first topology in Fig. A.6 in the Appendix A.6). A singlet fraction $F = 0.99$ characterizes all connections. Optimal routing through this network between Alice and Bob involves 6 intermediary nodes. Then we started introduce damaged connections (i.e., connections with $F = 0.6$), thus increasing the number of the intermediary nodes (8,10,12,14,16) required for finding the optimal solution. The optimal routing paths, under those circumstances are shown in Fig. A.6 as well. The performances of the three agents (PPO, Monte-Carlo, Dijkstra) are summarized in Tab. 5.1.

The Monte Carlo method offers comparable performance to PPO only in the case of the simplest scenario (fully operational network with 6 intermediary nodes to find a solution). The more complex the scenario is, the more prominent the PPO's performance gain becomes. More specifically, in the case of a network where at least 16 intermediary nodes are required to find a solution, PPO outperforms the Monte Carlo method by a factor of about 5000. For visualization see Fig. 5.3. Given the additivity of white noise, the Dijkstra algorithm significantly outperforms the PPO and Monte Carlo in these almost classical scenarios. However, the situation changes with the introduction of purely quantum noise.
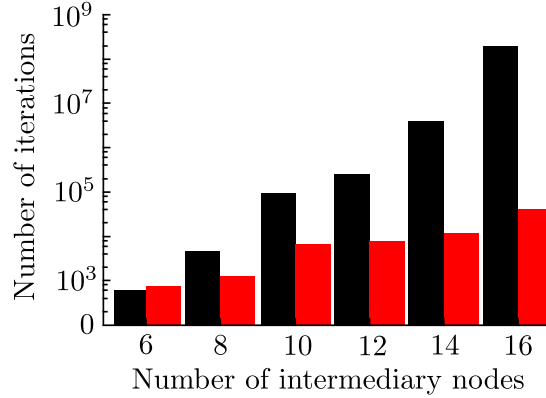
Figure 5.3: The graph compares the performance of the PPO algorithm, represented by the red (right) columns, and the Monte Carlo algorithm, depicted by black (left) columns, on different scenarios requiring a given number of passes through intermediary nodes in the quantum networks.

5.4.2 Network affected by amplitude damping

Amplitude damping, as introduced in Eq. 5.6, skews the amplitude balance towards one of the two components ($|01\rangle$ or $|10\rangle$). As a result, the singlet fraction decreases. Two connections with mutual opposite component damping can rebalance the amplitudes increasing the singlet fraction (at the expense of overall losses). This feature is intractable by greedy or dynamic algorithms such as Dijkstra, Bellman-Ford, or A*. In order to use those algorithms, one needs to save all preliminary solutions and compare them, which would cause exponential scaling of the algorithm complexity. Ultimately, the agent needs to figure out that in order to complete the task, it needs to find such a route where individual amplitude damping cancel each other out as much as possible. We forced the agent to use this strategy by designing scenarios where the agent must choose at least one amplitude-damped connection to reach the final destination. Moreover, the resulting singlet fraction is maximized when a second (opposite) amplitude-damped connection is chosen by the agent. Similar to the previous subsection, we present the agent with scenarios ranging from 6–16 intermediary nodes (see Fig. A.7).

The agents' performance is summarized in Tab. 5.2 and plotted in Fig. 5.4. One can notice that due to these complex initial conditions, the Monte Carlo algorithm performs slightly better than PPO when the optimal path

Intermediary nodes (count)	6	8	10	12	14	16
	Number of iterations					
PPO	1740	13K	14K	15K	54K	60K
Monte Carlo	1K	14K	94K	2M	5M	200M

Table 5.2: Results of the two agents applied to the networks of different complexity, including effects such as amplitude damping. This complexity is parametrized by the minimal number of intermediary nodes (first row of the table) that need to be visited in order to find a valid routing solution. The number of iterations is the average number of iterations required to find a solution for a particular topology. Here $M = 10^6$ and $K = 10^3$.

consists of 6 intermediary nodes. Both methods show similar performance for the 8 intermediary nodes solution; as of 10 intermediary nodes solution onward, the PPO significantly outperforms the Monte-Carlo. In the most complex scenario, i.e. 16 intermediary nodes, the PPO outperforms the Monte Carlo method by a factor of about 3300.

5.4.3   Network affected by correlated phase noise

This subsection demonstrates how agents handle another type of reversible damage caused by the correlated phase noise. These scenarios are motivated by one of the practical approaches towards quantum information distribution proposed by Xu *et al.* [101]. Testing Dijkstra algorithms is again pointless for the reasons we mentioned in the previous subsection. To demonstrate the versatility of the PPO agent, a brand new set of scenarios involving 6-16 intermediary nodes were generated. For more details, see Fig. A.8. In the current scenario, the agent starts from the initial node Alice and in the first action, it can only choose from paths damaged by the correlated phase noise. The agent aims to search the network for a suitable path to reverse the initial correlated phase shift. If successful, it must then find the final node, Bob.

Results of this test are shown in Tab. 5.3 and plotted in Fig. 5.5. One can notice that in the case of the 6 intermediary nodes scenario, the Monte
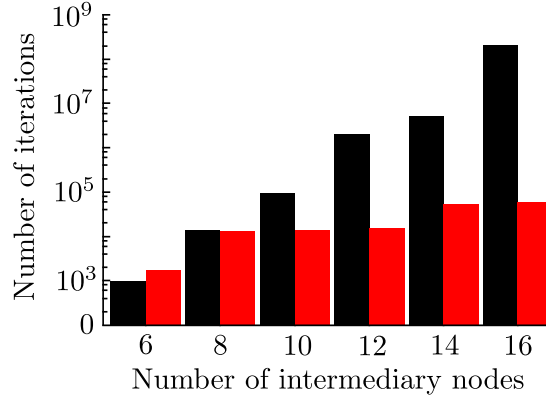
Figure 5.4: The graph compares the performance of the PPO algorithm, represented by the red (right) columns, and the Monte Carlo algorithm, depicted by black (left) columns, on different scenarios in the quantum networks where we also introduced connections affected by amplitude damping.

Carlo slightly outperforms the PPO algorithm. However, the PPO agent performs significantly better for all more complex scenarios from 8 intermediary nodes onward.

5.4.4   Evolving quantum network

Ultimately, we test the agents on dynamically evolving scenarios in our quantum network. The agents' goal in this final test is to maximize the overall functionality of the network throughout the evolutions. These scenarios reflect the realistic behavior of real-world quantum networks where various errors appear at random places and times. The entire routing task lasts for 10^6 iterations, during which the quantum network undergoes ten scenarios (i.e., ten events when various connections become damaged or unperturbed). The evolution continues regardless of the agent's success. In this final test, we use all three types of errors discussed in previous chapters, namely white noise, amplitude dumping, and correlated phase noise. To make the interpretation of the results clear, we set some ground rules. Suppose the agent finds a solution (i.e., a path between Alice and Bob with $F > 0.8$) to the current scenario. In that case, it will use this solution for as long as its singlet fraction remains $F > 0.8$ (i.e., until the scenario evolves).

Intermediary nodes (count)	6	8	10	12	14	16
	Number of iterations					
PPO	1320	2700	10K	20K	27K	39K
Monte Carlo	780	4672	45K	500K	4M	22M

Table 5.3: Results of the two agents applied to the networks of different complexity, including effects such as correlated phase noise. This complexity is parametrized by the minimal number of intermediary nodes (first row of the table) that need to be visited in order to find a valid routing solution. The number of iterations is the average number of iterations required to find a solution for a particular topology. Here M = 10^6 and K = 10^3.

PPO agent at that point also saves its current policy. After the situation evolves, both agents search for a new solution. PPO starts searching from the last saved policy and Monte Carlo randomly from scratch. Each evolution introduces errors so that the previous solution is no longer valid ($F < 0.8$). Hence agents need to find a new route. This condition does not mimic the natural network behavior, but it is the most extreme case where the PPO agent faces the most disadvantageous conditions. All evolutions of the quantum network are depicted in Fig A.9. Resulting success rates are shown in Fig. 5.6. From the obtained results, it is clear that if we let agents deal with an undamaged or slightly damaged network (scenarios 1,2,10), both agents can keep the network functional for more than 95% of the time. If the scenario becomes a bit more complex (scenario 6), the PPO agent slightly outperforms the Monte Carlo agent. For even more complex scenarios, Monte Carlo could not find a solution in a given amount of iterations. Due to these poor results, Monte Carlo kept the network functional for 37.5% of the overall time. On the other hand, the PPO found a solution in 10/10 scenarios and kept the network functional for 93.4% of the overall time.
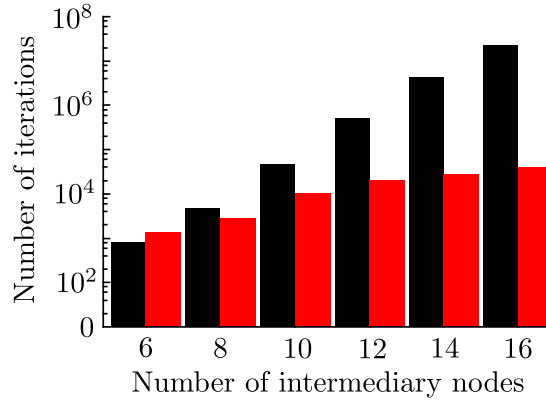
Figure 5.5: The graph compares the performance of the PPO algorithm, represented by the red (right) columns, and the Monte Carlo algorithm, depicted by black (left) columns, on different scenarios, staged in the quantum networks where we also introduced connections causing correlated phase noise.

5.5 Conclusions

This investigation compares three different algorithms (PPO, Djikstra, and Monte Carlo) for route-finding in quantum communications networks. We benchmark these algorithms on various scenarios in a realistic network topology using singlet fraction as the figure of merit. In these scenarios, we introduce additive white noise as well as purely quantum errors such as amplitude damping and correlated phase noise.

We explicitly show that the non-additivity of quantum errors prevents traditional graph path or tree-finding algorithms (Djikstra) from finding the optimal solution. While the Monte Carlo search allows finding such optimal solutions, its exponential scaling makes its deployment prohibitive in large complex networks. We demonstrate that reinforcement machine learning in the form of the PPO algorithm circumvents the limitations of both aforementioned approaches. It can cope with purely quantum errors and, simultaneously, does not suffer from unfavorable scaling.

Our numerical model reveals that the PPO advantage over mere Monte-Carlo search becomes significant when the number of intermediary nodes in the path increases (e.g., for 16 intermediary nodes, PPO outperforms Monte-Carlo by a factor of several thousand). Moreover, in a dynamically
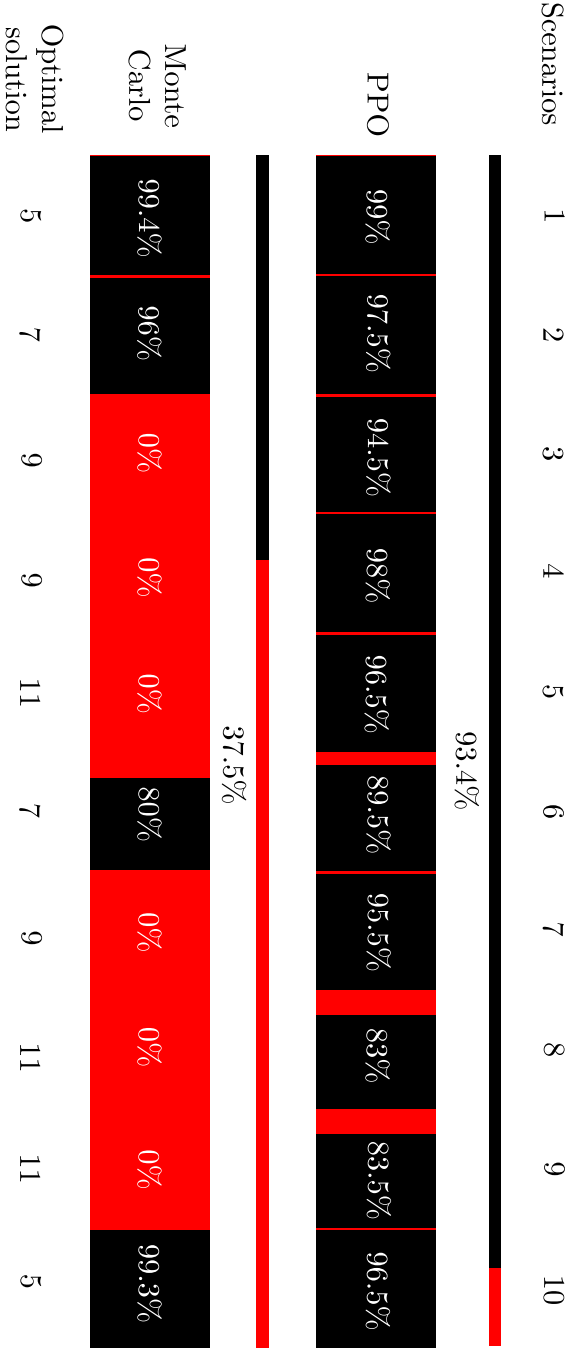
Figure 5.6: Illustration of the Agents' performance on the evolving quantum communication network. Thin stripes show the overall functionality of the quantum network throughout its evolution, and the thick stripes show the functionality during each scenario of its evolution.

evolving quantum network, the PPO could maintain an operational route for about 93% of the time, while Monte Carlo for less than 38%. We believe that our research further promotes reinforcement learning as an invaluable method for improving quantum communications.

Chapter 6

Conclusions

"*The saddest aspect of life right now is that science gathers knowledge faster than society gathers wisdom.*"

<div align="right">-Isaac Asimov</div>

Humankind stands on the verge of a new era, "The golden age" of artificial intelligence. Tasks that were just a few years ago mentioned only in the context of sci-fi literature are nowadays becoming reality. Despite all recent breakthroughs, there still lies a long road ahead to unveil the full potential of artificial intelligence. Based on the achieved results, artificial intelligence has already earned its place as a valuable tool in research. The author firmly believes that artificial intelligence has the potential to shed some light on the fundamental problems of science. Further deployment of artificial intelligence into fields such as quantum data processing may significantly speed up the development of essential technologies, such as large-scale quantum networks.

This thesis presented two fundamental problems of quantum physics and one of quantum data processing. The first problem focused on optimizing the detection of quantum states. The promising results in detecting entangled states motivated follow-up research focused on quantifying the amount of entanglement. The third research task was dedicated to the problem of finding the optimal route in quantum networks. In all three cases, the presented tasks have quantum nature, and to find the solution, we deployed artificial intelligence. That is why Chapter 2 briefly introduces the method and terminology of artificial intelligence and machine learning, and the second half of Chapter 2 establishes basic terms of

quantum data processing.

Chapter 3 highlights the potential of artificial neural networks to binary classify random two-qubit states as entangled or separable. Achieved results demonstrate that given the same amount of resources (i.e., the number of unique collective measurements), ANN surpassed all tested analytical entanglement witnesses. Furthermore, we showed that ANN trained on artificially generated data could be applied to actual experimental data with similar success.

In Chapter 4, we discussed the generalization of the idea from Chapter 3. Here we present the potential of the ANN not just to classify general two-qubit states but also the capability to quantify their amount of entanglement. The ANN aimed to match the negativity values obtained from the full-state tomography. We showed that, given fewer resources, ANN could still maintain comparable prediction capabilities as full-state tomography. Furthermore, we demonstrated that ANN performs favorably in comparison with polynomial regression.

In the fifth chapter, we moved from the fundamental problems of quantum physics to obstacles restricting progress in applied research. Here we tested three conceptually different approaches toward route finding in quantum networks. According to our results, the classical route-finding algorithms struggle to find an optimal solution due to the presence of quantum errors. On the other hand, the proximal policy optimization demonstrated the ability to solve even complex scenarios involving different types of errors while maintaining favorable scaling. During the ultimate test on the evolving quantum network, PPO dominated the Monte Carlo algorithm and decisively proved its potential.

As a closing thought, the author wants to declare that the presented results have already caught the attention of the broader scientific community. Based on the results presented in Chapter 4, we established an international collaboration focused on the follow-up research with a promise to unveil some fundamental dependencies of entanglement detection. We also plan to build an experimental setup capable of doing collective measurements in the minimal set of tomographic projections to test the ANN quantification of entangled states on a real-experimental dataset.

Author's publications

[A-1] J. Roik, K. Bartkiewicz, A. Černoch, and K. Lemr, "Accuracy of entanglement detection via artificial neural networks and human-designed entanglement witnesses," *Physical Review Applied*, vol. 15, no. 5, p. 054006, 2021.

[A-2] J. Roik, K. Bartkiewicz, A. Černoch, and K. Lemr, "Entanglement quantification from collective measurements processed by machine learning," *Physics Letters A*, vol. 446, p. 128270, 2022.

[A-3] J. Roik, K. Bartkiewicz, A. Černoch, and K. Lemr, "Routing in quantum communications networks using reinforcement machine learning", submitted (2023).

[A-4] J. Roik, K. Lemr, A. Černoch, and J. Soubusta, "Calibration of commercially available RGB colorimeters using a spectrometer," *Jemná mechanika a optika*, vol. 67, p. 24, 2022.

[A-5] J. Roik, K. Lemr, and A. Černoch, "Testování a kalibrace RGB kalorimetrů," *Jemná mechanika a optika*, vol. 63, p. 170, 2018.

[A-6] J. Roik, K. Lemr, A. Černoch, and K. Bartkiewicz, "Interplay between strong and weak measurement: comparison of three experimental approaches to weak value estimation," *Journal of Optics*, vol. 22, no. 6, p. 065202, 2020.

[A-7] K. Bartkiewicz, P. Tulewicz, J. Roik, and K. Lemr, "Collaborative generative quantum machine learning on a quantum computer," arXiv preprint arXiv:2112.13255, 2021.

Bibliography

[1] R. N. Carleton, "Fear of the unknown: One fear to rule them all?," *Journal of anxiety disorders*, vol. 41, pp. 5–21, 2016.

[2] J. Lindow, *Norse mythology: A guide to gods, heroes, rituals, and beliefs.* Oxford University Press, 2002.

[3] G. Pinch, *Egyptian mythology: A guide to the gods, goddesses, and traditions of ancient Egypt.* Oxford University Press, USA, 2004.

[4] H. J. Rose, *A handbook of Greek mythology.* Routledge, 2004.

[5] A. Einstein, B. Podolsky, and N. Rosen, "Can quantum-mechanical description of physical reality be considered complete?," *Phys. Rev.*, vol. 47, pp. 777–780, May 1935.

[6] J. S. Bell, "On the Einstein Podolsky Rosen paradox," *Physics*, vol. 1, no. 3, p. 195, 1964.

[7] P. G. Kwiat, E. Waks, A. G. White, I. Appelbaum, and P. H. Eberhard, "Ultrabright source of polarization-entangled photons," *Physical Review A*, vol. 60, no. 2, p. R773, 1999.

[8] T. Juffmann, A. Milic, M. Müllneritsch, P. Asenbaum, A. Tsukernik, J. Tüxen, M. Mayor, O. Cheshnovsky, and M. Arndt, "Real-time single-molecule imaging of quantum interference," *Nature nanotechnology*, vol. 7, no. 5, pp. 297–300, 2012.

[9] T. Maudlin, *Quantum non-locality and relativity: Metaphysical intimations of modern physics.* John Wiley & Sons, 2011.

[10] C. Gearhart, *Black-Body Radiation*, pp. 39–42. Berlin, Heidelberg: Springer Berlin Heidelberg, 2009.

[11] M. Planck, "On the law of distribution of energy in the normal spectrum," *Annalen der physik*, vol. 4, no. 553, p. 1, 1901.

[12] A. Einstein, "Über einen die erzeugung und verwandlung des lichtes betreffenden heuristischen gesichtspunkt," *Annalen der physik*, 1905.

[13] H. Werner, "Über quantentheoretische umdeutung kinematischer und mechanischer beziehungen," *Zeitschrift für Physik*, vol. 33, pp. 879–893, 1925.

[14] E. Schrödinger, "Quantisierung als eigenwertproblem," *Annalen der physik*, vol. 385, no. 13, pp. 437–490, 1926.

[15] E. A. Paschos, *Electroweak theory*. Cambridge University Press, 2007.

[16] W. Marciano and H. Pagels, "Quantum chromodynamics," *Physics Reports*, vol. 36, no. 3, pp. 137–276, 1978.

[17] V. B. Berestetskii, E. M. Lifshitz, and L. P. Pitaevskii, *Quantum Electrodynamics: Volume 4*, vol. 4. Butterworth-Heinemann, 1982.

[18] I. N. Levine, D. H. Busch, and H. Shull, *Quantum chemistry*, vol. 6. Pearson Prentice Hall Upper Saddle River, NJ, 2009.

[19] G. S. Agarwal, *Quantum optics*. Cambridge University Press, 2012.

[20] F. A. Zwanenburg, A. S. Dzurak, A. Morello, M. Y. Simmons, L. C. Hollenberg, G. Klimeck, S. Rogge, S. N. Coppersmith, and M. A. Eriksson, "Silicon quantum electronics," *Reviews of modern physics*, vol. 85, no. 3, p. 961, 2013.

[21] G. Grosso and G. P. Parravicini, *Solid state physics*. Academic press, 2013.

[22] W. D. Callister, D. G. Rethwisch, *et al.*, *Materials science and engineering: an introduction*, vol. 9. Wiley New York, 2018.

[23] T. D. Ladd, F. Jelezko, R. Laflamme, Y. Nakamura, C. Monroe, and J. L. O'Brien, "Quantum computers," *Nature*, vol. 464, no. 7285, pp. 45–53, 2010.

[24] W. P. Schleich, K. S. Ranade, C. Anton, M. Arndt, M. Aspelmeyer, M. Bayer, G. Berg, T. Calarco, H. Fuchs, E. Giacobino, *et al.*, "Quantum technology: from research to application," *Applied Physics B*, vol. 122, no. 5, pp. 1–31, 2016.

[25] N. Gisin and R. Thew, "Quantum communication," *Nature photonics*, vol. 1, no. 3, pp. 165–171, 2007.

[26] S. Pirandola, U. L. Andersen, L. Banchi, M. Berta, D. Bunandar, R. Colbeck, D. Englund, T. Gehring, C. Lupo, C. Ottaviani, *et al.*, "Advances in quantum cryptography," *Advances in optics and photonics*, vol. 12, no. 4, pp. 1012–1236, 2020.

[27] D. G. Nocera, "The artificial leaf," *Accounts of chemical research,* vol. 45, no. 5, pp. 767–776, 2012.

[28] C. L. Degen, F. Reinhard, and P. Cappellaro, "Quantum sensing," *Reviews of modern physics*, vol. 89, no. 3, p. 035002, 2017.

[29] V. Giovannetti, S. Lloyd, and L. Maccone, "Advances in quantum metrology," *Nature photonics*, vol. 5, no. 4, pp. 222–229, 2011.

[30] W. Lu and C. M. Lieber, "Nanoelectronics from the bottom up," *Nature materials*, vol. 6, no. 11, pp. 841–850, 2007.

[31] S. Barnett, *Quantum information*, vol. 16. Oxford University Press, 2009.

[32] M. M. Wilde, *Quantum information theory*. Cambridge University Press, 2013.

[33] D. P. DiVincenzo, "Quantum computation," *Science*, vol. 270, no. 5234, pp. 255–261, 1995.

[34] C. Shao, Y. Li, and H. Li, "Quantum algorithm design: techniques and applications," *Journal of Systems Science and Complexity*, vol. 32, no. 1, pp. 375–452, 2019.

[35] F. M. Reza, *An introduction to information theory*. Courier Corporation, 1994.

[36] D. Gottesman, A. Kitaev, and J. Preskill, "Encoding a qubit in an oscillator," *Physical Review A*, vol. 64, no. 1, p. 012310, 2001.

[37] C. Flühmann, T. L. Nguyen, M. Marinelli, V. Negnevitsky, K. Mehta, and J. Home, "Encoding a qubit in a trapped-ion mechanical oscillator," *Nature*, vol. 566, no. 7745, pp. 513–517, 2019.

[38] P. Kok, W. J. Munro, K. Nemoto, T. C. Ralph, J. P. Dowling, and G. J. Milburn, "Linear optical quantum computing with photonic qubits," *Reviews of modern physics*, vol. 79, no. 1, p. 135, 2007.

[39] D. Loss and D. P. DiVincenzo, "Quantum computation with quantum dots," *Physical Review A*, vol. 57, no. 1, p. 120, 1998.

[40] M. Kjaergaard, M. E. Schwartz, J. Braumüller, P. Krantz, J. I.-J. Wang, S. Gustavsson, and W. D. Oliver, "Superconducting qubits: Current state of play," *Annual Review of Condensed Matter Physics*, vol. 11, pp. 369–395, 2020.

[41] I. Marcikic, H. de Riedmatten, W. Tittel, V. Scarani, H. Zbinden, and N. Gisin, "Time-bin entangled qubits for quantum communication created by femtosecond pulses," *Physical Review A*, vol. 66, no. 6, p. 062308, 2002.

[42] I. L. Chuang, N. Gershenfeld, and M. Kubinec, "Experimental implementation of fast quantum searching," *Physical review letters*, vol. 80, no. 15, p. 3408, 1998.

[43] P. W. Shor, "Algorithms for quantum computation: discrete logarithms and factoring," in *Proceedings 35th annual symposium on foundations of computer science*, pp. 124–134, Ieee, 1994.

[44] T. Monz, D. Nigg, E. A. Martinez, M. F. Brandl, P. Schindler, R. Rines, S. X. Wang, I. L. Chuang, and R. Blatt, "Realization of a scalable Shor algorithm," *Science*, vol. 351, no. 6277, pp. 1068–1070, 2016.

[45] P. Vikstål, M. Grönkvist, M. Svensson, M. Andersson, G. Johansson, and G. Ferrini, "Applying the quantum approximate optimization algorithm to the tail-assignment problem," *Physical Review Applied*, vol. 14, no. 3, p. 034009, 2020.

[46] H.-S. Zhong, H. Wang, Y.-H. Deng, M.-C. Chen, L.-C. Peng, Y.-H. Luo, J. Qin, D. Wu, X. Ding, Y. Hu, *et al.*, "Quantum computational advantage using photons," *Science*, vol. 370, no. 6523, pp. 1460–1463, 2020.

[47] "IBM unveils 400 qubit-plus quantum processor and next-generation IBM Quantum System Two," *IBM Newsroom*, Nov 9, 2022.

[48] V. Chauhan, S. Negi, D. Jain, P. Singh, A. K. Sagar, and A. K. Sharma, "Quantum computers: A review on how quantum computing can boom ai," in *2022 2nd International Conference on Advance Computing and Innovative Technologies in Engineering (ICACITE)*, pp. 559–563, IEEE, 2022.

[49] I. M. Georgescu, S. Ashhab, and F. Nori, "Quantum simulation," *Reviews of Modern Physics*, vol. 86, no. 1, p. 153, 2014.

[50] L. Zhu, H. L. Tang, G. S. Barron, F. Calderon-Vargas, N. J. Mayhall, E. Barnes, and S. E. Economou, "Adaptive quantum approximate optimization algorithm for solving combinatorial problems on a quantum computer," *Physical Review Research*, vol. 4, no. 3, p. 033029, 2022.

[51] P. Gachnang, J. Ehrenthal, T. Hanne, and R. Dornberger, "Quantum computing in supply chain management state of the art and research directions," *Asian Journal of Logistics Management*, vol. 1, no. 1, pp. 57–73, 2022.

[52] Y. Cao, J. Romero, and A. Aspuru-Guzik, "Potential of quantum computing for drug discovery," *IBM Journal of Research and Development*, vol. 62, no. 6, pp. 6–1, 2018.

[53] A. Pandey and V. Ramesh, "Quantum computing for big data analysis," *Indian Journal of Science*, vol. 14, no. 43, pp. 98–104, 2015.

[54] J. Biamonte, P. Wittek, N. Pancotti, P. Rebentrost, N. Wiebe, and S. Lloyd, "Quantum machine learning," *Nature*, vol. 549, no. 7671, pp. 195–202, 2017.

[55] V. Hassija, V. Chamola, V. Saxena, V. Chanana, P. Parashari, S. Mumtaz, and M. Guizani, "Present landscape of quantum computing," *IET Quantum Communication*, vol. 1, no. 2, pp. 42–48, 2020.

[56] R. De Wolf, "The potential impact of quantum computers on society," *Ethics and Information Technology*, vol. 19, no. 4, pp. 271–276, 2017.

[57] P. W. Shor, "Polynomial-time algorithms for prime factorization and discrete logarithms on a quantum computer," *SIAM review*, vol. 41, no. 2, pp. 303–332, 1999.

[58] N. Gisin, G. Ribordy, W. Tittel, and H. Zbinden, "Quantum cryptography," *Rev. Mod. Phys.*, vol. 74, pp. 145–195, Mar 2002.

[59] W. K. Wootters and W. H. Zurek, "A single quantum cannot be cloned," *Nature*, vol. 299, no. 5886, pp. 802–803, 1982.

[60] D. J. Bernstein and T. Lange, "Post-quantum cryptography," *Nature*, vol. 549, no. 7671, pp. 188–194, 2017.

[61] H. J. Kimble, "The quantum internet," *Nature*, vol. 453, no. 7198, pp. 1023–1030, 2008.

[62] H. Zhou, K. Lv, L. Huang, and X. Ma, "Quantum network: Security assessment and key management," *IEEE/ACM Transactions on Networking*, 2022.

[63] M. Pompili, S. L. Hermans, S. Baier, H. K. Beukers, P. C. Humphreys, R. N. Schouten, R. F. Vermeulen, M. J. Tiggelman, L. dos Santos Martins, B. Dirkse, *et al.*, "Realization of a multinode quantum network of remote solid-state qubits," *Science*, vol. 372, no. 6539, pp. 259–264, 2021.

[64] R. Jozsa, D. S. Abrams, J. P. Dowling, and C. P. Williams, "Quantum clock synchronization based on shared prior entanglement," *Physical Review Letters*, vol. 85, no. 9, p. 2010, 2000.

[65] A. S. Cacciapuoti, M. Caleffi, F. Tafuri, F. S. Cataliotti, S. Gherardini, and G. Bianchi, "Quantum internet: networking challenges in distributed quantum computing," *IEEE Network*, vol. 34, no. 1, pp. 137–143, 2019.

[66] L. Gyongyosi and S. Imre, "Advances in the quantum internet," *Communications of the ACM*, vol. 65, no. 8, pp. 52–63, 2022.

[67] M. Pant, H. Krovi, D. Towsley, L. Tassiulas, L. Jiang, P. Basu, D. Englund, and S. Guha, "Routing entanglement in the quantum internet," *npj Quantum Information*, vol. 5, no. 1, pp. 1–9, 2019.

[68] K. Azuma and G. Kato, "Aggregating quantum repeaters for the quantum internet," *Physical Review A*, vol. 96, no. 3, p. 032332, 2017.

[69] S. B. Kotsiantis, I. Zaharakis, P. Pintelas, *et al.*, "Supervised machine learning: A review of classification techniques," *Emerging artificial intelligence applications in computer engineering*, vol. 160, no. 1, pp. 3–24, 2007.

[70] Z. Ghahramani, "Unsupervised learning," in *Summer school on machine learning*, pp. 72–112, Springer, 2003.

[71] P. Y. Glorennec, "Reinforcement learning: An overview," in *Proceedings European Symposium on Intelligent Techniques (ESIT-00), Aachen, Germany*, pp. 14–15, Citeseer, 2000.

[72] D. Maulud and A. M. Abdulazeez, "A review on linear regression comprehensive in machine learning," *Journal of Applied Science and Technology Trends*, vol. 1, no. 4, pp. 140–147, 2020.

[73] T. S. Madhulatha, "An overview on clustering methods," *arXiv:1205.1117*, 2012.

[74] X. Huang, L. Wu, and Y. Ye, "A review on dimensionality reduction techniques," *International Journal of Pattern Recognition and Artificial Intelligence*, vol. 33, no. 10, p. 1950017, 2019.

[75] S. J. Russell, *Artificial intelligence a modern approach.* Pearson Education, Inc., 2010.

[76] O. I. Abiodun, A. Jantan, A. E. Omolara, K. V. Dada, N. A. Mohamed, and H. Arshad, "State-of-the-art in artificial neural network applications: A survey," *Heliyon*, vol. 4, no. 11, p. e00938, 2018.

[77] I. Goodfellow, J. Pouget-Abadie, M. Mirza, B. Xu, D. Warde-Farley, S. Ozair, A. Courville, and Y. Bengio, "Generative adversarial networks," *Communications of the ACM*, vol. 63, no. 11, pp. 139–144, 2020.

[78] J. Oppenlaender, "The creativity of text-to-image generation," in *25th International Academic Mindtrek conference*, pp. 192–202, 2022.

[79] Y. Wu, M. Schuster, Z. Chen, Q. V. Le, M. Norouzi, W. Macherey, M. Krikun, Y. Cao, Q. Gao, K. Macherey, *et al.*, "Google's neural machine translation system: Bridging the gap between human and machine translation," *arXiv preprint arXiv:1609.08144*, 2016.

[80] C. Badue, R. Guidolini, R. V. Carneiro, P. Azevedo, V. B. Cardoso, A. Forechi, L. Jesus, R. Berriel, T. M. Paixao, F. Mutz, *et al.*, "Self-driving cars: A survey," *Expert Systems with Applications*, vol. 165, p. 113816, 2021.

[81] B. Zolfaghari, G. Srivastava, S. Roy, H. R. Nemati, F. Afghah, T. Koshiba, A. Razi, K. Bibak, P. Mitra, and B. K. Rai, "Content delivery networks: state of the art, trends, and future roadmap," *ACM Computing Surveys (CSUR)*, vol. 53, no. 2, pp. 1–34, 2020.

[82] H. Zhang and T. Yu, "Alphazero," in *Deep Reinforcement Learning*, pp. 391–415, Springer, 2020.

[83] K. Arulkumaran, A. Cully, and J. Togelius, "Alphastar: An evolutionary computation perspective," in *Proceedings of the genetic and evolutionary computation conference companion*, pp. 314–315, 2019.

[84] Y. Mintz and R. Brodie, "Introduction to artificial intelligence in medicine," *Minimally Invasive Therapy & Allied Technologies*, vol. 28, no. 2, pp. 73–81, 2019.

[85] X. Mei, H.-C. Lee, K.-y. Diao, M. Huang, B. Lin, C. Liu, Z. Xie, Y. Ma, P. M. Robson, M. Chung, *et al.*, "Artificial intelligence–enabled rapid diagnosis of patients with covid-19," *Nature medicine*, vol. 26, no. 8, pp. 1224–1228, 2020.

[86] R. Fjelland, "Why general artificial intelligence will not be realized," *Humanities and Social Sciences Communications*, vol. 7, no. 1, pp. 1–9, 2020.

[87] K. Lemr, K. Bartkiewicz, A. Černoch, and J. Soubusta, "Resource-efficient linear-optical quantum router," *Physical Review A*, vol. 87, no. 6, p. 062333, 2013.

[88] E. Meyer-Scott, M. Bula, K. Bartkiewicz, A. Černoch, J. Soubusta, T. Jennewein, and K. Lemr, "Entanglement-based linear-optical qubit amplifier," *Physical Review A*, vol. 88, no. 1, p. 012327, 2013.

[89] J. Jašek, K. Jiráková, K. Bartkiewicz, A. Černoch, T. Fürst, and K. Lemr, "Experimental hybrid quantum-classical reinforcement learning by boson sampling: how to train a quantum cloner," *Optics express*, vol. 27, no. 22, pp. 32454–32464, 2019.

[90] A. Harrow, P. Hayden, and D. Leung, "Superdense coding of quantum states," *Physical review letters*, vol. 92, no. 18, p. 187901, 2004.

[91] S. Pirandola, J. Eisert, C. Weedbrook, A. Furusawa, and S. L. Braunstein, "Advances in quantum teleportation," *Nature photonics*, vol. 9, no. 10, pp. 641–652, 2015.

[92] Ł. Rudnicki, P. Horodecki, and K. Życzkowski, "Collective uncer-
      tainty entanglement test," *Physical Review Letters*, vol. 107, no. 15,
      p. 150502, 2011.

[93] J. F. Clauser, M. A. Horne, A. Shimony, and R. A. Holt, "Proposed
      experiment to test local hidden-variable theories," *Phys. Rev. Lett.*,
      vol. 23, pp. 880–884, Oct 1969.

[94] K. Bartkiewicz, P. Horodecki, K. Lemr, A. Miranowicz, and K. Ży-
      czkowski, "Method for universal detection of two-photon polariza-
      tion entanglement," *Phys. Rev. A*, vol. 91, p. 032315, Mar 2015.

[95] V. Vedral and M. B. Plenio, "Entanglement measures and purification
      procedures," *Phys. Rev. A*, vol. 57, pp. 1619–1633, Mar 1998.

[96] J. Gao, L.-F. Qiao, Z.-Q. Jiao, Y.-C. Ma, C.-Q. Hu, R.-J. Ren, A.-L. Yang,
      H. Tang, M.-H. Yung, and X.-M. Jin, "Experimental machine learning
      of quantum states," *Phys. Rev. Lett.*, vol. 120, p. 240501, Jun 2018.

[97] O. Gühne and G. Tóth, "Entanglement detection," *Physics Reports*,
      vol. 474, no. 1-6, pp. 1–75, 2009.

[98] J. Řeháček, B.-G. Englert, and D. Kaszlikowski, "Minimal qubit to-
      mography," *Phys. Rev. A*, vol. 70, p. 052321, Nov 2004.

[99] K. Życzkowski, P. Horodecki, A. Sanpera, and M. Lewenstein, "Vol-
      ume of the set of separable states," *Phys. Rev. A*, vol. 58, pp. 883–892,
      Aug 1998.

[100] R. Fortes and G. Rigolin, "Fighting noise with noise in realistic quan-
      tum teleportation," *Phys. Rev. A*, vol. 92, p. 012338, Jul 2015.

[101] J.-S. Xu, M.-H. Yung, X.-Y. Xu, J.-S. Tang, C.-F. Li, and G.-C. Guo, "Ro-
      bust bidirectional links for photonic quantum networks," *Science
      advances*, vol. 2, no. 1, p. e1500672, 2016.

[102] J. Schulman, F. Wolski, P. Dhariwal, A. Radford, and O. Klimov, "Prox-
      imal policy optimization algorithms," *arXiv:1707.06347*, 2017.

[103] Y. Yuan, Y. Zhao, B. Zong, and S. Parolari, "Potential key technolo-
      gies for 6g mobile communications," *Science China Information Sci-
      ences*, vol. 63, no. 8, pp. 1–19, 2020.

[104] M. H. Hassoun *et al.*, *Fundamentals of artificial neural networks*.
      MIT press, 1995.

[105] M. Uzair and N. Jamil, "Effects of hidden layers on the efficiency of neural networks," in *2020 IEEE 23rd international multitopic conference (INMIC)*, pp. 1–6, IEEE, 2020.

[106] A. K. Jain, J. Mao, and K. M. Mohiuddin, "Artificial neural networks: A tutorial," *Computer*, vol. 29, no. 3, pp. 31–44, 1996.

[107] S. Sharma, S. Sharma, and A. Athaiya, "Activation functions in neural networks," *Towards Data Sci*, vol. 6, no. 12, pp. 310–316, 2017.

[108] J. Lederer, "Activation functions in artificial neural networks: A systematic overview," *arXiv preprint arXiv:2101.09957*, 2021.

[109] H. Pratiwi, A. P. Windarto, S. Susliansyah, R. R. Aria, S. Susilowati, L. K. Rahayu, Y. Fitriani, A. Merdekawati, and I. R. Rahadjeng, "Sigmoid activation function in selecting the best model of artificial neural networks," in *Journal of Physics: Conference Series*, vol. 1471, p. 012010, IOP Publishing, 2020.

[110] J. Schmidt-Hieber, "Nonparametric regression using deep neural networks with ReLU activation function," *The Annals of Statistics*, vol. 48, no. 4, pp. 1875 – 1897, 2020.

[111] I. Kouretas and V. Paliouras, "Simplified hardware implementation of the softmax activation function," in *2019 8th international conference on modern circuits and systems technologies (MOCAST)*, pp. 1–4, IEEE, 2019.

[112] P. Ramachandran, B. Zoph, and Q. V. Le, "Searching for activation functions," *arXiv preprint arXiv:1710.05941*, 2017.

[113] S. Kohli, S. Miglani, and R. Rapariya, "Basics of artificial neural network," *International Journal of Computer Science and Mobile Computing*, vol. 3, no. 9, pp. 745–751, 2014.

[114] S. Ruder, "An overview of gradient descent optimization algorithms," *arXiv preprint arXiv:1609.04747*, 2016.

[115] L. Bottou *et al.*, "Stochastic gradient learning in neural networks," *Proceedings of Neuro-Nımes*, vol. 91, no. 8, p. 12, 1991.

[116] R. Hecht-Nielsen, "Theory of the backpropagation neural network," in *Neural networks for perception*, pp. 65–93, Elsevier, 1992.

[117] A. Lazaridis, A. Fachantidis, and I. Vlahavas, "Deep reinforcement learning: A state-of-the-art walkthrough," *Journal of Artificial Intelligence Research*, vol. 69, pp. 1421–1471, 2020.

[118] C. Beattie, J. Z. Leibo, D. Teplyashin, T. Ward, M. Wainwright, H. Küttler, A. Lefrancq, S. Green, V. Valdés, A. Sadik, *et al.*, "Deepmind lab," *arXiv preprint arXiv:1612.03801*, 2016.

[119] J. Schulman, S. Levine, P. Abbeel, M. Jordan, and P. Moritz, "Trust region policy optimization," in *International conference on machine learning*, pp. 1889–1897, PMLR, 2015.

[120] G. Brockman, V. Cheung, L. Pettersson, J. Schneider, J. Schulman, J. Tang, and W. Zaremba, "Openai gym," *arXiv preprint arXiv:1606.01540*, 2016.

[121] P. A. M. Dirac, "A new notation for quantum mechanics," in *Mathematical Proceedings of the Cambridge Philosophical Society*, vol. 35, pp. 416–418, Cambridge University Press, 1939.

[122] A. Messiah, *Quantum mechanics.* Courier Corporation, 2014.

[123] K. Blum, *Density matrix theory and applications*, vol. 64. Springer Science & Business Media, 2012.

[124] G. Jaeger, *Entanglement, information, and the interpretation of quantum mechanics.* Springer Science & Business Media, 2009.

[125] W. K. Wootters, "Quantum entanglement as a quantifiable resource," *Philosophical Transactions of the Royal Society of London. Series A: Mathematical, Physical and Engineering Sciences*, vol. 356, no. 1743, pp. 1717–1731, 1998.

[126] A. Salles, F. de Melo, M. P. Almeida, M. Hor-Meyll, S. P. Walborn, P. H. Souto Ribeiro, and L. Davidovich, "Experimental investigation of the dynamics of entanglement: Sudden death, complementarity, and continuous monitoring of the environment," *Phys. Rev. A*, vol. 78, p. 022322, Aug 2008.

[127] R. T. Thew, K. Nemoto, A. G. White, and W. J. Munro, "Qudit quantum-state tomography," *Physical Review A*, vol. 66, no. 1, p. 012303, 2002.

[128] J. B. Altepeter, E. R. Jeffrey, and P. G. Kwiat, "Photonic state tomography," *Advances in atomic, molecular, and optical physics*, vol. 52, pp. 105–159, 2005.

[129] A. Peres, "Separability criterion for density matrices," *Phys. Rev. Lett.*, vol. 77, pp. 1413–1415, Aug 1996.

[130] M. Horodecki, P. Horodecki, and R. Horodecki, "Separability of mixed states: necessary and sufficient conditions," *Physics Letters A*, vol. 223, no. 1, pp. 1–8, 1996.

[131] O. Gühne and N. Lütkenhaus, "Nonlinear entanglement witnesses," *Phys. Rev. Lett.*, vol. 96, p. 170502, May 2006.

[132] L. Rudnicki, Z. Puchała, P. Horodecki, and K. Życzkowski, "Collectibility for mixed quantum states," *Phys. Rev. A*, vol. 86, p. 062329, Dec 2012.

[133] C. H. Bennett, G. Brassard, C. Crépeau, R. Jozsa, A. Peres, and W. K. Wootters, "Teleporting an unknown quantum state via dual classical and einstein-podolsky-rosen channels," *Physical review letters*, vol. 70, no. 13, p. 1895, 1993.

[134] N. Lütkenhaus, J. Calsamiglia, and K.-A. Suominen, "Bell measurements for teleportation," *Physical Review A*, vol. 59, no. 5, p. 3295, 1999.

[135] M. Zukowski, A. Zeilinger, M. A. Horne, and A. K. Ekert, ""Event-ready-detectors" bell experiment via entanglement swapping.," *Physical review letters*, vol. 71, no. 26, 1993.

[136] E. Schrödinger, "Discussion of probability relations between separated systems," *Mathematical Proceedings of the Cambridge Philosophical Society*, vol. 31, no. 4, p. 555–563, 1935.

[137] M. B. Plenio and S. Virmani, "An introduction to entanglement theory," in *Quantum Information and Coherence*, pp. 173–209, Springer, 2014.

[138] R. Horodecki, P. Horodecki, M. Horodecki, and K. Horodecki, "Quantum entanglement," *Rev. Mod. Phys.*, vol. 81, pp. 865–942, Jun 2009.

[139] F. Mintert, A. Carvalho, M. Kuś, and A. Buchleitner, "Measures and dynamics of entangled states," *Physics Reports*, vol. 415, no. 4, pp. 207 – 259, 2005.

[140] A. Steane, "Quantum computing," *Reports on Progress in Physics*, vol. 61, pp. 117–173, feb 1998.

[141] D. Bouwmeester, J.-W. Pan, K. Mattle, M. Eibl, H. Weinfurter, and A. Zeilinger, "Experimental quantum teleportation," *Nature*, vol. 390, pp. 575–579, Dec 1997.

[142] K. Bartkiewicz, B. Horst, K. Lemr, and A. Miranowicz, "Entanglement estimation from Bell inequality violation," *Phys. Rev. A*, vol. 88, p. 052105, Nov 2013.

[143] P. Horodecki, "From limits of quantum operations to multicopy entanglement witnesses and state-spectrum estimation," *Phys. Rev. A*, vol. 68, p. 052101, Nov 2003.

[144] F. A. Bovino, G. Castagnoli, A. Ekert, P. Horodecki, C. M. Alves, and A. V. Sergienko, "Direct measurement of nonlinear properties of bipartite quantum states," *Phys. Rev. Lett.*, vol. 95, p. 240407, Dec 2005.

[145] A. R. R. Carvalho, F. Mintert, and A. Buchleitner, "Decoherence and multipartite entanglement," *Phys. Rev. Lett.*, vol. 93, p. 230501, Dec 2004.

[146] Z.-H. Chen, Z.-H. Ma, O. Gühne, and S. Severini, "Estimating entanglement monotones with a generalization of the Wootters formula," *Phys. Rev. Lett.*, vol. 109, p. 200503, Nov 2012.

[147] L. Aolita and F. Mintert, "Measuring multipartite concurrence with a single factorizable observable," *Phys. Rev. Lett.*, vol. 97, p. 050501, Aug 2006.

[148] S. P. Walborn, P. H. Souto Ribeiro, L. Davidovich, F. Mintert, and A. Buchleitner, "Experimental determination of entanglement with a single measurement," *Nature*, vol. 440, pp. 1022–1024, Apr 2006.

[149] P. Badziag, i. c. v. Brukner, W. Laskowski, T. Paterek, and M. Żukowski, "Experimentally friendly geometrical criteria for entanglement," *Phys. Rev. Lett.*, vol. 100, p. 140403, Apr 2008.

[150] M. Huber, F. Mintert, A. Gabriel, and B. C. Hiesmayr, "Detection of high-dimensional genuine multipartite entanglement of mixed states," *Phys. Rev. Lett.*, vol. 104, p. 210501, May 2010.

[151] O. Gühne, M. Reimpell, and R. F. Werner, "Estimating entanglement measures in experiments," *Phys. Rev. Lett.*, vol. 98, p. 110502, Mar 2007.

[152] J. Eisert, F. G. S. L. Brandão, and K. M. R. Audenaert, "Quantitative entanglement witnesses," *New Journal of Physics*, vol. 9, pp. 46–46, mar 2007.

[153] R. Augusiak, M. Demianowicz, and P. Horodecki, "Universal observable detecting all two-qubit entanglement and determinant-based separability tests," *Phys. Rev. A*, vol. 77, p. 030301, Mar 2008.

[154] A. Osterloh and P. Hyllus, "Estimating multipartite entanglement measures," *Phys. Rev. A*, vol. 81, p. 022307, Feb 2010.

[155] L. Rudnicki, P. Horodecki, and K. Życzkowski, "Collective uncertainty entanglement test," *Phys. Rev. Lett.*, vol. 107, p. 150502, Oct 2011.

[156] B. Jungnitsch, T. Moroder, and O. Gühne, "Taming multiparticle entanglement," *Phys. Rev. Lett.*, vol. 106, p. 190502, May 2011.

[157] Ł. Rudnicki, Z. Puchała, P. Horodecki, and K. Życzkowski, "Constructive entanglement test from triangle inequality," *Journal of Physics A: Mathematical and Theoretical*, vol. 47, p. 424035, oct 2014.

[158] L. Zhou and Y.-B. Sheng, "Detection of nonlocal atomic entanglement assisted by single photons," *Phys. Rev. A*, vol. 90, p. 024301, Aug 2014.

[159] H. S. Park, S.-S. B. Lee, H. Kim, S.-K. Choi, and H.-S. Sim, "Construction of an optimal witness for unknown two-qubit entanglement," *Phys. Rev. Lett.*, vol. 105, p. 230404, Dec 2010.

[160] W. Laskowski, D. Richart, C. Schwemmer, T. Paterek, and H. Weinfurter, "Experimental Schmidt decomposition and state independent entanglement detection," *Phys. Rev. Lett.*, vol. 108, p. 240501, Jun 2012.

[161] Y.-C. Ma and M.-H. Yung, "Transforming Bell's inequalities into state classifiers with machine learning," *npj Quantum Information*, vol. 4, p. 34, Jul 2018.

[162] S. Lu, S. Huang, K. Li, J. Li, J. Chen, D. Lu, Z. Ji, Y. Shen, D. Zhou, and B. Zeng, "Separability-entanglement classifier via machine learning," *Phys. Rev. A*, vol. 98, p. 012315, Jul 2018.

[163] C. H. Bennett, D. P. DiVincenzo, J. A. Smolin, and W. K. Wootters, "Mixed-state entanglement and quantum error correction," *Phys. Rev. A*, vol. 54, pp. 3824–3851, Nov 1996.

[164] K. Bartkiewicz, K. Lemr, A. Černoch, and A. Miranowicz, "Bell non-locality and fully entangled fraction measured in an entanglement-swapping device without quantum state tomography," *Phys. Rev. A*, vol. 95, p. 030102, Mar 2017.

[165] A. S. M. de Castro and V. V. Dodonov, "Covariance measures of inter-mode correlations and inseparability for continuous variable quantum systems," *Journal of Optics B: Quantum and Semiclassical Optics*, vol. 5, pp. S593–S608, oct 2003.

[166] M. Abadi, P. Barham, J. Chen, Z. Chen, A. Davis, J. Dean, M. Devin, S. Ghemawat, G. Irving, M. Isard, *et al.*, "Tensorflow: A system for large-scale machine learning," in *12th {USENIX} symposium on operating systems design and implementation ({OSDI} 16)*, pp. 265–283, 2016.

[167] K. Lemr, K. Bartkiewicz, and A. Černoch, "Experimental measurement of collective nonlinear entanglement witness for two qubits," *Phys. Rev. A*, vol. 94, p. 052334, Nov 2016.

[168] M. A. Nielsen and I. L. Chuang, "Quantum computation and quantum information," *Phys. Today*, vol. 54, no. 2, p. 60, 2001.

[169] C. Hughes, J. Isaacson, A. Perry, R. F. Sun, and J. Turner, *Quantum computing for the quantum curious.* Springer Nature, 2021.

[170] B. C. Hiesmayr, "Free versus bound entanglement, a NP-hard problem tackled by machine learning," *Scientific Reports*, vol. 11, Oct. 2021.

[171] L. Gurvits, "Classical deterministic complexity of edmonds' problem and quantum entanglement," in *Proceedings of the thirty-fifth ACM symposium on Theory of computing - STOC '03*, ACM Press, 2003.

[172] S. Gharibian, "Strong NP-hardness of the quantum separability problem," *Quantum Information & Computation,* vol. 10, no. 3&4, p. 343–360, 2010.

[173] Y. Huang, "Computing quantum discord is NP-complete," *New Journal of Physics,* vol. 16, p. 033027, Mar. 2014.

[174] K. Bartkiewicz, A. Černoch, K. Lemr, and A. Miranowicz, "Priority choice experimental two-qubit tomography: Measuring one by one all elements of density matrices," *Scientific Reports,* vol. 6, p. 19610, Jan 2016.

[175] M. Paris and J. Rehacek, *Quantum state estimation,* vol. 649. Springer Science & Business Media, 2004.

[176] S. Hill and W. K. Wootters, "Entanglement of a pair of quantum bits," *Physical review letters,* vol. 78, no. 26, p. 5022, 1997.

[177] V. Vedral, M. B. Plenio, M. A. Rippin, and P. L. Knight, "Quantifying entanglement," *Physical Review Letters,* vol. 78, no. 12, p. 2275, 1997.

[178] K. Bartkiewicz, J. c. v. Beran, K. Lemr, M. Norek, and A. Miranowicz, "Quantifying entanglement of a two-qubit system via measurable and invariant moments of its partially transposed density matrix," *Phys. Rev. A,* vol. 91, p. 022323, Feb 2015.

[179] M. Mohri, A. Rostamizadeh, and A. Talwalkar, *Foundations of machine learning.* MIT press, 2018.

[180] K. Hornik, M. Stinchcombe, and H. White, "Multilayer feedforward networks are universal approximators," *Neural networks,* vol. 2, no. 5, pp. 359–366, 1989.

[181] C. Ren and C. Chen, "Steerability detection of an arbitrary two-qubit state via machine learning," *Phys. Rev. A,* vol. 100, p. 022314, Aug 2019.

[182] Y.-Q. Zhang, L.-J. Yang, Q.-L. He, and L. Chen, "Machine learning on quantifying quantum steerability," *Quantum Information Processing,* vol. 19, no. 8, 2020.

[183] A. Canabarro, S. Brito, and R. Chaves, "Machine learning nonlocal correlations," *Phys. Rev. Lett.,* vol. 122, p. 200401, May 2019.

[184] F. F. Fanchini, G. b. u. Karpat, D. Z. Rossatto, A. Norambuena, and R. Coto, "Estimating the degree of non-markovianity using machine learning," *Phys. Rev. A,* vol. 103, p. 022425, Feb 2021.

[185] D. Koutnỳ, L. Ginés, M. Moczała-Dusanowska, S. Höfling, C. Schneider, A. Predojević, and M. Ježek, "Deep learning of quantum entanglement from incomplete measurements," *arXiv preprint arXiv:2205.01462,* 2022.

[186] D. Gross, Y.-K. Liu, S. T. Flammia, S. Becker, and J. Eisert, "Quantum state tomography via compressed sensing," *Physical review letters,* vol. 105, no. 15, p. 150401, 2010.

[187] C. A. Riofrio, D. Gross, S. T. Flammia, T. Monz, D. Nigg, R. Blatt, and J. Eisert, "Experimental quantum compressed sensing for a seven-qubit system," *Nature communications,* vol. 8, no. 1, p. 15305, 2017.

[188] C. A. Fuchs and R. Schack, "Quantum-bayesian coherence," *Reviews of modern physics,* vol. 85, no. 4, p. 1693, 2013.

[189] D. P. Kingma and J. Ba, "Adam: A method for stochastic optimization," *arXiv preprint arXiv:1412.6980,* 2014.

[190] K. Jiráková, A. Černoch, K. Lemr, K. Bartkiewicz, and A. Miranowicz, "Experimental hierarchy and optimal robustness of quantum correlations of two-qubit states with controllable white noise," *arXiv preprint arXiv:2103.03691,* 2021.

[191] J.-W. Pan, D. Bouwmeester, H. Weinfurter, and A. Zeilinger, "Experimental entanglement swapping: Entangling photons that never interacted," *Phys. Rev. Lett.,* vol. 80, pp. 3891–3894, May 1998.

[192] V. c. v. Trávníček, K. Bartkiewicz, A. Černoch, and K. Lemr, "Experimental diagnostics of entanglement swapping by a collective entanglement test," *Phys. Rev. Applied,* vol. 14, p. 064071, Dec 2020.

[193] F. Chollet *et al.,* "Keras," 2022.

[194] S. Miyagawa, S. Ojima, R. C. Berwick, and K. Okanoya, "The integration hypothesis of human language evolution and the nature of contemporary languages," *Frontiers in psychology,* vol. 5, p. 564, 2014.

[195] M. D. Hauser, *The evolution of communication.* Cambridge, Massachusetts: MIT press, 1996.

[196] B. M. Leiner, V. G. Cerf, D. D. Clark, R. E. Kahn, L. Kleinrock, D. C. Lynch, J. Postel, L. G. Roberts, and S. Wolff, "A brief history of the internet," *ACM SIGCOMM Computer Communication Review*, vol. 39, no. 5, pp. 22–31, 2009.

[197] C. H. Bennett and G. Brassard, "Quantum cryptography: Public key distribution and coin tossing," *arXiv preprint arXiv:2003.06557*, 2020.

[198] A. K. Ekert, "Quantum cryptography and Bell's theorem," in *Quantum Measurements in Optics*, pp. 413–418, Boston, MA: Springer, 1992.

[199] Y. Cao, Y. Zhao, Q. Wang, J. Zhang, S. X. Ng, and L. Hanzo, "The evolution of quantum key distribution networks: On the road to the qinternet," *IEEE Communications Surveys & Tutorials*, vol. 24, no. 2, pp. 839–894, 2022.

[200] M. Hillery, V. Bužek, and A. Berthiaume, "Quantum secret sharing," *Physical Review A*, vol. 59, no. 3, p. 1829, 1999.

[201] D. Gottesman and I. L. Chuang, "Demonstrating the viability of universal quantum computation using teleportation and single-qubit operations," *Nature*, vol. 402, no. 6760, pp. 390–393, 1999.

[202] S. Wehner, D. Elkouss, and R. Hanson, "Quantum internet: A vision for the road ahead," *Science*, vol. 362, no. 6412, p. eaam9288, 2018.

[203] A. Singh, K. Dev, H. Siljak, H. D. Joshi, and M. Magarini, "Quantum internet—applications, functionalities, enabling technologies, challenges, and research directions," *IEEE Communications Surveys & Tutorials*, vol. 23, no. 4, pp. 2218–2247, 2021.

[204] L. Gyongyosi and S. Imre, "Topology adaption for the quantum internet," *Quantum Information Processing*, vol. 17, no. 11, pp. 1–12, 2018.

[205] K. Goodenough, D. Elkouss, and S. Wehner, "Optimizing repeater schemes for the quantum internet," *Physical Review A*, vol. 103, no. 3, p. 032610, 2021.

[206] W. J. Munro, Y.-H. Luo, M.-C. Chen, M. Erhard, H.-S. Zhong, D. Wu, H.-Y. Tang, Q. Zhao, X.-L. Wang, K. Fujii, *et al.*, "Teleportation in

quantum edge networks (conference presentation)," in *Quantum Communications and Quantum Imaging XX*, p. PC122380G, SPIE, 2022.

[207] H.-J. Briegel, W. Dür, J. I. Cirac, and P. Zoller, "Quantum repeaters: the role of imperfect local operations in quantum communication," *Physical Review Letters*, vol. 81, no. 26, p. 5932, 1998.

[208] B. Jacobs, T. Pittman, and J. Franson, "Quantum relays and noise suppression using linear optics," *Physical Review A*, vol. 66, no. 5, p. 052307, 2002.

[209] L. Fu, D. Sun, and L. R. Rilett, "Heuristic shortest path algorithms for transportation applications: State of the art," *Computers & Operations Research*, vol. 33, no. 11, pp. 3324–3343, 2006.

[210] K. Mattle, H. Weinfurter, P. G. Kwiat, and A. Zeilinger, "Dense coding in experimental quantum communication," *Physical Review Letters*, vol. 76, no. 25, p. 4656, 1996.

[211] M. Horodecki, P. Horodecki, and R. Horodecki, "General teleportation channel, singlet fraction, and quasidistillation," *Physical Review A*, vol. 60, no. 3, p. 1888, 1999.

[212] K. Mehlhorn, P. Sanders, and P. Sanders, *Algorithms and data structures: The basic toolbox*, vol. 55. Berlin: Springer, 2008.

[213] R. Bellman, "On a routing problem," *Quarterly of applied mathematics*, vol. 16, no. 1, pp. 87–90, 1958.

[214] P. E. Hart, N. J. Nilsson, and B. Raphael, "A formal basis for the heuristic determination of minimum cost paths," *IEEE transactions on Systems Science and Cybernetics*, vol. 4, no. 2, pp. 100–107, 1968.

[215] A. Raffin, A. Hill, A. Gleave, A. Kanervisto, M. Ernestus, and N. Dormann, "Stable-baselines3: Reliable reinforcement learning implementations," *Journal of Machine Learning Research*, 2021.

[216] J. Maziero, "Random sampling of quantum states: a survey of methods," *Brazilian Journal of Physics*, vol. 45, pp. 575–583, Dec 2015.

[217] C.-K. LI, R. ROBERTS, and X. YIN, "Decomposition of unitary matrices and quantum gates," *International Journal of Quantum Information*, vol. 11, no. 01, p. 1350015, 2013.

[218] Digital supplement containing source codes and trained ANN's parameters is available on Physics Letters A website.

Apendix

Text adopted from appendix sections of author's publications [A-1],[A-2] and [A-3]. Due to similarities in the preparation process of investigated states in Chapter 2 and Chapter 3, their original appendix sections about the preparation process were merged into one.

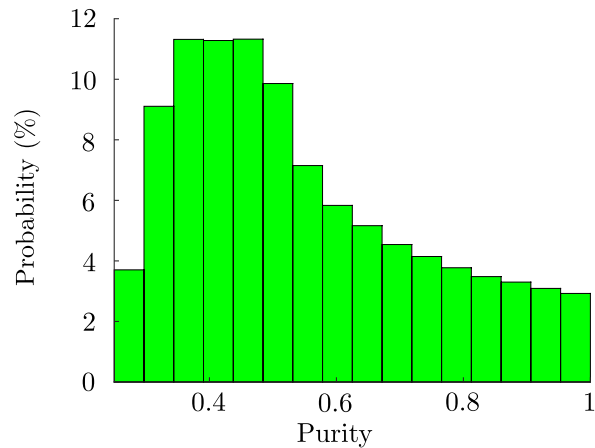## A.1   Preparation of general two-qubit states

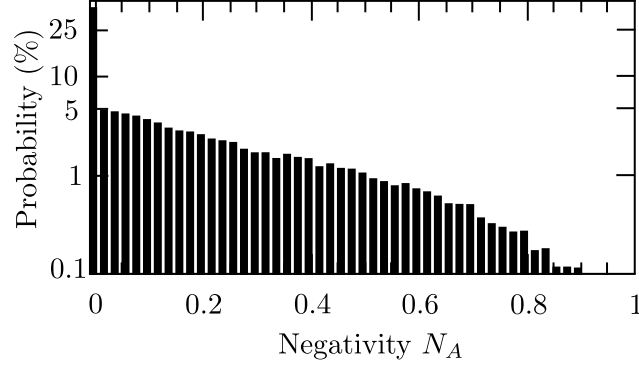Figure A.1: Purity distribution of the training and test states.

Figure A.2: Distribution of negativity N as the function of the probability of occurrence in generated states $\hat{\rho}$. The resulting histogram is in line with the general expectation that at least 30% of random two-qubit states are separable [99] and that the probability of observing a maximally entangled pure state is negligible [216].

Random two-qubit states were generated from 4×4 diagonal matrix $\hat{\rho}_i$ according to Ref. [216]

$$\hat{\rho}_i = \begin{pmatrix} \rho_{11} & 0 & 0 & 0 \\ 0 & \rho_{22} & 0 & 0 \\ 0 & 0 & \rho_{33} & 0 \\ 0 & 0 & 0 & \rho_{44} \end{pmatrix}, \tag{A.1}$$

where $\rho_{11} = r_1$; $\rho_{22} = r_2(1 - \rho_{11})$; $\rho_{33} = r_3(1 - \rho_{11} - \rho_{22})$; $\rho_{44} = r_4(1 - \rho_{11} - \rho_{22} - \rho_{33})$; r_n for $n = 1,2,3,4$ are uniformly distributed random numbers from range $[0,1]$. In the next step, the proper random unitary transformation was used in order to create a density matrix of a general random 2-qubit state [217]

$$U = \begin{pmatrix} 1 & 0 & 0 & 0 \\ 0 & 1 & 0 & 0 \\ 0 & 0 & & U_1 \\ 0 & 0 & & \end{pmatrix} \begin{pmatrix} 1 & 0 & 0 & 0 \\ 0 & & U_2 & 0 \\ 0 & & & 0 \\ 0 & 0 & 0 & 1 \end{pmatrix} \begin{pmatrix} & U_3 & 0 & 0 \\ & & 0 & 0 \\ 0 & 0 & 1 & 0 \\ 0 & 0 & 0 & 1 \end{pmatrix}$$

$$\begin{pmatrix} 1 & 0 & 0 & 0 \\ 0 & 1 & 0 & 0 \\ 0 & 0 & & U_4 \\ 0 & 0 & & \end{pmatrix} \begin{pmatrix} 1 & 0 & 0 & 0 \\ 0 & & U_5 & 0 \\ 0 & & & 0 \\ 0 & 0 & 0 & 1 \end{pmatrix} \begin{pmatrix} 1 & 0 & 0 & 0 \\ 0 & 1 & 0 & 0 \\ 0 & 0 & & U_6 \\ 0 & 0 & & \end{pmatrix}, \tag{A.2}$$

where

$$U_j = e^{i\alpha_j} \begin{pmatrix} e^{i\psi_j} \cos\phi_j & e^{i\chi_j} \sin\phi_j \\ -e^{-i\chi_j} \sin\phi_j & e^{-i\psi_j} \cos\phi_j \end{pmatrix}, \qquad j = 1,\dots,6 \qquad \text{(A.3)}$$

with $0 \le \phi \le \frac{\pi}{2}, 0 \le \alpha, \psi, \chi < 2\pi$. The homogenous distribution of states was ensured by $\phi_j = \arcsin\sqrt{\xi_j}, \xi_j \in [0,1]$. Parameters $\phi_j, \psi_j, \chi_j, \alpha_j$ and ξ_j are picked from their respective intervals with uniform probability. The final density matrix was obtained as $\hat{\rho} = U\hat{\rho}_i U^\dagger$. We present a histogram for the negativity of these randomly generated states in Fig. A.2. To mathematically describe the collective measurement, a 4-qubit density matrix of the entire system $\hat{\rho}_4$ was defined as $\hat{\rho}_4 = \hat{\rho} \otimes SWAP\,\hat{\rho}\,SWAP$ where

$$SWAP = \begin{pmatrix} 1 & 0 & 0 & 0 \\ 0 & 0 & 1 & 0 \\ 0 & 1 & 0 & 0 \\ 0 & 0 & 0 & 1 \end{pmatrix}. \qquad \text{(A.4)}$$

A.2   Collectibility

In order to calculate collectibility we used the formula by Rudnicky *et al.* [132] represented in computational bases, i.e., $H \to |0\rangle$; $V \to |1\rangle$; $D \to |+\rangle = (|0\rangle + |1\rangle)/\sqrt{2}$; $A \to |-\rangle = (|0\rangle - |1\rangle)/\sqrt{2}$; $R \to (|0\rangle - i|1\rangle)/\sqrt{2}$ and, $L \to = (|0\rangle + i|1\rangle)/\sqrt{2}$

$$\begin{aligned} W(\hat{\rho}) = \frac{1}{2}[\eta &+ p_0^2(1 - r_{00}) + (1 - p_0)^2(1 - r_{11}) \\ &+ 2p_0(1 - p_0)(1 - r_{01}) - 1], \end{aligned} \qquad \text{(A.5)}$$

where

$$\eta = 8p_0(1 - p_0)\sqrt{r_{00}r_{11}} + 2p'. \qquad \text{(A.6)}$$

In the equations above single-photon projection probability $p_0 = \hat{\rho}_{00} + \hat{\rho}_{11}$ and $p' = \max\{p_{++}, p_{--}\}$. P_{xy} represents probabilities of single Bell state projection of non-locally measured qubit conditioned on local projection onto $|x\rangle$ and $|y\rangle$ states. [132]

A.3   Other two-copy witnesses

A class of two-copy entanglement witnesses can be calculated using elements of the symmetric matrix [164]

$$R_{i,j} = R_{j,i} = \left\langle \sigma_i^{(a_1)} \otimes \sigma_j^{(a_2)} \otimes |\Psi_{b_1,b_2}^-\rangle\langle\Psi_{b_1,b_2}^-| \right\rangle, \qquad \text{(A.7)}$$
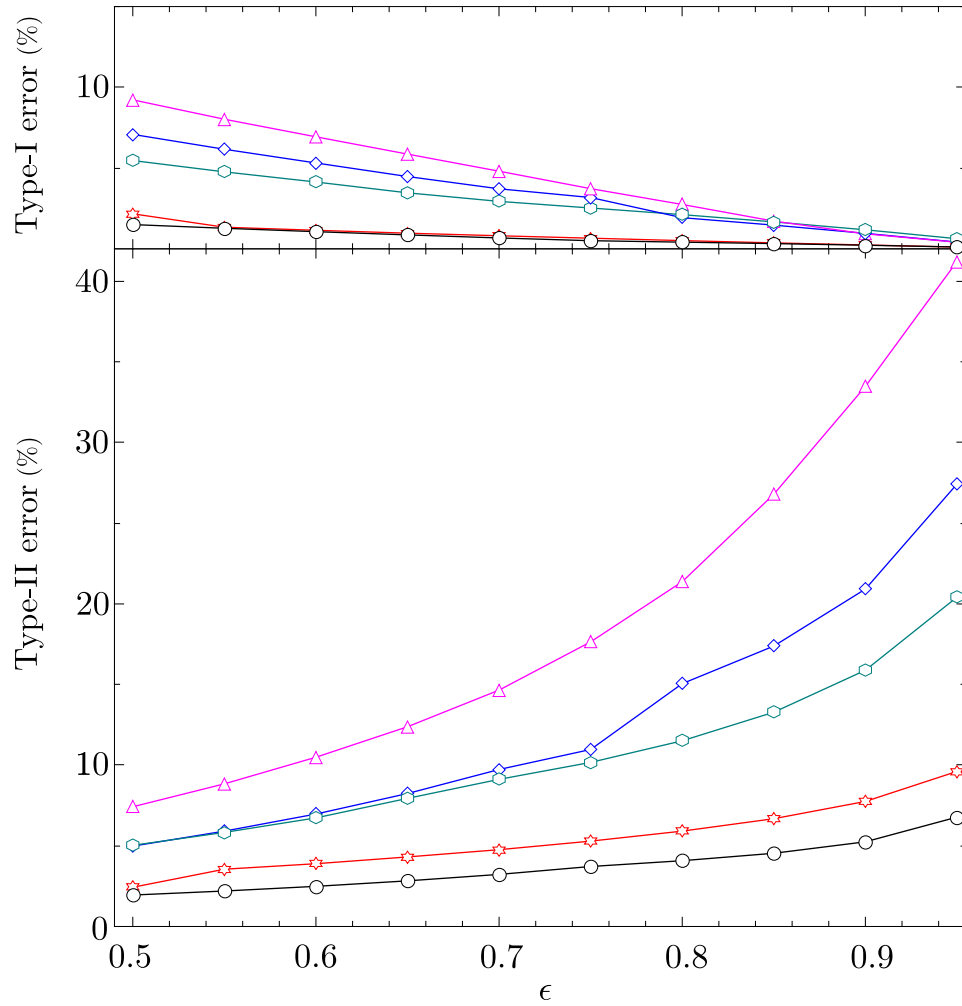
Figure A.3: Dependence of Type I and Type II errors on ϵ threshold for varying numbers of projections. Here purple triangles represent $B = 3$, blue diamonds represent $B = 5$, green hexagons represent $B = 6$, red stars represent $B = 12$, and black circles represent $B = 15$.

B	3		5		6		12		15	
ϵ	T-I	T-II	T-I	T-II	T-I	T-II	T-I	T-II	T-I	T-II
0.5	9.23	7.42	7.09	4.98	5.47	5.03	2.17	2.43	1.50	1.94
0.55	8.03	8.84	6.17	5.91	4.77	5.83	1.34	3.55	1.27	2.19
0.6	6.94	10.49	5.32	6.97	4.14	6.73	1.15	3.89	1.06	2.48
0.65	5.87	12.38	4.48	8.24	3.47	7.94	0.97	4.31	0.86	2.82
0.7	4.81	14.65	3.72	9.73	2.94	9.12	0.81	4.76	0.67	3.22
0.75	3.73	17.64	3.18	10.97	2.53	10.17	0.66	5.29	0.50	3.71
0.8	2.75	21.37	1.93	15.05	2.12	11.51	0.51	5.91	0.41	4.07
0.85	1.72	26.79	1.47	17.38	1.67	13.28	0.37	6.68	0.32	4.53
0.9	0.93	33.47	0.96	20.91	1.18	15.88	0.24	7.75	0.22	5.24
0.95	0.41	41.21	0.42	27.42	0.63	20.41	0.11	9.61	0.11	6.77

Table A.1: Evolution of Type-I and Type-II error for different thresholds ϵ. T-I and T-II represent Type-I and Type-II errors respectively and are listed in percentages.

where the expectation values are calculated on two copies of ρ, i.e., $\rho_{a_1,b_1} \otimes \rho_{a_2,b_2}$. To estimate the number of projections let use the resolution of two-qubit identity operator valid for an arbitrary $i, j = 1, 2, 3$, which reads

$$\hat{1}^{\otimes 2} = \sum_{r,s=0,1} |r_i s_j\rangle\langle r_i s_j|, \tag{A.8}$$

where $|0_i\rangle$ and $|1_i\rangle$ are eigenstates of σ_i operator associated with ± 1 eigenvalues, respectively. A product of two Pauli operators reads

$$\sigma_i^{(a_1)} \otimes \sigma_j^{(a_2)} = |0_i 0_j\rangle\langle 0_i 0_j| + |1_i 1_j\rangle\langle 1_i 1_j|$$
$$- (|0_i 1_j\rangle\langle 0_i 1_j| + |1_i 0_j\rangle\langle 1_i 0_j|). \tag{A.9}$$

By adding the corresponding sides of Eq. (A.8) to Eq. (A.9) and subtracting $\hat{1}^{\otimes 2}$ we obtain

$$\sigma_i^{(a_1)} \otimes \sigma_j^{(a_2)} = 2(|0_i 0_j\rangle\langle 0_i 0_j| + |1_i 1_j\rangle\langle 1_i 1_j|) - \hat{1}^{\otimes 2}. \tag{A.10}$$

This means that measuring all 6 different elements of R (i.e., $i \leq j$ for $i, j = 1, 2, 3$) requires 12 projections in total. These projections read

$$|D\rangle|D\rangle, |A\rangle|A\rangle, |D\rangle|L\rangle, |A\rangle|R\rangle,$$
$$|D\rangle|H\rangle, |A\rangle|V\rangle, |L\rangle|L\rangle, |R\rangle|R\rangle, \tag{A.11}$$
$$|L\rangle|H\rangle, |R\rangle|V\rangle, |H\rangle|H\rangle, |V\rangle|V\rangle.$$

B	$\lvert i\rangle\lvert j\rangle$
3	$\lvert H\rangle\lvert H\rangle, \lvert V\rangle\lvert V\rangle, \lvert H\rangle\lvert V\rangle$
5	$\lvert H\rangle\lvert H\rangle, \lvert V\rangle\lvert V\rangle, \lvert H\rangle\lvert V\rangle, \lvert D\rangle\lvert D\rangle, \lvert A\rangle\lvert A\rangle$
6	$\lvert H\rangle\lvert H\rangle, \lvert V\rangle\lvert V\rangle, \lvert H\rangle\lvert V\rangle, \lvert D\rangle\lvert D\rangle, \lvert R\rangle\lvert R\rangle, \lvert L\rangle\lvert L\rangle$
12	$\lvert D\rangle\lvert D\rangle, \lvert A\rangle\lvert A\rangle, \lvert D\rangle\lvert L\rangle, \lvert A\rangle\lvert R\rangle, \lvert D\rangle\lvert H\rangle, \lvert A\rangle\lvert V\rangle,$ $\lvert L\rangle\lvert L\rangle, \lvert R\rangle\lvert R\rangle, \lvert L\rangle\lvert H\rangle, \lvert R\rangle\lvert V\rangle, \lvert H\rangle\lvert H\rangle, \lvert V\rangle\lvert V\rangle,$
15	$\lvert D\rangle\lvert D\rangle, \lvert A\rangle\lvert A\rangle, \lvert D\rangle\lvert L\rangle, \lvert A\rangle\lvert R\rangle, \lvert D\rangle\lvert H\rangle, \lvert A\rangle\lvert V\rangle, \lvert L\rangle\lvert L\rangle,$ $\lvert R\rangle\lvert R\rangle, \lvert L\rangle\lvert H\rangle, \lvert R\rangle\lvert V\rangle, \lvert H\rangle\lvert H\rangle, \lvert V\rangle\lvert V\rangle, \lvert D\rangle\lvert R\rangle, \lvert D\rangle\lvert V\rangle, \lvert L\rangle\lvert V\rangle$

Table A.2: List of specific projections settings used for the learning of the artificial neural network.

By using these 12 projections we determine matrix Q used to calculate entanglement witnesses. Fully entangled fraction f can be used to construct an entanglement witness [164]

$$F = 2f - 1 = \tfrac{1}{2}[\mathrm{Tr}(\sqrt{Q}) - 1]. \tag{A.12}$$

This and the following witnesses are positive, if entanglement is detected and negative, otherwise. The maximum value is 1.

Furthermore, by using an optimal CHSH inequality we can construct an entanglement witness [164] as

$$M = \mathrm{Tr}(Q) - \min[\mathrm{eig}(Q)]. \tag{A.13}$$

It is also possible to use Q to express an entropic entanglement witness [164]

$$E = \tfrac{1}{2}[\mathrm{Tr}(Q) - 1]. \tag{A.14}$$

A.4   Polynomial fits of the negativity function

Polynomial models provide estimates of negativity, and their precision improves with the order of the polynomial. The quadratic regression model for the negativity can be formally written as $N_p = \vec{\theta}_B \cdot \vec{x}$, where the vector $\vec{x} = (1, x_1, x_2, ..., x_B, x_1^2, x_1 x_2, ..., x_1 x_B, x_2^2, x_2 x_3, ..., x_2 x_B, ..., x_B^2)$ contains vector elements $x_1, x_2 ..., x_B$. This model performs worse than the ANNs but allows extracting an approximate analytical formula for negativity as a function of the input vector of collective measurements.
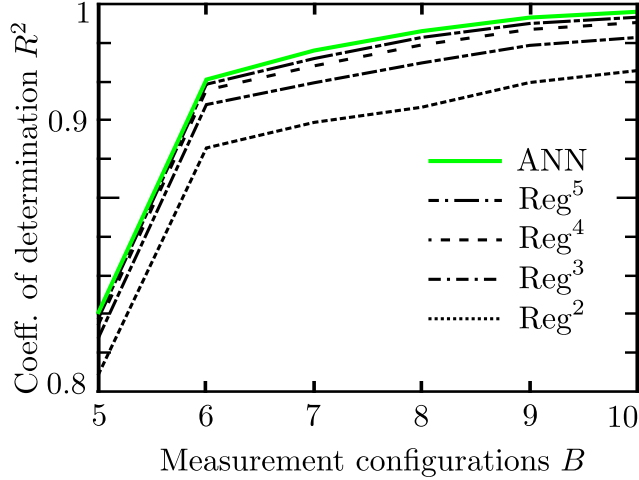
Figure A.4: Comparison of polynomial regression models and the ANNs in terms of the coefficient of determination R^2 as function of input feature vector length B.

	ANN		REG2		REG3	
B	R^2	τ	R^2	τ	R^2	τ
5	0.841	0.08	0.809	0.09	0.828	0.08
6	0.961	0.04	0.926	0.06	0.948	0.05
7	0.976	0.03	0.938	0.05	0.959	0.04
8	0.986	0.02	0.947	0.05	0.970	0.04
9	0.993	0.02	0.959	0.04	0.979	0.03
10	0.996	0.01	0.965	0.04	0.983	0.03

Table A.3: Comparison of the results obtained by ANN and quadratic/ cubic regressions REG2/ REG3 for B = 5 to 10. Where R^2 represents the coefficient of determination and τ stands for standard deviation.

Higher-order polynomial regression models are straightforward expansions of the quadratic model having considerably more parameters for fitting and therefore are less useful as an analytical approximation of the negativity function. On the other hand, the linear model is too simple to provide helpful approximation for negativity. As indicated in Tab. A.3, neither the quadratic nor cubic model outperforms the ANNs. Moreover, we plot the dependence of the coefficient of determination R^2 as a function of the
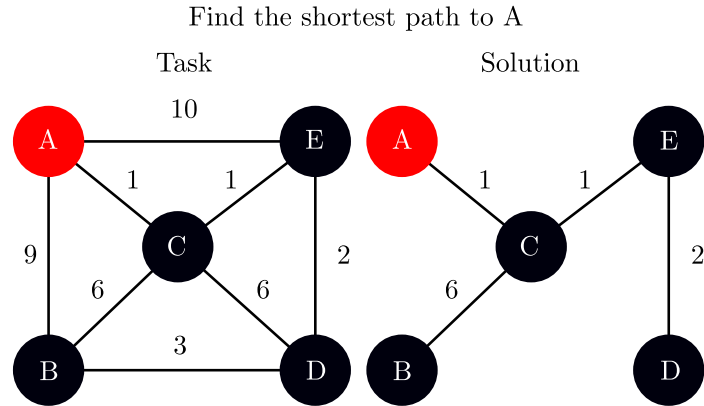
Figure A.5: Depiction of an illustrative communications network where the red circle A marks the initial position and the numbers beside the connections correlate to the distance.

input vector length *B* in Fig. A.4 to prove the ANNs superiority over these models up to the fifth order. The optimized polynomial model parameters are presented in the Digital Supplement [218].

A.5   Djikstra algorithm

The Dijkstra algorithm is designed to find the shortest distance from one node to every other node in the network. The working principle of this algorithm is as follows. In the first step, we choose the initial node, i.e., Alice. Then the algorithm starts filling a table storing all the information about the distances from the initial node to every other node. Distance is set to infinity if there is a nonexisting direct connection from the initial node. In the next step, it moves from the initial node to the closest node. The distance table is updated by replacing nonoptimal (longer) distances with optimal (shorter) distances from the initial node to every node, assuming the new path passes through the current node. This procedure continues until the algorithm visits all nodes and obtains the optimal path from Alice to all nodes. For an illustration, see Fig. A.5 and Tab. A.4.

Actions:	1	2	3	4	5
Unvisited nodes:	B,C,D,E	B,D,E	B,D	D	
Current node:	A	C	E	D	B
Distance					
A → A:	0	0	0	0	0
A → B:	9	7	7	7	7
A → C:	1	1	1	1	1
A → D:	∞	7	4	4	4
A → E:	10	2	2	2	2

Table A.4: Description of the evaluation of the Dijkstra algorithm on the illustrative communication network showcased in Fig. A.5

A.6   PPO algorithm

This section provides a graphical representation of the performance of the PPO agent deployed on the various scenarios in quantum networks. Fig. A.6 visualizes scenarios where we considered connections affected by white noise only. Fig. A.7 displays scenarios where connections are affected by white noise and amplitude dumping. Fig. A.8 shows scenar- ios where connections are affected by white noise and correlated phase noise. Last but not least, in Fig. A.9, one can see a visual representation of ten unique subsequent scenarios used to assess the agent performance on evolving quantum networks.
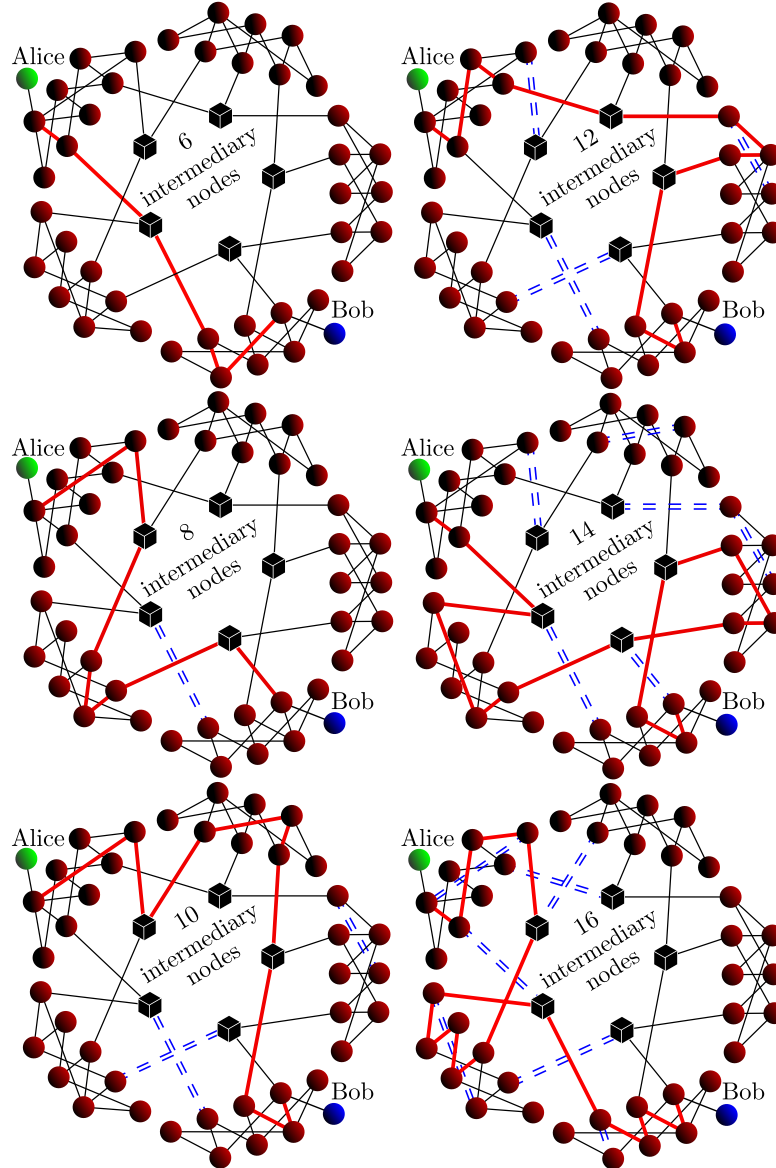
Figure A.6: The figure shows various quantum network scenarios where we consider connections affected by white noise only. We prepared scenarios ranging from simplest solvable using 6 intermediary nodes to complex requiring up to 16 intermediary nodes. The thick red line marks one of the optimal solutions to the presented scenario, and the double blue dashed lines represent irreversibly damaged connections.
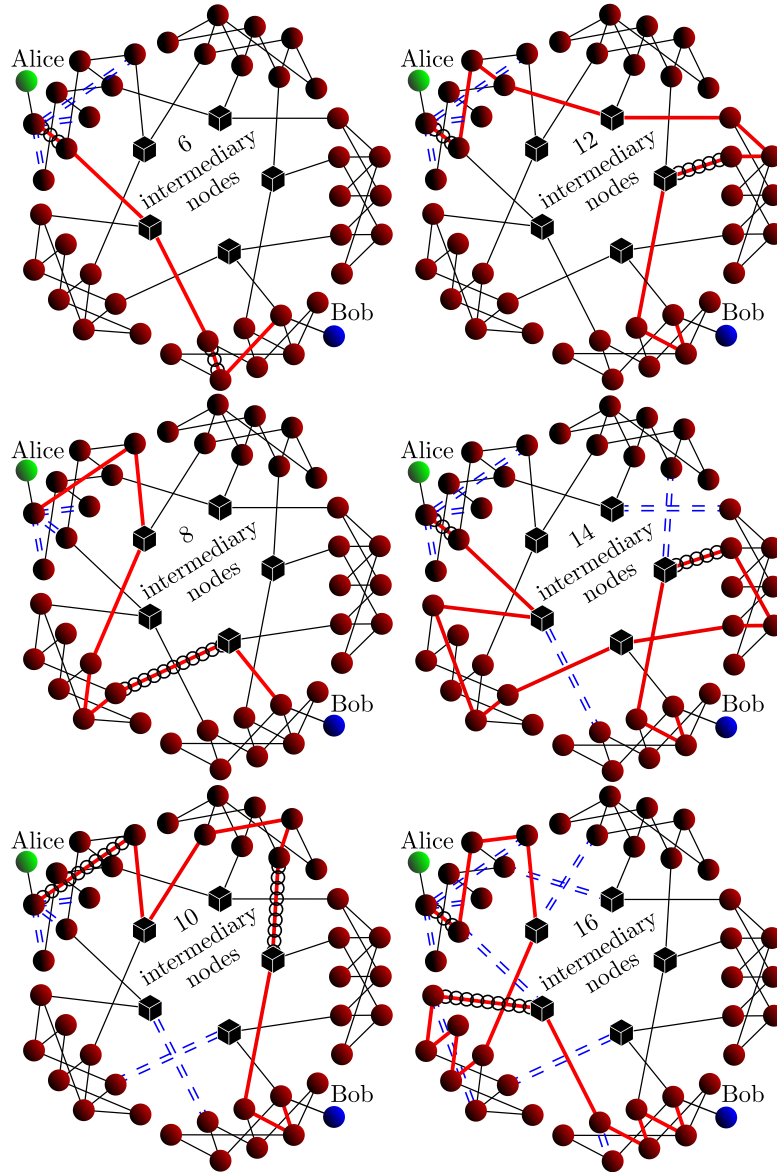
Figure A.7: The figure shows various quantum network scenarios where we consider connections affected by white noise and amplitude dumping. We prepared scenarios ranging from simplest solvable using 6 intermediary nodes to complex requiring up to 16 intermediary nodes. The thick red line marks one of the optimal solutions to the presented scenario, double blue dashed lines represent irreversibly damaged connections, and black chain marks connections cause amplitude damping.
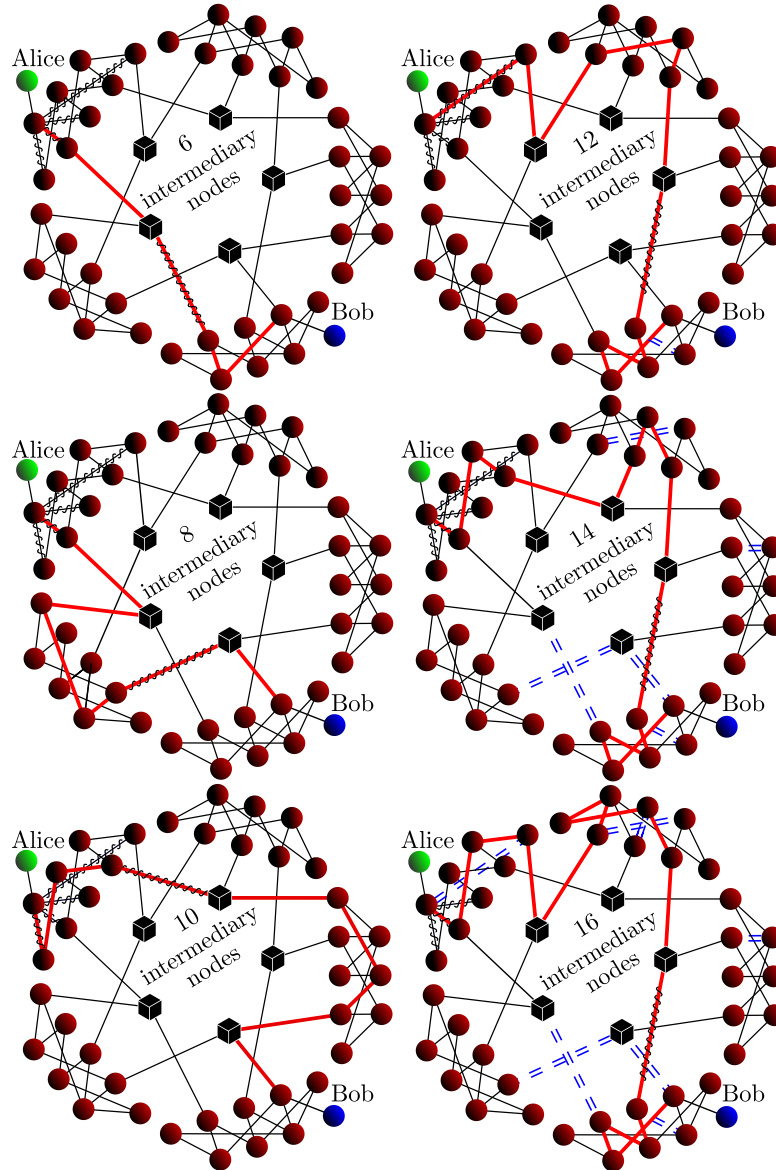
Figure A.8: The figure shows various quantum network scenarios where we consider connections affected by white noise and correlated phase noise. We prepared scenarios ranging from simplest solvable using 6 intermediary nodes to complex requiring up to 16 intermediary nodes. The thick red line marks one of the optimal solutions to the presented scenario, double blue dashed lines represent irreversibly damaged connections, and wrap-around lines mark connections causing correlated phase noise.
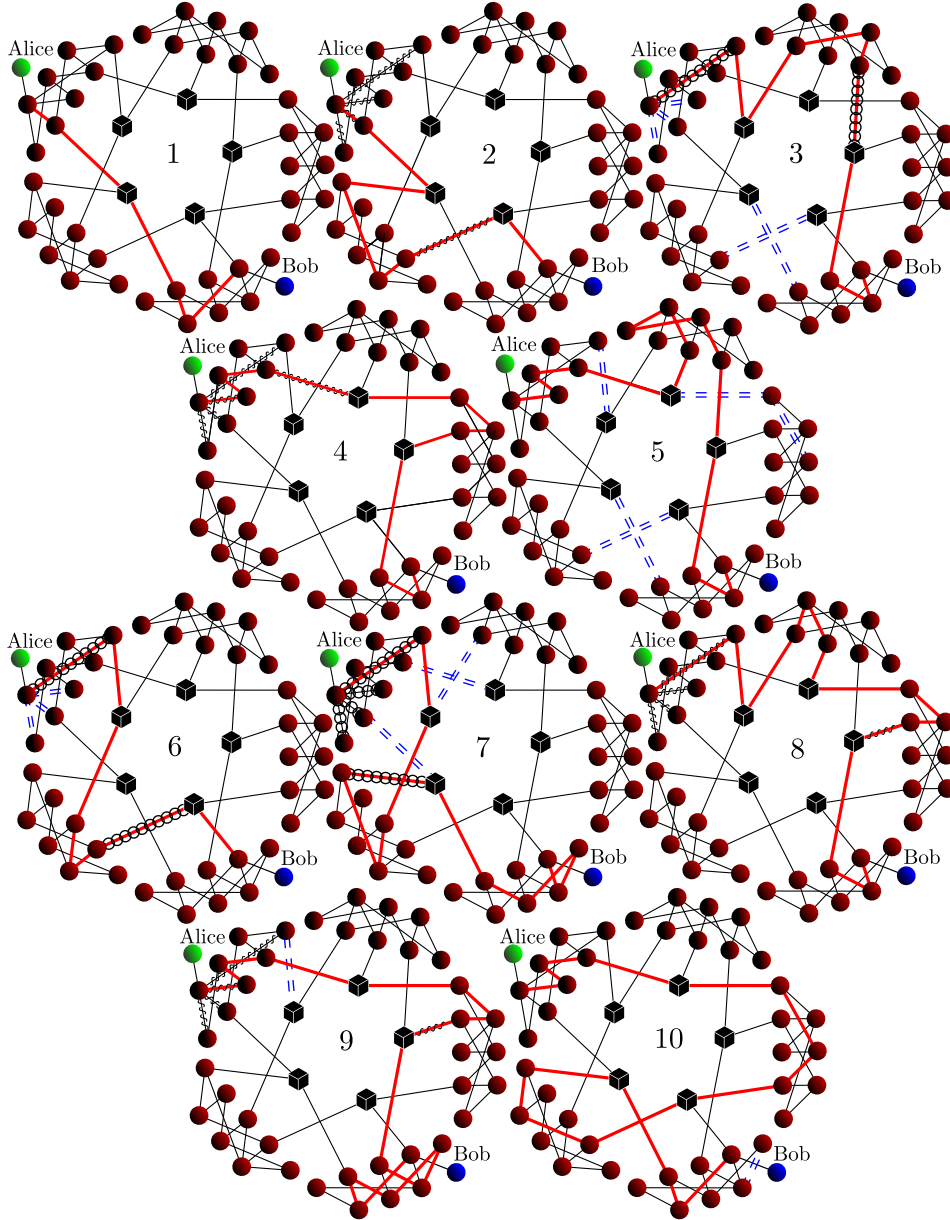
Figure A.9: The figure shows evolving quantum communications network and the response of the PPO agent to those changes. The thick red line marks the PPO's solution in the final iterations before the change in the current scenario. Double-blue dashed lines represent damaged connections, wrap-around lines mark connections causing correlated phase noise and black chain marks connections causing amplitude damping.

Confirmation of contribution

As the supervisor to Mgr. Jan Roik and corresponding author of his publications

[1] J. Roik, K. Bartkiewicz, A. Černoch, and K. Lemr, "Accuracy of entanglement detection via artificial neural networks and human-designed entanglement witnesses," Phys. Rev. Appl. **15**, 054006 (2021),

[2] J. Roik, K. Bartkiewicz, A. Černoch, and K. Lemr, "Entanglement quantification from collective measurements processed by machine learning," Phys. Lett. A **446**, 128270 (2022),

[3] J. Roik, K. Bartkiewicz, A. Černoch, and K. Lemr, "Routing in quantum communications networks using reinforcement machine learning," submitted (2023)

I hereby certify that Mgr. Jan Roik significantly contributed to the scientific investigation presented in these publications. Typically, he programmed the machine learning models, evaluated obtained data and dominantly contributed to writing of the manuscripts. Extracts of the publications directly quoted in his thesis are of his own writing.

Olomouc, 6th March 2023   ....

doc. Mgr. Karel Lemr, Ph.D.
Joint Laboratory of Optics

Confirmation of contribution

As the co-author of Mgr. Jan Roik publications:

[1] J. Roik, K. Bartkiewicz, A. Cernoch, and K. Lemr, "Accuracy of entanglement detection via artificial neural networks and human-designed entanglement witnesses," Phys. Rev. Appl. 15, 054006 (2021),

[2] J. Roik, K. Bartkiewicz, A. Černoch, and K. Lemr, "Entanglement quantification from collective measurements processed by machine learning," Phys. Lett. A 446, 128270 (2022),

[3] J. Roik, K. Bartkiewicz, A. Černoch, and K. Lemr, "Routing in quantum communications networks using reinforcement machine learning," submitted (2023)

I hereby certify that Mgr. Jan Roik significantly contributed to the scientific investigation presented in these publications. Typically, he programmed the machine learning models, evaluated obtained data and dominantly contributed to writing of the manuscripts. Extracts of the publications directly quoted in his thesis are of his own writing.

Olomouc, 6th March 2023

....

Mgr. Antonín Černoch, Ph.D.
Joint Laboratory of Optics

6.03.2023, Poznań

To whom it may concern,

I declare that Mgr. Jan Roik contributed significantly to the scientific research presented in the publications [1,2,3]. His contributions included implementing and applying artificial intelligence methods to solve the particular research tasks, processing the obtained data, and dominantly contributing to the writing of manuscripts. He wrote the extracts of the publications quoted directly in his thesis.

[1] J. Roik, K. Bartkiewicz, A. Černoch, and K. Lemr, "Accuracy of entanglement detection via artificial neural networks and human-designed entanglement witnesses," Physical Review Applied, vol. 15, no. 5, p.054006, 2021.

[2] J. Roik, K. Bartkiewicz, A. Černoch, and K. Lemr, "Entanglement quantification from collective measurements processed by machine learning," Physics Letters A, vol. 446, p. 128270, 2022.

[3] J. Roik, K. Bartkiewicz, A. Černoch, and K. Lemr, "Routing in quantum communications networks using reinforcement machine learning," MANUSCRIPT SUBMITTED FOR PUBLICATION, 2023.

Prof. UAM dr hab. Karol Bartkiewicz